UNIVERSITY OF SOUTHAMPTON

MODELLING SOUND SOURCE REGIONS FOR THE PREDICTION OF COAXIAL JET NOISE

by
Giles Andrew Preston

A Thesis submitted for the award of
Doctor of Philosophy

FACULTY OF ENGINEERING AND APPLIED SCIENCE

INSTITUTE OF SOUND AND VIBRATION RESEARCH

February 1995

UNIVERSITY OF SOUTHAMPTON

ABSTRACT

FACULTY OF ENGINEERING AND APPLIED SCIENCE
INSTITUTE OF SOUND AND VIBRATION RESEARCH

Doctor of Philosophy

MODELLING SOUND SOURCE REGIONS FOR THE PREDICTION OF COAXIAL JET NOISE

by Giles Andrew Preston

This thesis describes work undertaken in a fundamental study of the mixing noise of coaxial jet exhausts using acoustic data obtained principally from work carried out at the Noise Test Facility at DRA Pyestock on model scale jets. For modelling purposes, the noise from coaxial jets has been divided into three components, each of which behaves as though it were emitted by part of a single isolated jet. The characteristics of these single equivalent jets have been identified from mean flow and turbulence features observed within different regions of the coaxial flow, and subsequent calculation of the noise from each region has been achieved using an empirical single jet prediction method.

A noise prediction model for coaxial jets has been developed on the basis of a limited database of noise from static, isothermal, fixed area jets, which has subsequently been successfully applied to jets of widely different conditions of temperature and area ratio, both statically and in simulated flight.

Noise measurements from cold and hot coaxial jets at an area ratio of four have been predicted with success despite a lack of any information about the turbulence or velocity profiles at such a geometry, by means of a minor alteration to the aerodynamic behaviour of one of the contributing single jets.

In respect of the noise from coaxial model jets in simulated flight, it has been shown that correcting each equivalent jet to flight conditions leads to satisfactory prediction for different temperature and area ratio jets, suggesting that those aspects of coaxial jets which change in the flight situation are being suitably modelled.

Contents

For my parents, Jo and Pen

When it was first said that the sun stood still and the earth turned round, the common sense of mankind declared the doctrine false; but the old saying of *Vox populi, vox Dei,* as every philosopher knows, cannot be trusted in science.

Charles Darwin

...Georges, then Doug, disappeared up the slope above, pulling the mad tangle of ropes, trying to claw their way to the notch. They made it on their third attempt, and my rope went tight. A dark shape hurtled past. "God, no, somebody's fallen." It was George's sack. I struggled after them, pulled by the ropes, hauling myself through the notch with my ice axe. It was like trying to crawl into a jet engine at full throttle.

Peter Boardman

...the words "DON'T PANIC" in large, friendly letters...

Douglas Adams

Acknowledgements

I would like to express my deepest thanks to Dr. C. L. Morfey for initiating this study and for his hours of patient tutelage, and also to Dr. M. J. Fisher for so enthusiastically adopting the role of replacement supervisor. I am entirely indebted to him for his unstinting support and humour, the time he spent discussing problems during which he constantly broadened my understanding of aeroacoustics, and for a couple of great trips abroad.

The work would not have been possible without the financial support of the Defence Research Agency at Pyestock, to whom I am also indebted for the supply of a detailed coaxial jet noise database culled from extensive and rigorous experiment.

I am very grateful to Mr. W. D. Bryce for his help, friendship and support during my visits to Pyestock, and also to Mr. R. Pinker and the rest of the staff at the Noise Section, DRA Pyestock, for continual encouragement and precise technical support.

My sincere thanks go out to Prof. J. K. Hammond who convinced me to persevere during a crisis of confidence, by taking me drinking on 2nd Street, Long Beach in California. I would also like to recognise the efforts of Dr. A. C. R. Tavner and Ms. A. (Dr. Pending) Keary of the Mechanical Engineering Department for helping me to maintain an interest in other things.

My working environment has been most pleasant thanks to the friendship and support of all my colleagues in 15 University Crescent, and I would also like to thank Ms. S. Hellon for always having a ready smile, even on rainy days.

I extend my gratitude to the Aeronautical Engineering Department at Loughborough University, for giving me a sense of reality, before which I thought things always went according to plan.

Finally, I would like to thank Dr. Kate, for finding and showing me my sense of purpose, convincing me to move to Southampton, providing unlimited love and support, and now for moving away from Southampton again.

Nomenclature

A	Jet cross sectional area	m^2
D	Jet diameter	m
T	Jet temperature	K
u'	Turbulence velocity	m/s
V	Jet centreline velocity	m/s
α	Turbulence intensity u'/V_j	%
β	Area ratio A_s/A_p	
λ	Velocity ratio V_s/V_p	
δ	Density ratio ρ_s/ρ_p	
τ	Temperature ratio Tj/T_o	

Subscripts

e	Effective jet
m	Mixed jet
p	Primary jet
s	Secondary jet
o	Ambient condition

Declaration

The author has developed a unique aerodynamic and acoustic model of coaxial jet exhaust flow which comprises sections of three separate, single jet flows, each defined by certain aspects of the coaxial jet. Of the three components, two are similar to those found in previous work, but one is quite new and possesses unique and previously unrecognised turbulence characteristics, which are quantifiably lower in intensity than the levels found in single jets.

The components of the aerodynamic model have been carefully defined in spatial terms by referring to established experimental data, and the single jet spectra have been curtailed using a unique method derived from an analysis of cited source location data.

The influence of turbulence intensity on far field sound intensity has been derived for both quadrupole and dipole sources and hence the noise spectrum from the third, unique jet component may be adjusted to correctly represent the noise from either a cold or a hot jet with reduced turbulence levels.

The model was developed from a limited database of stationary, isothermal model jet noise at a single area ratio of two. It has subsequently predicted the subtle spectral changes due to a heated primary flow and, by applying a standard flight correction scheme, the spectra of both hot and cold model jets in simulated flight have been successfully predicted.

Finally, noise data from model jets at an area ratio of four, for which there is no turbulence data, have been closely predicted by making a reasonable and clearly argued assumption about the nature of one of the model components.

Synopsis

Since the introduction into service of the De Havilland Comet in 1952, the noise of jet engines has been recognised as a problem. The dramatic increase in perceived noise levels for communities close to airports due to the sudden introduction of turbojet engined aircraft led to immediate public outrage, and in the United States of America a number of court cases were brought against the airlines and airports. By the early seventies, due largely to the Boeing 707 with Pratt and Whitney JT3 and JT4 engines, the particularly busy airports of Heathrow and Idlewild (now JFK) had started imposing enforceable local noise limits, but the Federal Aviation Authority in America had already decided on a national certification scheme for American built aircraft which was introduced in 1971, and in Europe the International Civil Aviation Organisation followed suit with a standard set by their Committee on Aircraft Noise. Despite initial differences, the two standards are now almost identical, as described by Smith [1]. They set a maximum level of sound of 108 EPNdB measured at three fixed positions relative to the runway and flight path, namely an approach reference with the aircraft descending at an angle of 3° at an altitude of 120m, a sideline measurement 450m and 90° from the runway, and a point 6.5 miles beyond the start of takeoff as the aircraft climbs away. Subsequently, different acceptable noise levels were introduced for different engine configurations due to the safe takeoff requirements of two, three and four engined aircraft.

Despite the controls imposed by the FAA and ICAO, environmental noise restrictions imposed locally by domestic airports on the airlines which use them are more strict now than ever before. John Wayne airport in Orange County, California for example is so strict that a wide range of older aircraft with noisy engines simply cannot land, while others are limited to an operational window of no more than half an hour in the middle of the day, an expensive time to operate.

As a result of the limitations outlined above, there are huge commercial and financial benefits for engine manufacturers who can design quiet power units and sell them to the airlines who want to operate out of modern airports. The ability to accurately predict a significant part of the jet engine noise, namely that due to the exhaust mixing, would

greatly assist the design stage of engine development as well as helping to understand and modify the noise characteristics of current engine designs.

This thesis describes the development and testing of a model for the prediction of coaxial jet noise, based on data collected during an extended project of experimental testing in the anechoic test facility at DRA Pyestock on model scale coplanar jet nozzles. Initial analysis of the data by Pyestock staff indicated that the far field noise could be divided into three parts, each of which behaved differently to changes in the coaxial jet conditions. In particular, one part of the total mixing noise appeared to act as if it were emanating from a single jet at the core or primary velocity.

Previous studies of the structure and sound source locations in the coaxial exhaust flow have suggested that highly turbulent noise producing regions can be identified in the secondary to ambient shear layer, the primary to secondary shear layer and the downstream, fully mixed region. However, the experimental work at Pyestock was expressly designed to isolate any noise from the complex mixing region proposed to be downstream of the coincidence of the two shear layers. It was found that excess noise from such a region was in fact significant, and that it exhibited a dependence on primary jet velocity. The aim of this thesis was to find some physical justification for the different sound producing regions, in order to establish a workable prediction scheme based on the characteristics of the coaxial jet.

Working initially with isothermal jets at a secondary to primary area ratio of two, three sound producing regions were modelled, important evidence for which was found in the rigorous turbulence measurement work of Ko and Kwan [2], which identified three characteristic flow zones within the coaxial exhaust. One of the zones corresponded approximately to the complex mixing region as proposed by Pyestock, and it was evident from [2] that the region is unusual in its turbulence behaviour. This insight enabled the model to be refined, and very satisfactory predictions have subsequently been obtained for the far field noise at a range of jet velocity ratios.

Extending the model to predict the noise from hot jets by estimating the relative strengths of dipole and quadrupole sources it has been possible to predict the noise from a high temperature complex mixing region, leading to further predictive success.

Measured spectra from model jets with nozzles at an area ratio of four were initially predicted with equivalent jet conditions derived

from the model based on the smaller area ratio. This led to some significant predictive errors, due to an overestimate of the noise from the complex mixing zone. To correct these errors, it has been assumed that the velocity dependence of the complex mixing zone changes as the area ratio increases. With an optimum reduction in the equivalent jet which models the complex mixing region, satisfactory predictions have been obtained for isothermal jets and heated jets at a range of angles for the available velocity ratios, although small systematic discrepancies indicate that the model is being pushed close to its limits.

Finally, the model predictions have been incorporated into a static to flight noise prediction scheme in order to estimate the noise measured from model jets in a simulated flight situation, with some success.

Chapter 1

A General Review of Jet Mixing Noise.

1.1 Introduction

In this chapter, some aspects of jet mixing noise are discussed in terms of their relevance to noise prediction. An outline of the work leading to an understanding of the noise generated by turbulence is followed by a brief discussion of the effects of density fluctuations on turbulent noise production, which are of practical relevance in the case of hot jet engines. The merits of various approaches to single jet noise prediction are appraised, and complications introduced by coaxial jet configurations are then outlined; these include changes in velocity profiles and the size and strength of shear layers in the flow, all of which have been reported extensively and are reviewed only briefly here.

1.2 Single Jet Mixing Noise

The foundations of fundamental jet noise research were laid by Lighthill in the early fifties when he presented his works [3] and [4] on the aerodynamic generation of sound. He proposed that a distribution of acoustic sources located in a stationary ambient medium would produce precisely the same sound field as the highly non-linear turbulent motion generating the true sound field, as long as the strengths of the sources were precisely defined by the turbulence structure of the real flow. The sound field was identified as being equivalent to that from a distribution of moving quadrupoles, their source strength density being equal to a turbulence stress tensor $\overset{\leftrightarrow}{T}_{ij} = \rho v_i v_j + \left(p - c_o{}^2 \rho\right)\delta_{ij} + \sigma_{ij}$. The quadrupole nature of the proposed sources implied that the generation of aerodynamic noise is a very inefficient process. By approximating the stress tensor to just the fluctuating Reynolds stress $\rho v_i v_j$ (or the mean momentum flux tensor), dimensional analysis showed that the sound intensity from a

quadrupole distribution leads to the now familiar V_j^8 law for low speed isothermal jet mixing noise.

Although modifications to Lighthill's approach were put forward in 1960 by Phillips [5] and subsequently by Ribner in 1969 [6] to include the effect of refraction of the sound by the mean flow, the only significant change to be widely accepted involved applying the theory to noise radiation from the more appropriate moving sources in a jet by Ffowcs Williams [7] in 1963. The continued success of Lighthill in predicting the overall sound pressure levels of jet noise meant that the simple V^8 law went unchallenged for several more years.

Carefully conducted experimental work involving analysis in proportional frequency bands led Lush [8] in 1971 to report on systematic discrepancies observed in the variation of measured spectra with angle when compared with that predicted by the Lighthill theory. These were attributed to significantly lower levels of convective amplification than that predicted by theory. The observations of Lush were subsequently confirmed by the independent measurements of Tanna [9] who, by use of convergent-divergent nozzles, was able to obtain data for much higher jet velocities while maintaining an isothermal static jet temperature.

The principal problem with the Lighthill equation is that although the theory is exact, the source term contains all the true flow effects and source mechanisms, which are impossible to define precisely. This fact, combined with the observations of Lush and Tanna, led Lilley *et al.* [10] and [11] to develop an alternative formulation which more clearly separated the source terms from the flow effects; an approach now commonly known as flow-acoustic interaction.

By reformulating the Lighthill equation in terms of a convected wave equation, Lilley extracted other terms attributable to the effects of mean flow to obtain both a more reasonable 'real' source term and an expression which can be interpreted as the inhomogeneous wave equation driven by the turbulent velocity field, incorporating both shear and convection.

Application of the Lilley equation to measured data was carried out by Mani [12] in 1976. Using a simple plug model of a round jet for the flow field, it was shown that good agreement could be achieved if it was assumed that the sources did not communicate directly with the ambient surroundings but interact with the mean flow instead, essentially the process of refraction.

During the early seventies, a considerable quantity of high quality noise data became available through work carried out at Lockheed [17], Southampton [19] and Pyestock [15]. In collaboration with these studies, Tester & Morfey [20] developed a jet noise model based on a shear flow analogy governed by the Lilley equation, which took account of the interaction between the mean flow and the radiation of turbulence generated noise. This model incorporated the Mach number effects of turbulence non-compactness and source convection which they identified as the main causes of deviation from Lighthill by isothermal jets; flow-acoustic interaction, responsible for refraction of sound away from the region close to the downstream jet axis; and geometric acoustics in the shear layer to account for the reduction in intensity for higher speed hot jets. It appeared that for subsonic isothermal jets, the problems were nearly over.

1.2.1 Mixing Noise in Hot Jets.

In the treatment of flows containing variations of density, due for example to the presence of hot volumes of gas, Lighthill [4] argued that the fluctuation in momentum flux is such a dominant source of noise that variations in the other terms of the stress tensor, involving the local velocity of sound, will always be insignificant. The overriding effect of high temperature would therefore be to reduce the density in the Reynolds stress term, resulting in a universal reduction in the mixing noise. However, work by Hoch *et al.* [15], first presented in 1972, showed that this theory is only true at sufficiently high jet velocities, below which the hot jet is actually noisier than the cold. Subsequent work by Lush *et al.* [16] and also Tanna *et al.* [17] indicated the presence of an additional source of noise in the heated jet, based on the argument that in a source region with a sound speed different from the ambient sound speed, the second part of the Lighthill source term can no longer be ignored.

In trying to identify the nature of this second source, Lush opted for an uncorrelated fluctuating entropy term which, if assumed to be only a function of temperature, provided an acoustic intensity that scaled as V_j^4. From a more extensive series of tests including higher jet velocities, Tanna *et al.* adopted a fourth power of velocity for their new source, but could only repredict their experimental results by making the unprecedented assumption that the two sources must be statistically correlated.

At the same time as the experimental works described above, Morfey [18] carried out a rational and detailed study of the possible extra source term, prompted by the results of Hoch *et al*, in the limit as the sound speed tends to infinity. By rewriting Lighthill's wave equation in terms of pressure rather than density, and by relating the pressure and density at a point by the general energy equation, Morfey revealed that in flows of non-uniform density, a dipole order term is the most efficient source. In hot jet flows, there are therefore two dominant sound sources in the turbulent shear layer, equivalent to a fluctuating force field with components $\frac{(\rho-\rho_o)}{\rho}\frac{\partial p}{\partial x_i}$ as well as a fluctuating stress field with components $\rho_o v_i v_j$. The latter is the familiar fluctuating Reynolds stress term, but based on the ambient density ρ_o and thus independent of jet temperature, while the former is a dipole term. At low jet Mach numbers, it is appropriate to assume that these equivalent sources radiate out into the ambient medium, and scaling laws based on the ambient density and speed of sound indicate that additional noise above the V_j^8 line would therefore vary as $V_j^6(\Delta T/T_s)^2$ rather than a fourth power term.

Morfey also explained the decrease in noise at high jet speed, by arguing that the wavelength of the generated noise ceases to be large compared to the shear layer thickness at high jet speed, and therefore that the sound radiates into the local medium, with local conditions a_s and ρ_s. The principal result of basing the acoustic analogy on these local values is to reduce the radiated sound intensity at high Mach numbers. A further extension of this work by Morfey *et al.* [21] developed scaling laws for both dipole and quadrupole components of turbulent mixing noise, and used the numerical results of the previous work to justify the use of a high frequency geometric acoustics (GA) approximation.

By combining flow acoustic interaction with the theory of geometric acoustics and a better understanding of the effects of density fluctuations, Morfey and Szewczyk [22] developed a scheme which arguably was the first to fully rationalise the scaling of single jet noise data. Their scaling laws gave consistently good predictions for all conditions outside the 'cone of silence', the conical volume of space found at angles close to the downstream jet axis bounded by sound rays emitted parallel to the jet axis and subsequently refracted by the velocity profile. For sources within the cone of silence, it was proposed that the sound decayed away

exponentially until some transition point determined from the mean flow characteristics, after which it radiated normally. Satisfactory predictions were achieved for subsonic jets at angles inside the cone of silence, but the theory broke down as the eddy convection speed exceeded the ambient speed of sound. It seems probable that the reason is associated with eddy Mach wave radiation, for example in the form of Kelvin-Helmholtz instability waves as recently suggested by Seiner *et al.* [64].

Because of difficulties explained above, the prediction of single stream jet noise still relies heavily on empirical methods using systematic interpolation within a multi-dimensional database. The number of influential variables is limited and their effects are reasonably well understood, making interpolation the most reliable and cost effective method for single stream jets. The introduction of bypass flow complicates the issue significantly. Adding all the absolute variables of the outer flow, principally temperature, velocity and area, as well as the ratios of these parameters and factors such as nozzle geometry means that the construction of a useful database for coaxial jets is not straightforward.

1.3 The Coaxial Complication.

Since the early sixties, with the notable exception of Concord, commercial interest in single jets was waning in favour of coaxial or bypass jets. These were becoming dominant in the passenger transport market due to their greater fuel efficiency and significantly reduced generation of jet noise. To explain basically the reason behind the latter point, we can scale quadrupole jet noise as U^8D^2 whereas the thrust scales as U^2D^2, so the noise intensity per unit thrust is proportional to U^6 [23]. Any increase in overall size of the jet, which for the same thrust must be accompanied by a velocity reduction, will therefore drastically diminish the noise output of the jet. It has always been understood that the aerodynamic processes leading to the generation of noise in coaxial jet flows are the same as those responsible for single jet noise, but the physical structure of coaxial exhaust flow is much more complicated than single jet exhaust flow and there are many more variables.

Experimental work on the mean velocity profiles of coaxial jets had been reported as early as 1950 by Forstall and Shapiro [24], but it was the investigation into the physical structure of coaxial jets by Greatrex [25] in 1960 which led to the identification of three separate and distinct possible

noise producing regions. These comprised the shear layer between the inner and outer flows, the shear layer between the outer bypass flow and the stationary ambient medium and finally the portion of the inner core that extends downstream of the former shear layer which Greatrex assumed to be mixing with ambient air again. Subsequent studies by Chigier and Beer [26] and Williams *et al.* [27] for example observed characteristics such as extension of the inner potential core length, and similarity in the mean velocity profiles at positions downstream of the end of the potential core.

In an extensive series of tests carried out in 1971 at the Wyle labs, Eldred [28] scaled the results from three hundred different model coaxial jets in order to determine the reduction in overall sound power and peak sideline perceived noise levels as a function of velocity ratio and area ratio. The study made use of coaxial jets with primary jet Mach numbers between 0.85 and 1.47, primary to secondary jet velocity ratios between zero and one, area ratios of 1, 2, 5 and 10 and a wide range of primary jet temperatures. The findings of this extensive work include the observation that for coaxial jets of fixed thrust and area ratio, the greatest reduction is achieved at a velocity ratio of $\lambda = 0.5$. A simple model based on the three noise producing regions of Greatrex was developed for the coplanar nozzles, in which a significant factor was the scaling of the acoustic power from the inner shear layer as the product of four powers of fluctuating local turbulent velocity u' and four powers of jet Mach number, as originally suggested by Pau and Lowson [29]. The assumption that u' is proportional to the relative velocity led to a scaling law for the inner shear layer given by $W_{ps} \propto r_p^2 \left(V_p - V_s\right)^4 V_p^4 \Delta L$, where ΔL accounts for the stretching of the primary core due to the secondary flow.

Similarly extensive work was conducted by Olsen and Friedman [30] for a wide range of geometric and flow parameters, from which it was concluded that the spectral shape at a given angle did not change significantly with area ratio or velocity ratio. This allowed a spectral template for every angle to be provided which could subsequently be positioned according to the peak noise level and frequency, determined empirically. A further experimental study of coaxial jet noise was carried out by the N.G.T.E. at Pyestock in 1976, reported by Cocking [31] and outlining a semi-empirical prediction method based on the influence of the

secondary flow which is characterised by the velocity ratio λ, the area ratio β and the angle of observation θ.

At about the same time as the study by Olsen and Friedman, the introduction of hot wire anemometry allowed direct experimental measurement of the turbulence intensity and velocity profiles in coaxial jet flow, notably in North Carolina by Hammersley and Jones [32], followed by Ko and Kwan [2] in Hong Kong. Both of these studies observed the turbulence development from the nozzle plane to positions at least eight primary diameters downstream, and reported characteristic differences from the growth of turbulence in single jets. In particular, the work of Ko and Kwan reported similarity of velocity profiles in the mixing regions of the jet over the first three or four diameters downstream as well as the region found beyond six diameters downstream, leading them to divide the flow up into three axially distinct zones, with the 'intermediate' zone, found between three and six primary diameters, exhibiting no similarity.

By the mid-seventies, the flow-acoustic interaction work of Mani, Lush, Morfey etc. was being applied to the coaxial jet problem. In a rigorous study by Gliebe and Balsa [33], the parallel shear flow model of Mani [12] was used to simulate the propagation to the far field of a source spectrum, obtained from a slice-of-jet analysis wherein the single frequency band contributions were predicted from the mean velocity, temperature and axial turbulence distributions at the different axial positions. The prediction scheme based on this method achieved some success in matching the overall level measurements of Olsen [30], and the spectral predictions of cold jets at 90° exhibited many of the observed characteristics of the data. However, away from 90°, and particularly at high frequencies and low angles of observation, the data were not predicted with any success. It is the opinion of Tanna and Morris [34] that such a method of solution, for a wide range of operating conditions, would be extremely time consuming, considering the value of the information thus obtained.

In the aero-industry there was by this time a real need for some kind of noise prediction method to aid the design and development of the growing new generation of coaxial jet engines. With this in mind, Stone *et al.* of NASA [35] developed an empirical procedure, based on the use of the correlated results of Olsen and Friedman to adjust a master spectrum derived from NASA's single jet prediction scheme. Useful predictions of overall sound pressure level for a wide range of conventional velocity

profile jets were obtained. More recently in 1986, Lu [36] constructed a model based on the three coaxial jet noise producing regions of Greatrex placed inside an ambient flow, with the empirical parameters for spectral shapes and levels being provided by correlation of model jet noise and source location data for both static and simulated flight situations. The advantage of such a method is that the jet in flight is now the general case, and the stationary jet is simply the limiting case at zero ambient velocity. The model also incorporated acoustic and geometric near field effects which serve to increase and decrease the SPL respectively, and an adjustment to account for acoustic excitation.

Also in the late seventies, some interest was being directed toward jets with inverted velocity profiles; with a higher secondary flow velocity than the primary flow velocity. Models of such jets had shown significant reductions in broad band peak noise, suggested by Tanna [37] to be due to the source convection and axial turbulence levels being significantly lower than for the fully mixed jet. Conversely, the perceived noise levels, in PNdB, either did not change or increased, due to the weighting that the PNdB scale gives to the higher frequencies. Such results prompted a resurgence of interest in the physical processes of coaxial jet mixing, seen for example in the works of Kuznetsov and Munin in 1978 [38] and Tanna and Morris [34] in 1983, both of which were carried out with the express intention of studying inverted as well as conventional velocity profile jets. The former work investigated the now familiar three region coaxial jet in terms of acoustic power, with an annular jet, modelled by part of the flat or plane jet of Abramovich [39], as the limiting case of the full coaxial condition. By attributing the coaxial jet with the measured directivity patterns of an equivalent single jet, overall noise characteristics relative to the single jet were reproduced with some success.

In the work of Tanna and Morris mentioned above, a predictive model for coaxial jet mixing noise has been developed based on the acoustic contributions from parts of three single equivalent jets, which model the three source regions proposed by Greatrex. By careful analysis of a host of previous experimental observation work, the outer and inner mixing layers and the merged jet flow were each modelled as separate jets with characteristics imposed by the coaxial jet conditions. For example, the potential core of the single equivalent jet or SEJ, which models the merged zone, is assumed to occupy the same axial position as the true primary potential core, thus dictating that the exit plane for the SEJ is not the same

as the coaxial jet exit plane. Having defined the flow properties of the three single jets, the noise radiation and directivity were calculated using the principles of the geometric acoustics model proposed by Morfey *et al.* [21]. Predictions at 90° at a range of velocity ratios were achieved with notable success, but a problem arose at small angles which they attributed to the application of geometric acoustics to coaxial jet flows within the GA 'cone of silence'. In Morfey's model, the radiation level within the cone of silence is determined by allowing exponential decay of the sound until a transition point is reached, after which acoustic radiation can commence. The location of this transition point for single jets depends on the mean velocity and temperature profiles, but for the more complicated profiles found in coaxial jets, it appears to be less easily pinpointed.

Also in 1983 at Rolls Royce, a technique was being developed, based on an idea introduced by Fisher *et al.* [40], to allow direct measurement of the strengths of noise sources within jet flows. The 'Polar Correlation Technique' makes use of a Fourier transform relation between the cross power spectral densities from a radial array of far field microphones and the source strength of an assumed line source distribution, to determine at each frequency the location and relative strengths of the real axially distributed sound sources. Previous work with directional reflector microphones by Laufer *et al.* [14] and elliptic mirrors by Lu [36] obtained some useful results but a significant advantage of the method of Fisher, applied in detail to a range of models and engines by Strange *et al.* [41], is in improved resolution of the position and the magnitude of the sources. It has been concluded by Strange that the noise from coaxial jets at normal operating conditions seems to be generated by two spatially distinct but distributed source regions, and that the strength of these sources seems to depend upon the secondary jet velocity in the case of the upstream source region and the primary jet velocity in the downstream case.

Coming more up to date, a study carried out by Lee in 1984 [42] is devoted to analysing the large scale structures seen in the turbulence of low Reynolds number jets and inferring their existence in flows at high Reynolds number from similarities in the near field pressure and velocity perturbations. It is apparent that the influence of these structures on the noise production of the jet is not significant, and despite a number of subsequent works concentrating on large scale structures, their presence has not altered or significantly contributed to the fund of jet noise knowledge to date.

A study initiated at Pyestock by the Defence Research Agency in 1988 [43] involved a novel approach to the measurement of model scale coaxial jet noise, in that the datum for the primary to secondary velocity ratio was one. In other words, the secondary jet velocity remained constant while the primary jet velocity was increased and decreased from the same initial value. The aim of this stratagem was to try to isolate the noise produced by the complicated mixing seen to be occurring downstream of the end of the secondary potential core but before the end of the primary potential core, and some initial results, presented in 1991 [44] were very encouraging. Since the present work relies heavily on the results of the DRA project, more detailed discussion is given in the main body of this thesis.

Finally in this section it is worth mentioning the work presented in Aachen in 1992 by Michel and Böttcher [45], which describes the development of a prediction scheme for the noise from combat aircraft during high speed flyover. The method combines the empirical SAE noise prediction scheme for stationary jets [46] with a theoretically derived jet stretching factor and, more importantly, the ratio of quadrupole to dipole source strengths, to obtain significant improvement over the SAE method in flyover conditions, although the absolute quality of prediction in both the forward and rear arcs falls short of that at 90°.

1.4 Aims.

While the noise generated by the turbulent mixing of jet flows issuing from single nozzles is now relatively well understood, it is evident that no similar understanding exists in the case of coaxial jets. There is little doubt that the processes causing the noise in single stream jets are the same as those in coaxial jets, but the relative complexity of the flow field in the latter case makes for a far more difficult problem. Previous attempts to develop coaxial jet mixing noise prediction schemes have either relied heavily on empirical correlations of the coaxial jet characteristics, in which case they may not be extrapolated beyond the limits of the original database and rarely provide any useful information about the nature or effect of the large number of variables in such a flow field, or alternatively a rigorous theoretical approach with sources derived from estimates of the turbulent flow patterns has met with the problem of applying geometric acoustics, derived from analysis of single jets, to a coaxial jet flow.

The objective of the work reported in this thesis was to develop a better understanding of the physical and acoustic natures of coaxial jets, with the aim of producing a basic noise model reflecting the known aerodynamic characteristics of generalised coaxial flows to improve prediction techniques for coaxial jet mixing noise. Inspiration came from the detailed and systematic coaxial jet measurements from Pyestock, which suggested that the noise from simple coaxial jet nozzles could be constructed from a sum of contributions from single jets whose characteristics mirrored certain reliable parameters within the coaxial flow.

Chapter 2

Experimental details

The data which forms the basis of the prediction model developed in this thesis was taken as part of an extensive programme of study of the noise from scale model coaxial jets at DRA Pyestock. Their experimental method was prompted by the desire to isolate and better understand the noise producing process or processes within the coaxial flow.

Greatrex [25] identified three principal sources of sound in the flow field of coaxial jets, which are shown in figure (1) and consist of the secondary to ambient shear layer and the primary to secondary shear layer, which are primarily upstream, high frequency sources, and the region where the jet flows are fully mixed, further downstream. In the initial development of the test scheme at Pyestock, Flitcroft and Bryce [43] considered the existence of a fourth source region which they called the primary to secondary interaction region, shown in figure (2), which begins at the coincidence of the inner and outer shear layers and extends downstream as far as the end of the primary potential core. It was decided to operate coaxial jets at various velocity ratios by changing the primary jet velocity relative to a fixed secondary jet velocity. If the secondary jet velocity is fixed, and the primary jet velocity is slowly increased from the same value, various assumptions may be made about the four noise producing regions. The first of the sources as identified by Greatrex will remain constant, since the outer shear layer is unaffected by the inner flow until far downstream. The inner shear layer will certainly be negligible for a velocity ratio of unity, and will increase in strength only slowly as the primary velocity rises, due to the growth of the velocity difference causing the shear. The third of Greatrex's noise sources, the fully mixed region, will vary in strength with velocity ratio but only significantly in the low frequencies. Finally, an advantage of this method is that as the velocity ratio gets less, so any increase in noise is due entirely to the presence of the faster primary flow, and may be attributed in part to the fourth source as suggested by Flitcroft and Bryce. Another advantage lies in the fact that the datum velocity condition, at a velocity ratio of one, corresponds to the

full diameter secondary jet alone, and may be used as a reliable reference jet.

All the measurements were taken in the Noise Test Facility at Pyestock, with nozzles designed to have shallow taper angles and short parallel outlets to maintain axial flow at the exit. The nozzle exit planes were chosen to be coplanar, in order to minimise aerodynamic complications due to pressure differences in the two streams. The noise was measured with half-inch diameter microphones positioned in the far field at a nominal distance of twelve metres, in 10° intervals between 30° and 120° to the downstream jet axis.

The test programme was carried out in two stages. In the first series of noise tests outlined in table [1], a single coaxial jet geometry was operated at three secondary jet velocities and numerous primary jet velocities, keeping both flows as close to ambient temperature as practical. The primary jet nozzle was 33.2mm in diameter and the secondary nozzle was 58.2mm in diameter, providing an area ratio of 1.98. Measurements were also taken at the intermediate secondary velocity with the coaxial jet within a large diameter co-flowing stream to simulate flight conditions. The flight stream nozzle diameter was 0.54m, giving a flight stream to jet area ratio of never less than fifty. This has been identified by Way and Cocking [47] as the minimum ratio for successful flight simulation at all frequencies.

The intention behind this first set of isothermal tests was to try to remove any complications due to dipole noise [43]. All the data were corrected to a polar distance of six metres and to lossless atmospheric conditions and in addition the simulated flight data were corrected for shear layer refraction, a Doppler shift and an angle transposition so that the data were presented as if measured in flight [44].

Examples of measured spectra are given in figures (3) a), b) and c). The first illustrates the spectra measured at 90° to a jet with a secondary velocity of 136m/s and primary velocities between 136m/s and 214m/s, the second and third show spectra for a jet with a secondary velocity of 170m/s and primary velocities varying between 136m/s and 302m/s at 40° and 90° respectively. The effect of increasing primary velocity is immediately evident as a rise in noise levels which is most significant at the frequency of the spectral peak, and a decrease in noise levels for the inverted velocity profiles represented by velocity ratios greater than one.

nozzle of 43mm diameter and a secondary nozzle of 58mm diameter provided an area ratio 0.84 while a 33mm primary with a 75mm secondary gave an area ratio of 4.1. For these and the original nozzle configuration, tests were carried out at ambient temperatures and with a heated primary jet at the temperatures 600K and 800K. Jet noise in simulated flight was measured for all geometries and temperatures at only the highest and lowest velocity ratios, namely 1.24 and 0.63, of which the former represents an inverted velocity profile.

Table [1].

V_s/V_p	V_p(m/s)	V_s(m/s)	V_f(m/s)
1.00	136	136	0
0.89	152	136	0
0.80	169	136	0
0.71	192	136	0
0.64	214	136	0
1.24	137	170	0, 55.0
1.13	153	170	0, 55.0
1.00	171	170	0, 55.0
0.89	191	170	0, 55.0
0.79	216	170	0, 55.0
0.71	241	170	0, 55.0
0.63	267	170	0, 55.0
0.56	302	170	0, 55.0
1.42	190	270	0
1.26	214	270	0
1.12	241	270	0
1.00	269	270	0
0.89	302	270	0

Chapter 3

Coaxial Jets

The noise from an operational coaxial turbofan engine is the product of many different sound sources which are found both inside and outside the engine's physical structure. The majority of sources inside the jet engine can be substantially reduced by careful design and with the use of acoustic linings, but a significant proportion of jet noise is generated in the turbulence downstream of the nozzle exit plane. This noise producing region extends from the jet exit nozzle to a distance of at least twenty nozzle diameters downstream and is clearly not amenable to acoustic treatment. If we wish to examine only the mixing noise of a coaxial jet then some of the complications presented by the core noise of a real engine can be removed with the use of model nozzles supplied with high pressure gas from a remote reservoir. However, there are many factors inherent in the operation of a jet engine which effect the aerodynamic and acoustic properties of the exhaust flow, which must be understood if a useful model is to be developed.

The inner, primary jet exhaust of a turbojet engine consists of the products of combustion and is very hot, so it will contain temperature dependent sound sources as well as the quadrupole fluctuating stress sources of Lighthill, [3]. Operational engines are designed with all sorts of radial and axial nozzle configurations, but in order to simplify the analysis, the axial variation of nozzle geometry will be ignored and the present work will consider the effect of temperature and bypass ratio on the exhaust of a coaxial jet, but only for coplanar nozzles.

3.1 The Aerodynamic Structure of Coaxial Jet Flow.

The nature of coaxial jet flow was examined by Greatrex [25] in 1960, who postulated the existence of three discrete noise producing regions within the exhaust plume. These are shown in figure (1) and consist of the following zones: the shear layer which develops between the primary and secondary jet flows and the shear layer between the secondary jet and ambient atmosphere, both of which begin immediately

downstream of the nozzle exit plane, and a third shear layer which emerges from the mixing of the first two, downstream of the end of the secondary jet potential core and referred to as the primary to ambient shear layer. Much subsequent measurement work has identified these and other turbulent regions within the coaxial flow, and with the introduction of methods such as hot wire anemometry, for example in the works of Hammersley and Jones [32] and Ko and Kwan [2], access to useful turbulence velocity information has been achieved which allows the relative importance of these various turbulent regions to be ascertained. Since Ko's and Kwan's measurements play an important part in the development of this thesis, a brief discussion of some of their principal observations will follow.

Three zones have been identified at different axial positions within the initial jet, as shown in figure (4) reproduced from [2], but it cannot be over-stressed that these regions do not correspond to the three noise producing regions proposed by Greatrex. The first of Ko's zones lies immediately downstream of the jet nozzles and is termed the initial merging zone. It includes some of the primary potential core and most of the secondary potential core as well as the initial development of the inner and outer shear layers, and extends approximately to the downstream end of the secondary potential core. The length of the initial merging zone therefore depends on the secondary to primary velocity ratio λ but the termination is in fact defined by the breakdown of similarity in the local mean velocity profiles of the secondary mixing region. This happens typically three primary diameters downstream of the nozzle exits.

The zone which commences beyond the end of the initial merging zone exhibits no similarity in local mean velocities at any radial position, and Ko has likened it to the region of a single jet where mixing occurs due to the disappearance of the core flow. This so-called intermediate zone is found between the downstrean end of the initial zone and about six primary diameters downstream of the nozzles, depending on the velocity ratio. Beyond the intermediate zone, similarity of local mean velocities resumes, but for various velocity ratios and axial positions the similarity relates to a non-dimensional radial distance $\eta_e = (y - D_e/2)/x_e$, as shown in figure (9). This third zone is called the fully merged zone in [2], although this term is used to refer to a different region of the prediction model in the present work. The parameter η_e is based on a diameter D_e, derived from the work of Eldred *et al.*[28] which observes that the coaxial

jet at this stage may be represented by a single jet of the same thrust and the velocity of the primary jet V_p, which together dictate an effective diameter. The effective diameter is given in [28] by $D_e = D_p(1+\lambda^2\beta)^{1/2}$ where λ is the jet velocity ratio and β is the exit nozzle area ratio. The results of Williams, Ali and Anderson [27] also show similarity of mean velocity profiles, but only at a distance greater than six primary diameters downstream.

Ko and Kwan also observed similarity of turbulence-intensity profiles in their initial and fully merged zones, using the same non-dimensional radial parameters that were used for local mean velocity profiles. Slight deviation from absolute similarity was seen in the initial merging zone for different velocity ratios, attributed to inward entrainment of the secondary jet by the faster primary shear layer.

A significant illustration of the radial distribution of turbulence intensity at different axial positions for a jet with a velocity ratio of 0.7 is reproduced here as figure (5). Careful perusal shows that there are turbulent eddies developing at a radial position of $0.7D_i$, within the secondary potential core, which reach 3% of the primary velocity before the shear layers meet. As the flow moves further downstream, the turbulence intensity at this radial position grows, but at an axial displacement of eight primary diameters it is only 10% of V_p. According to Davies *et al.* [48], an isolated single jet has a typical peak turbulence intensity of 15% of the jet exit velocity, which develops within about three diameters of the nozzle. Now the observant reader will notice that at a velocity ratio of 0.7, 10% of the primary velocity is approximately 15% of the relative velocity, but figure (6), kindly supplied by Ko in private correspondence, illustrates equivalent measurements for a jet with a relative velocity of 0.5; The initial peaks in developing turbulence intensity can be seen to be about 7.5% of V_p for both shear layers, which corresponds to 15% of (V_p-V_s) for the inner shear layer and 15% of V_s for the outer, as expected. However as the layers merge in the region between six and eight primary diameters, the turbulence intensity is again 10% of V_p. The scaling of the turbulence intensity in this region on the primary velocity alone, rather than on the relative velocity causing the shear, was unexpected. However, the evidence described above, combined with coaxial jet noise measurements described in section 3.2 below indicate that this is the case. The development of these turbulence intensities differs significantly from that for a single jet, for which a peak value of 15% of V_p

is achieved relatively early in the jet development. If we accept that Ko's fully merged zone is represented by something like the equivalent jet of Eldred, even at the upstream end, then we must take account of the reduced turbulence intensity observed at the corresponding point in the coaxial jet.

It has been shown by Kuznetsov and Munin [38] that at a sufficient distance from the coaxial exit nozzle, velocity profile measurements do indeed coincide with a universal profile characterising a single jet, and Tanna and Morris [34] identify a single equivalent jet which extends downstream from the tip of the primary potential core to model the fully developed section of jet flow. It is interesting to note that Tanna and Morris make some allowance for reduced turbulence levels at the boundary of their equivalent jet.

3.1.1 The Effect of Temperature on the Aerodynamic Structure.

The use of hot wire anemometers in heated jets meets with obvious practical difficulties so in order to study the detailed turbulence within shear layers between flows of different temperatures, it has been necessary to use gases of different densities at ambient conditions to simulate the temperature difference. Mixtures of air and helium have frequently been used to represent hot air, as in the work of Brown and Roshko [49] and Panchapakesan and Lumley [50]. The results of these works indicate that there is very little change in the development of turbulent structure in the mixing of flows of different densities. Brown and Roshko measured the spread of the shear layer from the edge of a flat plate separating two flows with different densities, whose density ratio varied from 0.14 to 7.0, and found that the density had very little influence on the spreading rate. Panchapakesan's and Lumley's much more recent experimental work on vertical, upward flowing, single round jets of air and helium used modern computational techniques to obtain high order correlations of the density and velocity fields at distances from fifty diameters downstream. They observed two differences between air and helium jets, namely that the helium jet had slightly increased axial mean velocity across its whole width, and that its axial turbulence intensity is greater near the axis than it is for an air jet. The first point is attributed to increased momentum in the jet due to the buoyancy of helium in air, but the second, supported by

other investigators, is not easily explained without close scrutiny of the near field development of the jet.

If, as is generally accepted, the characteristics exhibited by a low density jet of helium are equivalent to those of a hot air jet, then the changes in specific flow characteristics outlined above will also occur in hot air jets, and account must be made for them when modelling the noise from hot jets.

3.2 Noise Characteristics of the Coaxial Jet.

Noise source location work carried out by Strange *et al.* [41] on model and full scale coaxial jets supports the view of aerodynamic structure suggested above by identifying two spatially distinct source regions at all velocity ratios less than one. The work utilises a refinement of the Polar Correlation technique first proposed by Fisher *et al.* [51] to enable overlapping individual source images to be resolved from the overall source image. The two source peaks are found at different axial positions and have been attributed by Strange to two of Greatrex's three source regions. They suggest that the higher frequency sound is being emitted by the secondary to ambient shear layer and that the lower frequency sound emerges from the primary to ambient shear layer. Evidence for these proposed sources is found in the scaling of their positions and strengths as velocity and velocity ratio are changed. They further surmise that in all their tests, the primary to secondary shear layer constitutes a source which is much weaker than the secondary to ambient shear layer and that the latter will therefore always dominate the noise generated at axial positions where they coexist.

The distributed noise sources identified by Strange *et al.* within the jet mixing regions, when illustrated on a source strength per unit length basis, have a characteristic shape, and an axial position which is a function of the emitted frequency. The strength per unit length of a distributed source, of any third octave band *i*, may be described by a curve given by

$$S(x,f) \propto x^{m_i-1}\exp\left(\frac{-m_i x}{X_i}\right) \qquad (3.2.1)$$

where x is any axial position, X_i is an estimate of the axial position of the centroid of the source distribution, and m is a frequency dependent shape parameter.

The third, neglected zone proposed by Greatrex will generate some noise, since it contains turbulent eddies and fluctuating shear forces, but it has not been identified explicitly by the polar correlation technique for a number of reasons. Firstly, the method looks primarily at the axial position of sound sources and does not differentiate between radial positions. Secondly, most of the relatively weak inner shear layer is shrouded within the outer shear layer, so any characteristic noise source distribution information will be swamped by the source image of the dominant outer source. This view is in agreement with Greatrex who carried out a simple scaling of the inner shear layer noise with velocity ratio and found that it would suffer a reduction due to reduced shear of up to 21dB at a velocity ratio of 0.5, despite a concomitant increase in core length and the noise producing volume.

The data used for the development of the present predictive model was also the subject of an initial empirical analysis by the Noise Section of DRA Pyestock [44]. By subtracting the noise expected from the secondary jet and the fully mixed jet regions from the full coaxial jet spectrum, a significant level of noise remained, which was attributed to the complex interaction region proposed in [43]. The variation in amplitude of this derived spectrum with velocity ratio was seen to be independent of secondary jet velocity but to increase in proportion to the eighth power of primary velocity, the result expected for a single jet. Frequency changes also showed an approximate scaling to the primary jet velocity and were independent of secondary velocity.

In order to account for the excess noise observed in [44], a further source mechanism must be identified in the acoustic model, since the two significant sound source regions of Greatrex do not contribute noise at sufficient levels, and it is tempting to consider more closely the fourth noise producing region of Flitcroft and Bryce [43]. Now the measurements of Strange *et al.* neither support nor explicitly preclude the existence of such a source region, which corresponds directly to Ko's intermediate zone so clearly demonstrated by turbulence measurements. It is likely that such a region, which is large in volume and characterised by complex turbulent mixing scaled on the primary jet velocity, will generate noise at a significant level relative to the total noise of the coaxial jet, but because of its proximity to the secondary jet source region it could not have been resolved by the work of Strange *et al.*

In conclusion, the noise from coplanar coaxial jets is significantly more complex than that from a single stream jet, but methodical analysis has shown that the noise is emitted by at least two axially distinct source regions. These consist of a low frequency source at downstream locations which is equivalent to the noise from a fully mixed single jet, and a higher frequency region of sound production comprising two characteristically different turbulent volumes, one of which is characterised by the secondary jet conditions and the other by the primary jet velocity. It will be assumed that the latter of these high frequency sources is responsible for significant levels of noise at low velocity ratios, where the combination of the other sources is insufficient to account for the measured far field coaxial jet noise.

Chapter 4

Isothermal Model

In the previous chapter the nature of coaxial jets was examined, in order to identify characteristics of the aerodynamic and acoustic behaviour which may be utilised to model the noise emissions of coaxial jets. The development of the model described in this thesis relies substantially upon the flow and turbulence measurements taken by Ko and Kwan, whose experiments did not include a heated primary jet flow, so the initial model developed in this chapter does not incorporate temperature effects. The effect of heat on the noise emitted by jet flows has been studied in great depth both theoretically and experimentally and the implications for coaxial jet noise prediction will be discussed in chapter 6.

In this chapter, separate source regions are identified by their flow characteristics and each is modelled as a part of an equivalent isolated single jet. The noise characteristics of and emissions from these equivalent single jets are established, from which a prediction of the total noise from the mixing of isothermal coaxial jet exhausts is obtained.

4.1 Aerodynamic Flow Model.

Three separate and independent source regions, each of which contribute noise at levels and frequencies which are dependent upon characteristics of the coaxial jet, are described below.

4.1.1 The Fully Mixed Region.

The characteristic region found furthest from the coaxial jet nozzle is equivalent to the downstream flow of a single isolated jet which provides the same thrust, mass flow and enthalpy as the full coaxial jet, and a diameter which is defined by the other constraints. The single jet chosen to represent the so called 'fully mixed' region has characteristics dictated by the respective conservation equations given below.

$$\rho_m A_m V_m = \rho_p A_p V_p + \rho_s A_s V_s, \qquad (4.1.1)$$

$$\rho_m A_m V_m^2 = \rho_p A_p V_p^2 + \rho_s A_s V_s^2. \tag{4.1.2}$$

$$T_m\left(m_p + m_s\right) = T_p m_p + T_s m_s \tag{4.1.3}$$

where mass $m = \rho A v$.

Combining the equations above we obtain equations for the mixed jet velocity,

$$V_m = V_p \frac{\left(1+\delta\beta\lambda^2\right)}{(1+\delta\beta\lambda)} \tag{4.1.4}$$

and $$\rho_m A_m = \rho_p A_p \frac{(1+\lambda\beta\delta)^2}{\left(1+\lambda^2\beta\delta\right)} \tag{4.1.5}$$

where $\lambda = \frac{V_s}{V_p}$, $\beta = \frac{A_s}{A_p}$ and $\delta = \frac{\rho_s}{\rho_p}$.

However, for the isothermal case, $\rho_s = \rho_p$ so an expression for the diameter of the fully mixed jet emerges, namely

$$D_m = D_p \frac{(1+\lambda\beta)}{\left(1+\lambda^2\beta\right)^{1/2}}. \tag{4.1.6}$$

The way that the mixed jet velocity V_m depends on velocity ratio is illustrated in figure (7) for the area ratios β = 1, 2, 3 and 4. It can be seen that the mixed jet velocity is equal to the primary velocity twice; firstly at zero velocity ratio, that is, when there is no secondary jet flow, and secondly at a velocity ratio of one, when it is also equal to the secondary velocity. Between these values the mixed jet velocity diverges from the primary velocity to a minimum which decreases with increased area ratio. The mixed jet velocity tends towards the secondary jet velocity, also shown on figure (7), as both the velocity ratio and the area ratio increase, until the velocity ratio becomes greater than one when the jet has what is called an inverse velocity profile. The mixed jet velocity can be seen always to lie between the primary and secondary jet velocities, even at velocity ratios greater than one.

The diameter of the mixed jet, shown in figure (8), behaves in a similar manner to its velocity, in that it diverges rapidly from the primary jet diameter and approaches the secondary jet diameter asymptotically. However, unlike the velocity, the mixed jet diameter remains relatively close to that of the secondary jet as the profile of the coaxial jet becomes inverted at $\lambda > 1$. It is reassuring to predict that for isothermal jets, the diameter of the fully mixed jet is never greater than the size of the actual secondary jet.

It is interesting to observe that for velocity ratios covered by the present experimental database, $0.5 < \lambda < 1.24$, the mixed jet diameter is very close to the secondary jet diameter. For example, at an area ratio of two, the mixed jet is only 7.4% smaller than the secondary jet at the lowest velocity ratio, and significantly closer at higher velocity ratios due to its asymptotic behaviour. The difference between the mixed and secondary diameters is even less for larger area ratios.

4.1.2 The Unmerged Primary and Secondary Shear Layers.

i) The shear layer which develops between the primary and secondary jet flows, starting at the primary jet nozzle lip, is assumed to spread radially at a rate dependent on the factor $(1-\lambda)/(1+\lambda)$, in the manner of a shear layer between co-flowing streams, as reported by Brown and Roshko [49] or the shear layer of a single jet in a parallel stream, described by Morris [52]. For velocity ratios greater than a half, this spread rate will be significantly less than that for the secondary or mixed jet flows. The turbulence levels in this shear layer will also be proportional to the velocity difference across the shear, which will never be more than one half of the primary velocity but often much less than this value. For the present model, the inner shear layer is assumed to be negligible in terms of noise production due to its low volume and turbulence. A brief analysis of the possible acoustic output of the inner shear layer is carried out in section 4.2.2, which supports the above omission.

ii) The results of Ko and Kwan show that the velocity and turbulence profiles of their coaxial jet in the region from the nozzles to the tip of the secondary potential core match those of a single jet with the diameter of the secondary nozzle and with the secondary velocity. In particular, this indicates that the shear layer has the dimensions, spread rate and turbulence levels of the single equivalent jet, so its noise output

may be predicted as if it were a single jet. This model of the initial region of coaxial jets is identical to that used by Tanna and Morris [34].

4.1.3 The Interaction Region.

The turbulence measurements of Ko and Kwan clearly indicate that between the two regions exhibiting similarity there exists a zone with a more complicated structure. Figure (9) is reproduced from their paper and shows a non-dimensional plot of mean velocity ratio for axial positions at six, seven and eight primary diameters downstream. The axial positions represented on this diagram correspond to the positions of most rapid growth of turbulence intensity, shown in figure (5) at a radius between the primary and secondary lip lines. These results suggest that in this region, where a large volume of highly turbulent flow exists, the velocity profiles are characteristic of a single jet at the primary velocity V_p and which scale on a diameter similar to that given by

$$D_e = D_p\left(1+\lambda^2\beta\right)^{1/2} \tag{4.1.7}$$

which is the Effective Jet of Eldred *et al.*, [28]. The significance of this jet at isothermal conditions is that it provides the same thrust as the full coaxial jet, although this is not the case for hot jets.

The effective jet diameter is therefore equal to the primary jet diameter at a velocity ratio of zero and the secondary jet diameter at a velocity ratio of one, varying smoothly between these limits. It may be useful at this stage to point out that Ko's intermediate zone only extends from three to about six primary diameters downstream whereas the region being proposed in this thesis continues certainly as far as the end of the primary potential core and is assumed to co-exist with the mixed jet far downstream.

The convincing collapse shown by Ko and Kwan of measured velocity profiles for a wide selection of secondary to primary velocity ratios when scaled on the primary velocity V_p is shown in figure (9). The fact that the secondary jet velocity has no apparent influence on the normalised velocity profiles in this region is somewhat unexpected, but may reflect the fact that the primary potential core is still present up to nine primary diameters downstream. It also encourages the argument that the local turbulence intensity will scale on the primary velocity as described in section 3.1. Such an argument breaks down significantly at

two particular points where the effective diameter D_e is necessarily correct, namely at velocity ratios of zero and one.

4.1.3.1 The Effective Jet at $\lambda = 0$

A velocity ratio of zero corresponds to the case with no secondary flow, so the jet is a single isolated jet which will naturally have the velocity and turbulence intensity profiles of a single jet, and the peak turbulence intensity will be 15% of the velocity. The incorporation of the effective jet into the model for the zero velocity ratio case is clearly improper since the jet may be exactly modelled by either the secondary jet or the fully mixed jet alone. It is safe to assume that the single jet characteristics will immediately break down with the introduction of a secondary flow, but use of the current effective jet at velocity ratios of less than a half is inappropriate.

4.1.3.2 The Effective Jet at $\lambda = 1$

A velocity ratio of one corresponds to the situation where the secondary velocity is the same as the primary velocity, which has been compared to a single jet with the secondary diameter and velocity. If this is the case, then the effective jet is again redundant. It may be argued at this point that the flow characteristics of such a single jet will indeed be very similar to those of a coaxial jet at $\lambda = 1$, but the presence of the inner nozzle, which must have a finite thickness and must also induce boundary layers in both flows prior to their exit, will cause complications in the development of the turbulent flow. It is difficult to estimate the magnitude of these proposed changes without experimental data and no attempt is made here to equate them with the effective jet, but it will be shown below that the influence of the effective jet diminishes dramatically as the velocity ratio increases, due to the increasing dominance of the secondary and fully mixed jets.

In terms of the predictive model, the effective jet is assumed to exist at velocity ratios of both zero and one despite the poor evidence for such an extrapolation, since the zero case is not of interest in coaxial jet studies and the unity ratio case experiences no significant contribution from the effective jet.

4.1.4 Summary.

It is proposed that the flow model comprises three regions with specific characteristics on which the acoustic estimates can be based. The model may be summarised as follows:

a) In the initial exit region of the jet we assume that the noise producing characteristics of the coaxial jet are the same as those of a single jet which has both the velocity and diameter of the secondary or bypass jet;

b) In the intermediate zone, found beyond the end of the secondary potential core, the flow is equivalent to that of a single jet with a velocity equal to the primary jet, V_p, and an effective diameter D_e, but containing significantly reduced turbulence intensity levels which will be shown to diminish the sound output compared to an isolated single jet;

c) In the downstream region where the primary and secondary jets have been shown to be completely mixed together, the flow field is characterised by the mixed jet velocity V_m and mixed jet diameter D_m, which are defined by the conservation of the mass flow and the momentum of the coaxial jet.

4.2 The Acoustic Model.

In this section we develop an acoustic model based on each of the flow regions described above. The developing prediction method uses parts of single equivalent jets to model characteristic sections of the true coaxial flow field, so firstly it is necessary to establish the spatial positions where each region exists, and to identify the corresponding frequencies so that only the appropriate portion of each single jet spectrum is comprised in the total predicted spectrum. Secondly, consideration is given to the attenuation of a spectrum from a source region which ends abruptly in space, and finally we determine the effect on the jet noise of a lower than typical turbulence level as attributed to the effective jet.

4.2.1 Spatial and Frequency Limits of Equivalent Single Jets.

The division of the coaxial jet flow into discrete regions is best illustrated initially by considering the condition of the jet flow at a velocity ratio of one, shown in figure (10). As mentioned above, the flow at unity velocity ratio is very similar to the single secondary jet, whose conditions are met by both the secondary and fully mixed equivalent jets. In fact these two equivalent jets are identical and will provide exactly the same spectra which would match that of the true nozzle but for the presence of the primary jet annulus. The model requires that the mixed jet represents the downstream flow while the secondary jet represents the upstream flow, so in order to maintain a continuous pattern of flow development, it is only necessary to ensure that as one region ceases to exist, the other replaces it. The most obvious position for this transition for the single jet might seem to be at the tip of the potential core, upstream of which there is still a secondary shear layer and unmixed flow. However, for velocity ratios other than one, the outer shear layer is only similar to that of the secondary jet until it intercepts the inner jet flow, as shown by Ko.

Figure (11) illustrates the more general flow condition found at velocity ratios of less than one, from which it can be seen that the shear layers coincide when the sum of their widths w_o and w_1 is equal to the size of the secondary annulus (r_s-r_p), at the point x_s. This position is another candidate for the transition between the secondary and the mixed jets, with the advantage that the secondary jet will only be modelled over the region where the true secondary shear layer exists at the reduced velocity ratios. A notable disadvantage is that the mixed jet is now required to model the noise from the flow downstream of point x_s, which includes the end of the primary potential core at V_p. However, the mixed jet is not the only source in this region, since the effective jet begins to make a significant contribution, as discussed below.

In order to locate the position of the point x_s it is necessary to consider the growth rates of the two converging shear layers. The outer shear layer is developing between a moving stream and a static medium, and as such will have a typical spread rate $\eta_o = w_1/x_s = 0.1$, but the inner is developing between two flows at different velocities. According to Brown and Roshko [49] in confirmation of Abramovich [39], the growth rate of such a shear layer is given by the velocity dependent function

$$\frac{\eta}{\eta_0} = \frac{V_1 - V_2}{V_1 + V_2} = \frac{1-\lambda}{1+\lambda}, \qquad (4.2.1)$$

where the new rate η is a function of the rate at $\lambda = 0$ which is η_o. We have said that at the coincidence of the shear layers, $W_1+W_2 = r_s-r_p$, which can now be written

$$r_s - r_p = 0.1x_s + 0.1\left(\frac{1-\lambda}{1+\lambda}\right)x_s = 0.1\left[\frac{1-\lambda}{1+\lambda}+1\right]x_s = \frac{0.2x_s}{1+\lambda} \qquad (4.2.2)$$

so $$x_s = 5(r_s-r_p)(1+\lambda) \qquad (4.2.3)$$

and since $w_1 = 0.1x_s$ we also find that $w_1 = 0.5(r_s-r_p)(1+\lambda)$.

Having established a reasonable position for the proposed transition from the secondary jet region to the fully mixed jet region it is now necessary to determine a measure of the frequency of the noise being generated at this point, so that the spectral contributions of the two models may be cut off appropriately.

We now compare the whole secondary jet with the portion which lies in the upstream zone, and assume that the secondary shear layer develops with a linear dependence on Strouhal number. It may be argued that the frequency of the noise generated at the end of the primary potential core, at the position x_j, is characterised by a Strouhal number of about one, and at the nozzle, for the sake of argument, by an infinite Strouhal number. In other words, the Strouhal number at the position x_s is given by the expression

$$S_{sec} = \frac{x_j}{x_s}. \qquad (4.2.4)$$

The end of the potential core of a single jet at the secondary diameter is found at about $5D_s$ so from equation (4.2.3) we have

$$S_{sec} = \frac{D_s}{(r_s - r_p)(1+\lambda)} = \frac{fD_s}{V_s}. \qquad (4.2.5)$$

The resultant variation of cut off frequency for the secondary jet with velocity ratio is shown in figure (12) for three area ratios. It can be seen that the frequency of cut off does not vary greatly with velocity ratio, particularly over the range $0.5 < \lambda < 1.0$ which is of practical interest, but the effect of changing the dimensions and hence the area ratio is very

marked. This is because the length of the undisturbed secondary flow is directly proportional to the width of the secondary flow annulus r_s-r_p. For example, the effect of increasing the area ratio is to widen the secondary jet annulus, this extends the secondary jet region downstream with a consequent reduction in the cut off frequency. The secondary jet therefore contributes noise over an increasing proportion of the developing coaxial jet as the area ratio is enlarged, and vice versa.

The spatial definition of the effective jet is more difficult to determine and justify. The evidence of Ko and Kwan indicates that the velocity or turbulence profiles of the secondary jet are unaffected within three primary diameters of the nozzle, but beyond this position there is an influence disturbing the further development of the shear layer. It seems reasonable to attribute this disturbance to the complex mixing zone modelled by the effective jet, which starts to have a significant effect on the flow characteristics from between three and four primary diameters downstream. For a velocity ratio of $\lambda = 0.5$, at which the effective jet is most significant, three primary jet diameters corresponds to two and a half effective jet diameters, or half way to the tip of the potential core of the effective jet. At $\lambda = 1$, this position in the effective jet is equal to $4.3D_p$. The significance of a position half way along the potential core is that the noise produced here is characterised by a Strouhal number of two. The coincidence of the start of Ko's intermediate zone with a characteristic effective jet Strouhal number suggests that the upstream end of the complex mixing region may be suitably modelled by an effective jet with a spectral contribution that is curtailed at a Strouhal number given by

$$S_e = \frac{fD_e}{V_p} = 2. \qquad (4.2.6)$$

Downstream of the start of the effective jet the model incorporates the effective and fully mixed equivalent jets, which produce comparable thrusts. It is well known that at low absolute frequencies, the spectra of equal thrust jets converge and become identical, from which it is apparent that there is a risk of 'double accounting', over predicting the noise generated by the coaxial jet at its downstream limit, unless care is taken in the assessment of the model in this region.

Referring again to the physical characteristics of the coaxial jet, it will be remembered that the potential core of the primary jet extends downstream for as much as ten primary diameters, well into the region

modelled by the mixed jet. There is certainly a need for some contribution from the effective jet in this area to account for the centre line velocity and hence the noise emission being so much higher than for the mixed jet. Beyond the tip of the true primary potential core the mixing on the centre line will still contain eddy velocities of the order of V_p, although it must be assumed that these will diminish at some point to values more typical of the mixed jet.

At the downstream positions where the spectra of two equal thrust jets converge, the effective jet will in fact be producing significantly less noise due to the reduced turbulence intensities it contains, a decrease amounting to approximately 7dB. Also, the work of Powell [53], extended by Ribner [54] suggests that the noise produced by a unit slice of jet in the far downstream region drops off at a rate of 21dB for every doubling of axial distance. In the light of these two considerations it was decided to incorporate all of the low frequency end of the effective jet spectrum in the full knowledge that the greatest error that will occur will be of the order of +0.8dB, due to the incorrect addition of another spectrum 7dB lower than the mixed jet spectrum.

4.2.2 The Method of Spectral Attenuation.

In the spatial model of the jet, the mixed and secondary regions meet at an interface at the point x_s which corresponds to a frequency given by equation (4.2.5). It is assumed that one source region ceases to exist at this interface and is replaced completely by the other. However, this abrupt spatial curtailment does not lead to a similarly immediate truncation of the spectra at the corresponding frequency, as we shall proceed to demonstrate.

The jet noise source location work carried out by Strange *et al.* [41] shows that each third octave frequency band is generated not at one discrete position but over a finite length of the jet, with the high frequencies issuing from compact, upstream distributions while the lower frequencies are emitted from progressively more extended sources further downstream. It is therefore evident that there will be source distributions which overlap the cut off position, and the noise levels from these partial sources will decline as less and less of each third octave source distribution remains in the modelled region. It is therefore necessary to determine the missing fraction of every third octave band source distribution which

overlaps the interface position. It will now be shown that the work of [41] enables us to determine such a fraction on one side of any arbitrary axial position, which can then be associated with the position of the model interface.

Referring to equation (3.2.1) it is straightforward to write an expression for the fraction of energy at a given frequency radiated from positions upstream of a point x_1, as follows:

$$F_u(x_1,f)=\frac{\int_0^{x_1} S(x,f)\partial x}{\int_0^{\infty} S(x,f)\partial x} \qquad (4.2.7)$$

and the fraction radiated from positions downstream of x_1 is given by

$$F_d(x_1,f)=1-F_u(x_1,f). \qquad (4.2.8)$$

Note that x is measured from the nozzle exit plane.

For a specific but typical value of the shape parameter m = 4, the numerator in (4.2.7) may be evaluated by parts, which results in

$$I(x_1)=\frac{-x_1^3}{\alpha}\exp(-\alpha x_1)-\frac{3x_1^2}{\alpha^2}\exp(-\alpha x_1)-\frac{6x_1}{\alpha^3}\exp(-\alpha x_1)-\frac{6}{\alpha^4}\exp(-\alpha x_1)+\frac{6}{\alpha^4}$$

where $\alpha = m/X_i$.

But if $x_1 \to \infty$,

$I(x_1,f)=\frac{6}{\alpha^4}$ which is equivalent to the denominator in (4.2.7). This expression therefore becomes

$$F_u(x_1,f)=1-\exp\left(\frac{-mx_1}{X_i}\right)\left[1+\frac{mx_1}{X_i}+\frac{1}{2}\left(\frac{mx_1}{X_i}\right)^2+\frac{1}{6}\left(\frac{mx_1}{X_i}\right)^3\right] \qquad (4.2.9)$$

We therefore see that for an axially distributed source which emits sound of frequency f, the fraction of energy generated upstream of the arbitrary point x_1 depends only upon the ratio of the axial distances of x_1 and the centroid of the distribution X_i from the nozzle exit plane. However, for spectral attenuation purposes it is more convenient to express the energy fraction in terms of frequency alone, which may be achieved if we can justify an equivalence between axial ordinates in space

and the frequencies of the source distributions which make up the spectrum of the jet noise.

It is possible to assume that the position of the centroid of each source distribution varies inversely with frequency, based on the observation that the peak frequency radiated at any axial position is related to the shear layer width W at that point, such that

$$\frac{fW}{U_j} = \text{constant}$$

We can therefore assume that every axial position x will correspond to the peak of a single frequency source distribution. By simply replacing every x_n with $1/f_n$ the energy fraction can be written

$$F_u(f_1, f) = 1 - \exp\left(\frac{-mf}{f_1}\right)\left[1 + \frac{mf}{f_1} + \frac{1}{2}\left(\frac{mf}{f_1}\right)^2 + \frac{1}{6}\left(\frac{mf}{f_1}\right)^3\right] \qquad (4.2.10)$$

so now our arbitrary point x_1 is identified with the peak of the source distribution of an arbitrary frequency f_1. The source distributions of other frequencies f overlap the position x_1 by varying degrees, and the expression above gives the fraction of energy emitted by the part of each source distribution which lies upstream of it.

If the point x_1 is made to coincide with the model interface position x_s then equation (4.2.10) represents the reduction in energy emitted at the frequency f due to the absence of the portion of the source distribution which is downstream of position x_s. Applied over the full frequency range, this expression yields a spectral attenuation function which can be applied to the secondary jet spectrum at any chosen cut on point and associated frequency given by equation (4.2.5) above. Similarly, (4.2.8) provides a function for the rate of cut off of the mixed jet spectrum due to the removal of the upstream end of its source distributions. The two attenuation functions are shown in figure (13) in decibels relative to the logarithm of frequency, with the value of the cut off frequency f_1 also shown.

In the interests of ease of calculation, the attenuation rates given above have been approximated to a standard rate of -6dB/octave in the predictions given below. Such a step presumes that the affected source distributions, i.e.:- those which overlap the model interface at x_s, are completely symmetrical about their centroids. These simplified attenuation curves have been included in figure (13) to illustrate their deviation from the more rigorous functions from above. It can be seen from figure (13)

that there is a very small difference between the two pairs of attenuation rates, where non-symmetry of the source distributions about their centroids results in the source whose energy is exactly halved being slightly further downstream than symmetry would dictate. The errors involved in adopting the simpler -6dB/octave rate are considered to be unimportant in their influence on the total prediction. In particular, the two rates F_d for the mixed jet attenuation are very close during the important initial cut off and only deviate significantly when the spectrum is already well reduced and therefore insignificant.

The application of functions which approximate to $F_u(x_1,f)$ and $F_d(x_1,f)$ has been justified in terms of a spatial interface which curtails the secondary jet model in favour of the mixed jet model at the axial position x_s. However, their principal value is in providing a smooth spectral transition between two of the component sources of a coaxial jet. The third source is discussed below.

The attenuation rate for the high frequency end of the effective jet spectrum now poses some problems. Physically there is not enough detailed information from Ko and Kwan about local turbulence and velocity profiles within the first few primary jet diameters to enable a modified source distribution or spectral cut off rate to be estimated, although it can be seen from figures (5) and (6) that there are perceptible turbulence levels developing within this axial distance at radial positions corresponding to the effective jet. It can therefore be argued that an immediate and complete spatial curtailment, with the associated -6dB per octave spectral attenuation, is too severe. On the other hand, incorporating the entire spectrum from the effective jet will undoubtedly lead to over prediction of the high frequencies. In practice, a cut off rate of -3dB per octave has been adopted as a compromise between cutting off completely, and including all of the effective jet, which disagrees with the aerodynamic model based on the observations of Ko and Kwan. The attenuation progresses at -3dB per octave from an initial 3dB down point at $S_e = 2$, (section 4.2.1) prior to which the rate is calculated to provide a smooth transition from the line of the full spectrum.

4.2.3 The Effect of Reduced Turbulence on Source Strength.

The noise generating mechanisms of turbulent flows are best understood by referring to the non-homogeneous Lighthill Equation first described in [3] which can be written

$$\frac{\partial^2\rho}{\partial t^2} - c_o{}^2 \frac{\partial^2\rho}{\partial x_i{}^2} = \frac{\partial Q}{\partial t} - \frac{\partial F_i}{\partial t} + \frac{\partial^2 T_{ij}}{\partial x_i \partial x_j} \qquad (4.2.11)$$

where $T_{ij} = \rho v_i v_j + p_{ij} - c_o{}^2 \rho_o \delta_{ij}$.

The three terms on the right hand side of (4.2.11) represent different acoustic source mechanisms, namely a mass introduction, a fluctuating applied force and the 'acoustic stress tensor' T_{ij} respectively. The exhaust of a free jet at constant mass flow will only contain sources derived from the third term, which itself comprises momentum fluctuations, viscous stresses and thermodynamic fluctuations. Further, for a jet of ambient density, the only significant perturbations of the stress tensor will be due to turbulent velocity fluctuations in the product $\rho u_i u_j$.

From the second part of Lighthill's work on aerodynamic sound [4], it can be shown that the acoustic pressure at a large distance r_o from a turbulent flow can be written

$$p(r_o, t) = \frac{1}{4\pi r_o c_o{}^2} \int \frac{\partial^2 T_{ij}}{\partial t^2}\left(\tilde{y}, t - \frac{r(y)}{c_o}\right) \partial V(\tilde{y}) \qquad (4.2.12)$$

where the integral is evaluated over the retarded time $t\text{-}r/c_o$ in the source region co-ordinates y. By neglecting differences in retarded time, Lighthill [4] argues that the intensity field per unit volume of turbulence in such a sound field is proportional to the average eddy volume and to the square of the quadrupole strength. The effect of retarded time may legitimately be ignored by considering only the sound emitted at 90° to the jet, from which it is possible to obtain a simple scaling law for the mean square pressure per unit volume,

$$d\left(\overline{p^2(r_o)}\right) \sim \frac{T_{ij}{}^2 \omega^4 L^3}{r_o{}^2 c_o{}^4} \partial V$$

where ω is a frequency typical of the local region and L^3 is the volume of a typical eddy, in agreement with [4]. For isothermal jets, $T_{ij} = \rho_o u_i u_j$ so the scaling law can be written

$$d\left(\overline{p^2(r_o)}\right) \sim \frac{\rho_o{}^2 (u')^4 \omega^4 L^3}{r_o{}^2 c_o{}^4} \partial V$$

where u' is the root mean square of local fluid (or turbulence) velocity. It is therefore apparent that the noise emitted by each local region is dependent on the root mean square turbulence level to the fourth power. This is in agreement with Pao and Lowson [29], who have developed scaling terms based on the 'self' and 'shear' noise sources of Ribner, and obtain a fourth power of turbulence dependence for both.

If a turbulence intensity parameter α is introduced such that $\alpha = u'/U_j$, and we assume that the flow is purely Strouhal number dependent, we can write a scaling expression for the overall noise of the jet at 90° thus:

$$\overline{p^2(r_o)} \sim \alpha^4 \frac{\rho_o{}^2 U_j{}^8 D^2}{r_o{}^2 c_o{}^4} \qquad (4.2.13)$$

It can now be seen that an isothermal mixing region having turbulence levels α which are characteristically different from those of an isolated single isothermal jet α_o will have a noise output at 90° which differs from that of the single jet by an amount

$$\Delta dB = 40 \log_{10}\left(\frac{\alpha}{\alpha_o}\right). \qquad (4.2.14)$$

The turbulence intensities within the intermediate mixing zone, which were observed by Ko and Kwan to be about 10% of the primary jet velocity, suggest that at 90° the noise output of the region will therefore suffer a reduction of 7.04dB compared with the noise from an isolated single jet with turbulence intensities which are typically 15% of U_j.

Extending these arguments to other angles of observation is not straightforward, because the subsequent convective amplification predictions of Lighthill [4] have been shown to diverge from measured data. However, although the level of noise from a jet is dependent upon its turbulence levels as shown above, both its spectral and directional characteristics are controlled principally by the mean flow field, through the agencies of eddy convection and sound ray refraction respectively. If these factors remain unchanged with local turbulence level, it is plain to see that the spectrum of the effective jet may be predicted to have the

spectral and directional characteristics of a single isolated jet with the effective jet diameter and the primary jet velocity, but at a noise level 7dB lower than the single jet spectrum.

In order to allow a wide prediction domain it was decided to resort to a single jet noise prediction database to provide the spectra for all three contributing source models. The use of an empirical method within what is ostensibly a theoretical work may be justified on two counts; firstly, the noise from single jets is already quite well understood and described by, for example Szewczyk [22], so any theoretical prediction scheme would hopefully provide very similar results to those from a database; and secondly, the range of such theoretical schemes is limited in the velocities it covers, which in turn would restrict the applicability of this coaxial prediction method. Having decided on an empirical scheme rather than a theoretical one, the database chosen for the prediction of single jet noise needs to be widely obtainable, with a well founded database derived from established experimental methods. One such scheme is provided by the Engineering Science Data Unit (ESDU), in software package number 89041 entitled 'Estimation of subsonic far-field jet-mixing noise from single stream circular nozzles', reference [55]. An advantage of this scheme lies in the fact that the data from which it was derived was measured in the same facility as the coaxial jet data used in this study.

4.2.4 A Test of the Predictive Quality of the ESDU Method.

The quality of prediction of the coaxial jet spectrum can obviously be no better than that of the single jet noise scheme used for the model contributions, so it will be useful here to qualify the ESDU database prediction method by predicting the noise from a few stationary single jets. Single jet noise data from two sources has been available, namely from the Lockheed tests of Tanna *et al.* described in [56] and the single jet noise database of Pyestock, from which the ESDU scheme was largely derived. Prediction of the latter data is essentially a test of the degree of generalisation built into the ESDU method, to reduce the effect of spurious measurements for example.

Figure (14) a) illustrates a 90° prediction and the corresponding data measured by Lockheed [56] for an isothermal jet at a velocity of 241m/s, giving $V_j/a_o = 0.7$. The data is marked by discrete points, the prediction by a solid line, and it is clear that the ESDU scheme does not provide an

accurate prediction of the noise measured by Lockheed at this jet condition. A hot jet at 410m/s is shown in figure (14) b), and the measured spectrum is predicted much more successfully, although there is still a disagreement of 0.5dB at the peak and a difference of about two third octaves between the peak frequencies. A selection of different comparisons has shown that the characteristics demonstrated by these two predictions are representative of the overall accuracy of the ESDU method as applied to the Lockheed database, in that the slower, cold jets are not well predicted but a general improvement is seen at higher temperatures and speeds.

Figures (15) a) and b) show the data and predictions for jet noise spectra at 90° and 40° for a very similar jet to that shown in (14) a), but from the Pyestock database. Similarly, figures (16) a) and b) are for a hot jet similar to that of (14) b). The quality of fit is good for all four spectra, but the 40° predictions are slightly in error at the high frequencies beyond the peak, under predicting by 0.5dB in the cold case and over predicting by a similar amount for the hot jet.

These comparative tests enable us to conclude firstly that the Pyestock data, on which the ESDU scheme relies, can be repredicted to a very acceptable degree of accuracy, and secondly that therefore the Pyestock and Lockheed measurements are not generally in close agreement. This second point is indicative of the great range of variation even within the relatively straightforward province of far field single stream jet noise measurement.

Since the coaxial jet noise measurements of this study were carried out in the anechoic chamber at Pyestock with the same methods and apparatus as the single stream work, it seems reasonable to assume that of the available methods, the ESDU scheme will provide the best estimate of noise from the model's single jet components.

4.3 Summary of the Isothermal Model.

The combination of aerodynamic and acoustic models of the separate regions of the coaxial jet derived above leads to three unique spectra whose shape and levels depend on the coaxial jet conditions. The final spectral contributions from the three source models are formalised below, from which the total noise prediction is obtained by calculating

their incoherent sum at each third octave frequency and each observation angle.

a) The Secondary Jet.

$$SPL_s(\theta,f) = SPL(V_s, D_s, \theta, f) + 10\log_{10} F_u(f_1, f) \qquad (4.3.1)$$

where $f_1 = \dfrac{V_s}{(r_s - r_p)(1+\lambda)}$ from (4.2.5).

In other words, the secondary jet spectrum at an angle θ and a third octave frequency f is equivalent to the spectrum of a single jet, at the same angle and frequency, which is curtailed by applying the attenuation factor F_u up to the frequency f_1 since the secondary jet model is only relevant upstream of its annular potential core.

b) The Effective Jet.

$$SPL_e(\theta,f) = SPL(V_p, D_e, \theta, f) - \Delta(f_e, f) + 10\log_{10}\left(\frac{\alpha}{\alpha_o}\right) \qquad (4.3.2)$$

where $S_e = \dfrac{f_e D_e}{V_p} = 2$, $\alpha = 10\%$, $\alpha_o = 15\%$,

and the high frequency attenuation factor is as follows:

$$\Delta = 3 + 10(\log_{10} f - \log_{10} f_e) \qquad f \geq f_e \qquad (4.3.3)$$

$$\Delta = 10\log_{10}\left(1 - 10^{-(0.3+2\log_{10} f_e - \log_{10} f)}\right) \qquad f < f_e \qquad (4.3.4)$$

The contribution of the effective jet is therefore calculated by predicting the noise from a single jet of diameter D_e and velocity V_p (at θ and f) which is then reduced by the turbulence factor (α term) and the high frequency tail of the spectrum is attenuated by a frequency-dependent reduction factor. The two terms for this factor represent firstly a rate of 3dB per octave starting at the third octave band containing f_e (4.3.3), and secondly a term to allow smooth transition into cut off for third octave frequency bands below f_e (4.3.4).

c) The Mixed Jet.

$$SPL_m(\theta,f) = SPL(V_m, D_m, \theta, f) + 10\log_{10} F_d(f_1, f) \qquad (4.3.5)$$

represents the mixed jet spectral contribution, which is equivalent to the noise from a single jet (D_m and V_m) at the same angle and frequency, but cut off by the factor F_d above the frequency f_1 where the mixed jet model is no longer relevant.

Chapter 5

Isothermal Predictions

In Chapter 4 a prediction scheme was set out which, it is proposed, enables the noise from isothermal coaxial jet nozzles to be predicted by adding the acoustic contributions from three incoherent sources modelled as portions of three single jets, whose conditions are dictated by the coaxial jet characteristics. In this chapter, isothermal jet noise data will be compared with corresponding predicted spectra for a series of coaxial jet conditions in order to test the validity of the model.

The proposed jet noise synthesis relies on interpolation within an empirically derived database to obtain the contributing single jet spectra described above, so it is important to establish a measure of the correlation between the predictive database and the data one is trying to repredict. To this end, the noise from a single nozzle with the secondary jet conditions was predicted and compared with the noise data from the coaxial jet at a velocity ratio of one.

Figure (17) shows a comparison between prediction and data for a single jet velocity of 170m/s at three angles. Agreement to within ±1dB is observed across the frequency range, although there is a tendency to under predict the data at the peak for the 40° and 90° angles by up to 1dB.

Now the measured noise has emerged from a coaxial jet nozzle with equal primary and secondary flow velocities, and such a configuration will undoubtedly give rise to a velocity profile discontinuity, at variance with the single jet case, due to the boundary layers on each side of the inner nozzle tube. The high level of agreement between data and prediction may therefore be explained in one of two ways; either the wake from the inner nozzle has almost no effect on the noise produced by the coaxial jet at λ = 1, or the extra noise produced by the disruption of the velocity profile has been coincidentally reproduced by the single jet prediction scheme. The application of Occam's Razor dictates that the former explanation is more appropriate.

Having argued that the database provides satisfactory spectral information for the conditions described, it needs to be shown that the model can predict the same spectra. The astute reader will already have noticed that the model's prediction at a velocity ratio of one cannot be the

same as the single jet spectrum since it incorporates the noise from the effective jet as well as that from the equivalent mixed and secondary jets. In fact the spectrum provided by the combination of attenuated mixed and secondary jets is equal to the single jet noise prediction, while the effective jet, with the same diameter and velocity as the single jet at $\lambda = 1$, will provide an identically shaped spectrum up to the frequency at which it is attenuated, but at a level 7dB below the single jet spectrum, thus raising the total prediction by 0.8dB as explained at the end of section 4.2.1. This additional noise coincides with the level of under prediction obtained for the angles 40° and 90° by the single jet calculations shown in figure (17), although such close agreement must be purely fortuitous. To conclude this brief section, it is the belief of the author firstly that the predictive database provides single jet spectra which are in good agreement with the data from Pyestock, and secondly that the noise emitted by a coaxial jet at a velocity ratio of one can be successfully predicted by the current model, by assuming that any extra turbulent sound sources due to the inner jet annulus are incorporated within the spectrum of the effective jet.

5.1 Analysis of Prediction Contributions at 90°.

Having established a measure of the accuracy achievable when predicting the data from a jet of unit velocity ratio, the following section describes and attempts to justify the changes observed in the spectra of the contributing jets as the data for lower velocity ratios is predicted. We shall concentrate on data for a secondary jet velocity of 170m/s with various velocity ratios and three angles of observation, the predictions at 90° being examined first. In all the figures described below, the data is shown as points marked with a cross and the prediction as a solid line, as well as the three spectral contributions from the physical model which are labelled individually.

5.1.1 Prediction for $\lambda = 0.56$

Figure (18)a) shows the data and prediction components for the lowest available velocity ratio, $\lambda = 0.563$, with a primary velocity of 301.9m/s. We notice that as expected, the mixed jet contribution dominates the low frequencies, although a small but significant noise contribution is needed from the effective jet to correctly match the data. In the region of the spectral peak, neither jet on its own provides either sufficient noise level or correct spectral shape, but by adding the contributions from both

mixed and effective jets, a satisfactory predicted spectrum is obtained. It is important to notice that while the spectrum of the mixed jet is being cut off above 4kHz, the attenuated portion continues to make a small but important contribution up to at least 10kHz. This demonstrates the importance of cutting off the contributing model source spectra on a rational basis such as that argued in section 4.2.2, rather than simply ignoring all contributions above some prescribed frequency. Lastly at this lowest velocity ratio one sees the generally negligible contribution that the secondary jet shear layer makes to the total prediction, particularly at frequencies below its marginally uncertain cut on frequency.

5.1.2 Prediction for $\lambda = 0.63$

The second figure in this series, (18)b) shows the data and prediction for the higher velocity ratio of $\lambda = 0.632$, obtained by reducing the primary jet velocity to 267.2m/s. The data is uniformly 3.3dB lower than for the previous velocity ratio and the total prediction reflects this change well, even though the three model source spectra have moved by different amounts. The mixed jet contribution has been reduced by 2.5dB due a decrease in both velocity and, to a lesser extent, diameter. The effective jet has been more significantly reduced, by about 3.5dB, due to the direct reduction of its velocity. The effective jet diameter is larger at this velocity ratio and one sees a shift of the effective jet contribution to slightly lower frequencies as a result. In addition, the secondary jet is now making a small but vital contribution to the noise of the effective jet at the frequencies above 10kHz, although it is at the same level as for the previous velocity ratio. The secondary jet contribution will obviously stay at the same level for all the predictions at one secondary velocity, but its contribution becomes more and more significant as the velocity ratio increases because the other model sources contribute less to the total prediction.

5.1.3 Prediction for $\lambda = 0.71$

By reducing the primary velocity to 241.4m/s one obtains a velocity ratio of $\lambda = 0.708$, illustrated in figure (18)c). Again it is seen that the measured spectrum is at a lower level and is successfully predicted by the model. It is very noticeable at this condition that the low frequencies are becoming increasingly dominated by the mixed jet alone, although the presence of the effective jet is justified due to the contribution it makes to the prediction at the peak frequencies. The secondary jet is now seen to be

within 2dB of the effective jet spectrum, making a vital addition to the high frequency prediction from 10kHz.

5.1.4 Prediction for $\lambda = 0.79$

Figure (18)d), which shows the next velocity ratio of $\lambda = 0.791$ given by a reduction in primary velocity to 216.0m/s, illustrates that the secondary jet has become a dominant source above a frequency of 8kHz. This is again due to a reduction in the level of contribution from both the effective and mixed jets, but their peak frequencies have also shifted down the spectrum as the diameters D_e and D_m move closer to the secondary jet diameter. Despite the resultant change in shape of the contributing source spectra, the fit of the prediction to the data is still very satisfactory. Another point to notice about this prediction is that at a frequency of about 5kHz, all three sources are contributing similar levels of noise which combine to produce a predicted level within 0.3dB of the data. This observation is interesting because it demonstrates the need for all three model components at the same frequency in the coaxial jet. Lastly for this case, the contribution from the effective jet is now seen to be low when compared with the mixed jet. This may be understood after considering the relative change in velocities of the two jets as the velocity ratio changes from 0.563 to 1.00. Over this range, the mixed jet velocity varies between 232.1m/s and 170m/s whereas the effective jet velocity is equal to V_p and consequently changes from 301.9m/s to 170m/s. As a result, the mixed jet is always slower than the effective jet and changing less rapidly with velocity ratio, so the effective jet spectrum, initially very similar in noise level to the mixed jet due to its reduced turbulence, drops away faster as the velocity ratio increases towards unity.

5.1.5 Prediction for $\lambda = 0.89$

Figure (18)e) illustrates the case for the velocity ratio of $\lambda = 0.894$ at a primary velocity of 191.1m/s. The effective jet noise level is now significantly lower than either the mixed or secondary jets, although it is still contributing a very useful 1dB to the total prediction at a frequency corresponding to the spatial interface of the other two jets. The low frequency data is now fully predicted by the mixed jet contribution and the high frequencies by the increasingly significant secondary jet spectral peak.

5.1.6 Prediction for $\lambda = 1.0$

The last figure in this series, (18)f) shows the full prediction and measured data at a velocity ratio of one; the same data as seen in figure

(17) but now with an additional contribution from the effective jet. As suggested at the beginning of this chapter, the prediction is in fact slightly improved by the addition of the effective jet spectrum, illustrated by the position of the solid line about 1dB above the dashed line of the mixed jet spectrum. Moving up the frequency range, the influence of the effective jet has started to diminish at the frequency where the mixed and secondary jets meet, so that the highest frequencies are completely dominated by the secondary jet spectrum.

To better illustrate the noise characteristics of the effective jet over the range of velocity ratios described above, figure (19) shows the predicted effective jet spectrum on its own for the same six values of velocity ratio. It can be seen that the gross effect of increasing the primary jet velocity on the effective jet part of the prediction model is to raise both the level and the frequency of its spectrum simultaneously, due to the fact that the diameter of the effective jet gets smaller as its velocity increases. This behaviour is in contrast to the Strouhal number dependence of a single isolated jet.

5.2 Analysis of Prediction Contributions at Other Angles.

Comparisons of data with predictions at an observation angle of 60° are shown in figures (20)a) to f). For the majority of the velocity ratios the quality of agreement is very similar to that at 90°. However, for the two lowest velocity ratios, shown in figures (20)a) and (20)b), there is some tendency for the data to be under predicted at and above the peak of the spectrum by up to -1.5dB. In fact at this angle the effective jet will be more dominant due to higher directivity at the primary jet velocity, but the shape and level of its spectral contribution are still not sufficient to correctly lift the total prediction to the data.

At an observation angle of 40°, shown in figures (21)a) to f), the discrepancies observed at 60° are even more apparent, amounting to an under prediction of as much as -3dB at a velocity ratio of $\lambda = 0.563$. They do however become progressively smaller as the velocity ratio increases, with very acceptable agreement being obtained at $\lambda = 0.708$ and above. The increased error observed as the observation angle moves closer to the downstream jet axis suggests that despite the natural augmentation of effective jet output, the full prediction is not accounting for all the convective amplification that the true noise sources are experiencing. It is

possible to create an improved fit at these small angles by attributing a turbulence level of 11% rather than 10% to the effective jet. The result of this assumption is to improve the fit at 40° and 60° without significantly impairing that at 90°. However, appraisal of simulated flight data, reported fully in Chapter 8, for which the effective jet becomes dominant at both larger angles and larger velocity ratios, shows that such an assumption then leads to significant and general over prediction.

In fact comparative studies of the current data strongly suggest that the origin of this isolated problem lies in a small difference between the predicted directivity of the effective jet and that of the real source in the interaction region, which is only apparent at low velocity ratios. It is suspected that the physical basis of the problem might be explained in terms of the large difference between the primary jet velocity and the mixed jet velocity found at low velocity ratios, which would result in a rapid deceleration of the centreline flow downstream of the tip of the primary potential core not found in an isolated jet. In this way, the flow field through which the noise of the effective jet must exit will be uncharacteristic and may influence the directional properties of the noise measured at angles close to the jet axis.

5.3 Miscellaneous Results.

In this final section of the chapter we shall briefly demonstrate the versatility of the prediction method as far as it has been developed, by illustrating three results taken from further afield in the database.

Figure (22) shows the measured and predicted 90° spectra for a jet of velocity ratio one at the high secondary velocity of 269m/s. Compared with the lower speed jet noise spectrum shown in figure (18) f), it can be seen that the increase in jet velocity produces a 16dB rise in noise levels as well as a change in the shape of the spectrum. These changes are well reproduced by the prediction model.

Figure (23) illustrates a case at the other end of the secondary velocity range, with V_s = 136m/s and a velocity ratio of $\lambda = 0.64$. Excellent agreement between measured and predicted spectra is evident, particularly at the peak of the data which coincides with the point where the prediction comprises similar contributions from both the effective jet and the mixed jet.

Lastly, figure (24) shows an attempt to predict the noise spectrum from an inverted velocity profile jet, that is, with a velocity ratio greater than one. The extreme case of $\lambda = 1.42$ is shown and it is clear that the prediction agrees well with the data over the majority of the spectrum, suffering an over prediction of no more than 1dB at the highest frequencies. In respect of the inverted velocity profile jet we note the following;

(a) For all such configurations, the contribution of the effective jet is likely to be insignificant since it has a velocity which is less than that of the secondary jet as well as a reduced turbulence level.

(b) The two significant contributions come from the mixed jet and the secondary shear layer at low and high frequencies respectively.

For the present test method, which employs a fixed secondary velocity for a number of primary flow velocities, we therefore expect that the low frequencies will be reduced as the profile becomes more inverted as a result of the diminishing mixed jet velocity. This can be seen in figure (24).

In terms of real jet engines it is useful to note the potential objective disadvantage with inverted velocity profiles; namely the almost constant production of high frequency noise as the thrust diminishes.

Chapter 6

The Effect of Temperature on Jet Noise.

In section 3.1.1, the effect of temperature on the physical structure of the turbulent jet mixing process was discussed in terms of the experiments carried out on low density jets of helium and similar gases. The conclusion was that very little change occurs in the observable, aerodynamic structure due to increased jet temperature.

Jet mixing noise certainly does change as the temperature of the flow is altered, and this has been convincingly attributed to changes in the nature of the sources which exist in the turbulent flow field, as described in the introductory review. It was the work of Morfey [18] which first proposed that in flows containing density fluctuations there exists a second kind of source which is of dipole nature, and whose strength is proportional to the sixth power of velocity. This theory neatly explains the transition seen in hot jet noise from being louder than isothermal jets at low velocities to being quieter at velocities above $M_j \approx 0.7$, and is adopted in this work in order to ascertain the noise produced by the different regions of the prediction model when the temperature of the primary flow is increased.

The effects of increased temperature on the previously developed isothermal model may be divided into two parts; the change in the far field noise spectrum which will be predicted by the database and is due to the increased temperature of the equivalent jets; and the effect of the presence of dipoles on the noise produced by a jet with reduced turbulence levels. The characteristics of the equivalent jets are obtained by applying similar constraints to those used in the isothermal case, described in detail below.

6.1 The Hot Jet Flow Model.

The addition of heat to the primary flow of a coaxial jet introduces a density factor to the conservation of momentum equation previously given by (4.1.1), which must now be written

$$\rho_T A_T v_T^2 = \rho_p A_p v_p^2 + \rho_s A_s v_s^2 = \rho_p A_p v_p^2 \left(1+\lambda^2\beta\delta\right) \quad (6.1.1)$$

This precipitates changes in the characteristics of the equivalent jets as follows;

i) The secondary jet models the behaviour of the outer shear layer immediately downstream of the nozzle, which is bounded by the unheated secondary flow on its inner boundary and the stationary ambient air at its outer boundary. The temperature of the primary flow therefore has no influence on the sound sources within the secondary shear layer. An identical secondary jet was used by Tanna & Morris [34] whose results suggest that it is still a good model for jets with heated primary flow, so the characteristics of the secondary jet remain the same as those in the isothermal case.

ii) The isothermal mixed jet had both the same thrust and mass flow as the coaxial jet, and may accommodate the hot primary flow provided also that it has the same enthalpy, given by equation (4.1.3). Assuming that the heat capacities of the two jet flows are equal, this may be stated as

$$T_m = \frac{\rho_p A_p v_p T_p + \rho_s A_s v_s T_s}{\rho_p A_p v_p + \rho_s A_s v_s} = T_p\left(\frac{1+\lambda\beta}{1+\lambda\beta\delta}\right) \quad (6.1.2)$$

The velocity of the mixed jet is given by equation (4.1.4), but the area is now inextricably linked to the density, the product of which is given by

$$\rho_m A_m = \rho_p A_p\left(\frac{(1+\lambda\beta\delta)^2}{1+\lambda^2\beta\delta}\right) \quad (6.1.3)$$

However, T_m is known, and since $\rho_p/\rho_m = T_m/T_p$ it can be stated that

$$A_m = A_p \frac{T_m}{T_p}\left(\frac{(1+\lambda\beta\delta)^2}{1+\lambda^2\beta\delta}\right) \quad (6.1.4)$$

iii) We still wish to scale the effective jet on the primary jet velocity so it is reasonable to attribute to it the temperature of the primary flow as well. With regard to the effective jet's diameter we will adopt the same physical dimensions as for the isothermal case. The concept of a turbulent region within the complex coaxial jet structure, which grows in size from the smallest to the largest limit of the jet stream as the velocity ratio varies between zero and one is intuitively sound, and furthermore has been observed for an isothermal coaxial jet, so it seems reasonable to adopt the same physical dimensions for the interaction zone of a heated jet.

6.2 The Acoustic Model

For the prediction of isothermal jets discussed in previous chapters, the high frequency part of the mixed jet's spectrum is cut off as the secondary jet is being cut on, in such a way that they are both attenuated by -3dB at some specified frequency. It is assumed in changing to a jet with a heated core that the physical structure of the coaxial flow is essentially unchanged, so the extent of the spectral contributions from the secondary and mixed jets will remain unaltered. Such assumptions cannot be made about the effective jet.

The noise emitted by the effective jet is less than that emitted by a conventional, isolated single jet because of the characteristically reduced turbulence level. It has been shown in section 4.2.3 that the noise emitted by the quadrupole sources of an isothermal jet is proportional to the fourth power of the root mean square of turbulence intensity. However, the noise from the hot effective jet proposed above is the product of both quadrupole and dipole sound sources, so it is necessary to scale the quadrupole noise and the dipole noise separately, as discussed below.

6.2.1 The Turbulence Dependence of Dipole Sources.

In order to scale the dipole noise correctly it is necessary to find the dependence of far field pressure fluctuations upon the turbulence velocity within the dipole source term, most generally given by

$$p(\tilde{x},t)=\frac{-1}{4\pi rc}\frac{x_i}{r}\int_V \frac{\partial F_i}{\partial t}\partial V(\tilde{y}) \qquad (6.2.1)$$

where F_i is the force per unit volume of each dipole within the source region bounded by the volume V. Morfey [18] has shown that the dominant sound radiation from hot jets is associated with the source term

$$q = -\frac{\partial}{\partial x_i}\left(\left(\frac{\rho-\rho_o}{\rho}\right)\frac{\partial p}{\partial x_i}\right).$$

Now if we assume that all the pressure fluctuations are due to the acceleration of pockets of different density gas, thus equating

$\frac{\partial p}{\partial x_i}$ with $\rho\frac{\partial U}{\partial t}$, we can rewrite the source term

$$q = \frac{-\partial}{\partial x_i}\left((\rho-\rho_0)\frac{\partial U}{\partial t}\right) \tag{6.2.2}$$

so we can say that in the far field,

$$p = \frac{-1}{4\pi r c_o}\frac{x_i}{r}\int_V \frac{\partial}{\partial t}\left((\rho-\rho_o)\frac{\partial U}{\partial t}\right)\partial V \tag{6.2.3}$$

However, $U = U_j + u'$, and U_j is invariant with time so

$$p = \frac{1}{4\pi r c_o}\frac{x_i}{r}\int_V \frac{\partial}{\partial t}\left((\rho-\rho_o)\frac{\partial u'}{\partial t}\right)\partial V. \tag{6.2.4}$$

Now for scaling law purposes we can scale the volume integral on a typical dimension D^3, and if we assume that we are looking at purely Strouhal dependant flow then the second time derivative scales on the square of frequency or $(U_j/D)^2$, resulting in a far field pressure

$$p_{farfield} \propto \frac{(\rho-\rho_0)U_j^2 u' D}{rc_0} \tag{6.2.5}$$

We can also describe the variation of far field sound intensity as

$$I \propto \frac{(\rho-\rho_0)^2 U_j^4 u'^2 D^2}{\rho_0 r^2 c_0^3} \tag{6.2.6}$$

So the sound intensity in the far field due to the dipole sources in a hot turbulent jet is proportional to the root mean square of turbulence

velocity squared. For the effective jet, whose turbulence velocity is characteristically 10% of U_j rather than 15%, the effect will be to reduce the dipole spectrum by an amount

$$\Delta dB = 20\log_{10}\left(\frac{10\%}{15\%}\right) = -3.52dB \qquad (6.2.7)$$

To summarise this section; it has been argued that if a single isolated jet contained only dipole sound sources, and the r.m.s. turbulence intensity levels were only 10% of the jet velocity, then the far field sound intensity would be 3.5dB lower than that from a similar jet with 15% turbulence levels.

6.2.2 The Ratio of Dipole to Quadrupole Sources in a Hot Jet.

It remains to determine how much of the predicted effective jet noise is produced by dipole sources and how much by quadrupole sources, so that the spectrum may be scaled appropriately. This information is not available from the empirical ESDU prediction method, so it is necessary to make use of the theoretical single jet analysis method developed by Szewczyk and Morfey [22].

By applying the Geometric Acoustics model of Morfey to the generation of sound by a hot jet, Szewczyk obtained normalised master spectra for quadrupole and volume displacement dipole sources which, when combined with mean flow-acoustic interaction, form the basis of a single jet prediction program. The 90° normalised radiation master spectra for dipole and quadrupole sources are shown in figure (25) relative to modified Strouhal number, from which the spectra of the two sources in a hot jet are predicted separately. The noise prediction program of reference [22] produces three spectra covering a specified range of frequencies which correspond to dipole noise, quadrupole noise and total noise.

The most obvious way to find the correct reduction delta for a jet containing both types of noise source is to use the scheme of [22] to predict the dipole and quadrupole spectra, then reduce these by 3.5dB and 7dB respectively before comparing their sum with the sum of the unattenuated spectra. This process may be written as follows,

$$\Delta dB_f = 10\log_{10}\left[\frac{\left(\alpha/\alpha_o\right)^2 I_d + \left(\alpha/\alpha_o\right)^4 I_q}{I_d + I_q}\right]_f \qquad (6.2.8)$$

where ΔdB_f is the reduction, in decibels, applied to the sound pressure level predicted at the third octave band f of the effective jet spectrum, and I_d and I_q are the separate far field dipole and quadrupole spectra for the same jet.

By examination, the frequency dependence of the reduction given by (6.2.8) will be greatest at a jet condition which produces dipole and quadrupole spectra with similar levels, at which point the difference in shape between the two master spectra is most influential. An example is a jet at 400 Kelvin and a jet velocity to ambient sound speed ratio of 0.9, whose quadrupole spectrum dominates at 15% turbulence level but after scaling to 10% turbulence has a dominant dipole spectrum, as shown by figure (26). The reduction in noise level calculated for such a jet is seen to vary by less than 0.5dB over the majority of the frequency range, figure (27), so it is tempting to propose that a simpler, overall noise reduction may be calculated which does not rely on the shapes of the master spectra but only on the overall noise levels of the two sources.

In simple terms, the intensity generated by dipole and quadrupole sources at 90° can be written

$$I_d = K_d\left(\frac{\Delta T}{T_s}\right)^2\left(\frac{T_o}{T_s}\right)^2 M_j{}^6 \qquad (6.2.9)$$

$$I_q = K_q\left(\frac{T_o}{T_s}\right)^3 M_j{}^8 \qquad (6.2.10)$$

where K_d and K_q are all embracing constants for the dipole and quadrupole master source spectra respectively, and $M_j = U_j/a_o$, from [22].

The ratio of dipole to quadrupole contributions may therefore be written

$$\frac{I_d}{I_q} = K\left(\frac{T_j - T_o}{T_s}\right)^2\left(\frac{T_s}{T_o}\right)M_j{}^{-2} \qquad (6.2.11)$$

where $K = \frac{K_d}{K_q}$. The value of this ratio may be found from the master spectra of [22] as shown in figure (25), for which K = 7 is a reasonable average.

It is noticeable at this point that the value of K derived from the master spectra is significantly frequency dependent. However, when the ratio of K values at 15% and 10% is calculated, the frequency dependence all but vanishes, as seen previously in the case shown by figures (26) and (27). The ratio of intensities may be rewritten as

$$\frac{I_d}{I_q} = Ky \tag{6.2.12}$$

$$\text{where} \quad y = \left(\frac{T_j - T_o}{T_s}\right)^2 \left(\frac{T_s}{T_o}\right) M_j^{-2} \tag{6.2.13}$$

but if $T_s = T_o + 0.65(T_j - T_o)$

and $\tau = T_j / T_o$

$$\text{we can now write} \quad y = \frac{(\tau - 1)^2}{1 + 0.65(\tau - 1)} M_j^{-2} \tag{6.2.14}$$

Let us now write similar expressions for the reduced turbulence jet, so that equations (6.2.9) and (6.2.10) become

$$I_d' = r^2 K_d \left(\frac{\Delta T}{T_s}\right)^2 \left(\frac{T_o}{T_s}\right)^2 M_j^{\,6} \tag{6.2.15}$$

$$I_q' = r^4 K_q \left(\frac{T_o}{T_s}\right)^3 M_j^{\,8} \tag{6.2.16}$$

where $r = 10/15$ allows for the reduced noise levels in the contributions due to the decreased turbulence.

The ratio given by (6.2.11) then becomes

$$\frac{I_d'}{I_q'} = r^{-2}K\left(\frac{T_j - T_o}{T_s}\right)^2\left(\frac{T_s}{T_o}\right)M_j^{-2} \qquad (6.2.17)$$

$$= r^{-2}Ky \qquad (6.2.18)$$

From these equations it is now possible to derive an expression for the ratio of total noise produced by 15% and 10% turbulence intensity jets. Modifying equations (6.2.12) and (6.2.18) gives us

$$\frac{I_d + I_q}{I_q} = 1 + Ky \quad \text{and} \quad \frac{I_d' + I_q'}{I_q'} = 1 + r^{-2}Ky$$

so the required ratio is

$$\frac{I_d' + I_q'}{I_d + I_q} = \frac{\left(1 + r^{-2}Ky\right)}{(1 + Ky)}\left(\frac{I_q'}{I_q}\right) \qquad (6.2.19)$$

However, it is noted that $I_q'/I_q = r^4 = 1/5$, so the noise reduction in a hot jet due to a decrease in turbulence level from 15% to 10% of U_j may be given by

$$\Delta(dB) = 10\log_{10}\left[\frac{(1+16y)}{5(1+7y)}\right] \qquad (6.2.20)$$

where again, $y = \dfrac{(\tau-1)^2}{1+0.65(\tau-1)}M_j^{-2}$

The variation of this overall attenuation with temperature ratio τ at four jet Mach numbers M_j is shown in figure (28). The extent of the reduction in effective jet noise is clearly greatest at a temperature ratio of one, corresponding to the isothermal jet which comprises only quadrupole sources. At the other extreme, a very hot effective jet contains a large proportion of dipole sources and consequently is only 3.5dB quieter than an equally hot conventional jet. The influence of jet velocity is negligible at these two points due to the complete dominance of the respective source mechanisms, but has some significant effect on the transition from one extreme to the other.

The general trend of the attenuation factor is to drop very rapidly from the isothermal value of 7dB and asymptote to the hot jet limit at 3.5dB. It can clearly be seen that the rate of decrease is less for fast jets, which is understood if we consider that the temperature at which the dipole spectrum exceeds the quadrupole must be higher for a fast jet than for a slow jet. From a practical viewpoint, the noise reduction will be within half a decibel of the full dipole jet factor when equation (6.2.20) gives $y \geq 0.5$. For a jet at Mach one, this corresponds to a temperature of about $1.8T_a$ while for a jet of Mach 1.5, the temperature needs to be no more than $2.4T_a$ for the same minimum (dipole dominant) reduction. It would therefore appear that for modelling typical aero-engine applications, the noise produced by the effective jet originates almost entirely from dipole sources, requiring a 3.5dB reduction in level to account for lower turbulence.

In summary, the hot coaxial jet predicted spectrum comprises the following spectral contributions;

i) The low frequencies from a mixed jet, given by

$$SPL_m(\theta,f) = SPL(V_m, T_m, D_m, \theta, f) + 10\log_{10}F_D(f_1, f) \qquad (6.2.21)$$

$$\text{where } \frac{f_1 D_m}{V_m} = 1. \qquad (6.2.22)$$

This equation describes the mixed jet third-octave sound pressure level at an angle θ and frequency f as the sound pressure level predicted for a single jet of diameter D_m, velocity V_m and temperature T_m at the same angle and frequency, cut off at frequencies above f_1 as described in section 4.2;

ii) The high frequencies from a secondary jet,

$$SPL_s(\theta,f) = SPL(V_s, T_s, D_s, \theta, f) + 10\log_{10}F_U(f_1, f). \qquad (6.2.23)$$

In this case the third-octave sound pressure level from the secondary jet at θ and f is given by the predicted sound pressure level from a jet with the velocity and diameter of the secondary jet at the same angle and frequency, cut off below the frequency f_1 given by (6.2.22);

iii) The spectrum from an effective jet whose predicted noise levels are scaled to a 10% turbulence intensity, so

$$SPL_e(\theta,f) = SPL(V_p, T_p, D_e, \theta, f) + \Delta dB \qquad (6.2.24)$$

The third-octave sound pressure level from the effective jet at θ and f is given by the sound pressure level predicted for a jet at the primary jet velocity and an effective diameter, reduced by a factor which varies between -3.5dB for a completely dipole-dominated jet to -7dB for an isothermal jet containing only quadrupoles. The value of the attenuation factor Δ is given by equation (6.2.20).

6.3 Predictions

The effects of a hot primary flow on the separate elements of the predictive model have already been discussed and illustrated, but it is a characteristic of the present modelling method that changes in individual components do not necessarily lead to similar changes in the final predicted spectrum. An example of this can be seen in the first comparisons between predicted and measured spectra described below.

6.3.1 Study of Overall Change Due to Hot Primary Flow.

As a general check on the effect of a hot core on the full prediction, figures (29) a), b) and c) compare equivalent predictions at $\lambda = 0.8$ and 90^{o} for the three temperatures covered by the data. The first and obvious difference is that the hotter jets are louder than the cold jet, which appears to be due primarily to the increased level of the effective jet spectrum at the higher temperatures. Conventional isolated jets at these conditions would experience a reduction in noise output because the reduction in quadrupole noise at high temperatures is greater than the increase in dipole noise. However, the effective jet's characteristically reduced turbulence intensity causes the dipole sources to become much more significant and thus the predicted noise from the effective jet increases with temperature. This unusual behaviour is due to reduced turbulence levels which have only been observed in isothermal coaxial jets. By extrapolating the effective jet model into the heated regime, we propose a sound source which is similar to a single jet but with fundamentally different behaviour at high temperatures. The hot effective jet spectrum constitutes the majority of the noise at the peak of the data and the fit is very good, which suggests that there is a source not dissimilar to the proposed effective jet within the real hot jet.

The increase in level is not the only change to be seen as the primary jet temperature increases. There is also a noticeable change in the shape of the measured spectrum towards a lower frequency peak level and a more rapid decrease to each side of the peak. The model succeeds in replicating this change largely by altering the balance of contributions to the total prediction, rather than changing their shapes. This observation illustrates the point that the influence of jet characteristics on the spectra of the isolated contributing sources is not the same as the effect on the total predicted spectrum.

The only major discrepancies between the measured and predicted spectra are at the lowest frequencies of the two hot jet spectra, which have been over predicted by up to 3dB. Such errors are not seen in the isothermal prediction, in which the effective jet makes a relatively minor contribution due to its lower level. The hot jet over prediction occurs at frequencies below 300Hz in both cases, and can be seen to follow the profile of the increasingly dominant effective jet spectrum. These spectra were measured from small scale air jets, so for a practical jet engine with a typical diameter thirty times larger than that of the model, assuming the effective jet scales on Strouhal number then the full sized jet prediction errors will start at 10Hz, which is too low to be of practical interest.

It may be seen on close inspection that the mixed jet noise levels increase slightly with temperature, but it must be remembered that the mixed jet is at a much lower velocity, close to or below the speed at which hot jets become noisier. The secondary jet remains constant within the constraints of experimental variation since the predicted spectrum is based upon the same jet conditions for all three cases.

6.3.2 Data and Predictions at a Velocity Ratio of 1.00.

Figures (30) a), b) and c) illustrate the predicted spectra and the data for the case where the primary velocity is equal to the secondary velocity, at the angles 40^{o}, 90^{o} and 120^{o}. At the velocity of 170m/s, a hot jet is very similar in noise output levels to an isothermal jet, so the contributions from each of the three sources within the model will not differ greatly from their cold counterparts. The secondary jet is at the ambient temperature anyway, whereas the mixed and effective jets are both hotter due to the hot primary flow. The sum of these spectra at all three angles constitutes a reasonable prediction of the measured jet noise, which is noticeably better

for the higher frequencies where all three sources are contributing at similar levels. The peaks of the predictions coincide with the peaks of the data in both level and frequency, except at 40° where the model over predicts by about 1dB. Again, the lowest frequencies are rather poorly matched; it seems that either the mixed jet or the effective jet alone would provide the downstream noise, but not both together.

An increase in the velocity of the $\lambda = 1$ hot jet will precipitate changes in the relative dominance of the contributing source models, particularly the effective jet whose spectrum is no longer similar to its cold equivalent. This is due to the increasing dominance of the quadrupole sources as the jet speed increases. Prediction and data for such a jet condition at 90° are illustrated in figure (31), which shows the results with a primary jet of velocity 270m/s and a temperature of 800K. It can indeed be seen that the effective jet spectrum now has a reduced influence over the majority of the frequency range. Combining this with the mixed and secondary jets, which are still very similar in nature, provides a satisfactory quality of prediction.

6.3.3 Predictions at Other Velocity Ratios.

As the primary jet velocity is increased, the velocity ratio becomes less than unity, and the noise from the coaxial jet increases. In terms of the model developed herein, the interaction region of the jet will become more and more dominant, as previously seen in section 6.3.1.

Figures (32) and (33) illustrate the data and predictions for jets at 600K, with velocity ratios of 0.79 and 0.63 respectively. Although these jets are not at the highest temperature, the effective jet is already dominant over most of the spectrum. It provides a satisfactory fit at the peak and in overall shape, but the predicted levels are too high at the lowest frequencies, as observed above, and some error may be seen beyond the peak frequency in figures (32) b), (32) c) and (33) a).

Three tests were carried out at a primary jet temperature of 800K, for which data and predictions are illustrated in figures (34), (35) and (36), corresponding to jet velocity ratios of 0.79, 0.71 and 0.63 respectively. Although there is no systematic deterioration in the quality of these predictions, the overall impression is one of reduced effectiveness. The over prediction of low frequencies is again evident, where either the mixed or effective jet alone would have provided a sufficient noise level, and at

small angles and high frequencies the levels are under predicted by about 2-3 dB.

Despite the anomalies in predictive accuracy seen in the figures, there are no obvious temperature dependent errors apparent in the predictions calculated so far, and it can be said that the variations are no worse than those seen in the isothermal predictions of Chapter 5. Since the majority of predictive errors are invariant with temperature and velocity ratio but consistent with measurement angle and jet velocity, it is tempting to suggest that there is some small but fundamental source of disagreement between the spectra of jets measured at Pyestock and those provided in the ESDU database.

6.4 In Summary.

The primary objective of this chapter was to extend the jet noise prediction model developed with isothermal, stationary coaxial jet data into the more practical field of heated primary flow coaxial jets. We may conclude the following;

The model developed on the basis of isothermal jet noise data may be modified straightforwardly to accommodate jets with hot primary flows with satisfactory accuracy in the predicted results.

The changes required of the cold model in order to predict hot jet data are as follows:

i) The effective jet is at the temperature of the primary jet flow, Tp;

ii) The mixed jet conditions are now dictated by the conservation of enthalpy as well as mass and momentum.

These changes, which are corollaries to basic assumptions made in the development of the cold model, precipitate minor complications in the prediction method due primarily to the occurrence of dipole as well as quadrupole sound sources in the hot effective jet, but the resultant noise predictions at all angles and velocities are of an accuracy comparable with predictions for isothermal jets.

Chapter 7

Predicting the Noise from a Jet of Area Ratio 4.

In previous chapters a predictive model for coaxial jet mixing noise has been developed which is based on data from various experimental works, all carried out on model jet rigs at an area ratio of about two. The model has been used to repredict the isothermal jet noise data from which it was initially derived, as well as predicting the noise from jets with a heated primary flow. An important argument in the extension of the model to hot jets was that the physical structure and dimensions of the turbulent mixing region remain unchanged. In this chapter the model will be applied to coaxial jets with an area ratio of four, which clearly requires a change in jet dimensions.

To recap, the experimental rig for this area ratio incorporated a primary nozzle of 33.2mm diameter, the same as that used for the smaller area ratio, but with a secondary nozzle of 75mm which gives an actual area ratio of $\beta = 4.01$. This configuration was operated at three secondary velocities, 135m/s, 170m/s and 270m/s, with various primary velocities to provide velocity ratios between 0.63 and 1.26. Experiments were also carried out with primary flow heated to a temperature of 800K, and with an annular flow of ambient air at about 55m/s to simulate a jet in flight at selected conditions.

Unfortunately the detailed turbulent structure information provided by Ko and Kwan [2] is limited to jets with an area ratio of two, so an extrapolation of the model into the realm of larger area ratios will be unsupported by experimental data.

7.1 Application of Model to Jets of Area Ratio Four.

The three single equivalent jets given by $\beta = 4$ in the formulae prescribed in chapter four, lead to total predicted spectra which are too high in noise level over a significant portion of the spectral range. A comparison between measured spectra and their predicted counterparts, from which figures (37) a)-c) are a selection, shows significant over-prediction at the majority of frequencies. A particular characteristic is

demonstrated by the cold jet data at 90°, where the prediction over estimates the noise level at the frequencies surrounding the peak of the measured data, while at 40° the low frequencies are more significantly over predicted. The hot jet data at 90° exhibits substantially greater error at high frequencies. In general, overprediction is more pronounced at the lowest velocity ratios and is markedly worse at 40° than at 90°, indicating a possible error in the directivity of the sources. In order to attempt a correction of the errors encountered in the area ratio four predictions, it is useful to investigate the changes we should expect as the secondary jet grows in size, and to compare these with the changes we obtain with the model at $\beta = 4$.

7.2 The Effect of Area Ratio on Measured Coaxial Jet Noise.

It has long been recognised that an increase in jet diameter at constant thrust will always lead to a reduction in jet noise, even when the larger diameter is associated with a bypass flow at some fraction of the primary jet velocity. Now, although the present experiments at the two area ratios have not been carried out at constant thrust, certain changes in the noise characteristics may be anticipated.

Firstly, at a velocity ratio of one, the only physical difference between equal velocity isothermal jets at the two area ratios is in the diameter of the outer nozzle. Both flows are at the same velocity for both area ratios, so in the far field the overall sound pressure level should be greater for the larger jet by the dimension factor

$$\Delta \text{OASPL} = 10\log_{10}\left(D_{\beta=4}/D_{\beta=2}\right)^2 \qquad (7.2.1)$$

The two jets are obviously not producing the same thrust at this condition.

As the velocity ratio is reduced from unity at a fixed secondary velocity by increasing the primary velocity, the thrust of both jets will increase. However, that of the area ratio four jet must rise at a slower rate because the increased primary flow constitutes a smaller proportion of the total coaxial flow momentum. Also, at the limiting velocity ratio of zero, the two jets will provide identical thrusts. As the velocity ratio drops from one towards zero therefore, the thrusts of the two jets will become more and more similar, approaching and at some point exceeding the condition where the larger jet is always quieter.

Olsen and Friedman [30] measured the OASPL of fixed primary velocity coaxial jets at a velocity ratio of $\lambda = 0.4$, for area ratios including both two and four, and found that the smaller area ratio jet produced noise levels which were consistently 2dB higher over all measurement angles. This trend was observed to continue for larger area ratio jets. Similar measured OASPL data from Cocking [31] over a range of velocity ratios show that while a jet of area ratio four is up to 4dB quieter than a jet of area ratio two at low velocity ratios, the situation is seen to be reversed above a velocity ratio of $\lambda = 0.7$. At this velocity ratio, the thrusts of the two jets have diverged to such an extent that the diameter of the jet becomes the dominant factor in noise level, as suggested above.

It is argued that the general changes which can be expected in the far field characteristics of coaxial jet noise in changing from an area ratio of two to four will be similar to those described above, such that there will be a reduction in the OASPL at a velocity ratio of one, a tangible increase at the velocity ratio of 0.63 and very little change at a velocity ratio of 0.8. It is to be assumed that any spectral changes will be due primarily to the increased diameter and length of the outer or secondary shear layer, and will be evident as a shift of the whole spectrum to lower frequencies.

Confirmation of the trends suggested above is given by a study of comparable data at both area ratios. Figures (38) a), b) and c) show pairs of measured noise spectra at 90° for three isothermal jets, each with a secondary velocity of 170m/s and velocity ratios of 1.0, 0.79 and 0.63 respectively, at the two area ratios. It is immediately clear from the first of these diagrams that the jet of area ratio four produces a higher level of sound at unit velocity ratio, due entirely to its larger diameter. The spectrum of this jet is shifted to lower frequencies, suggesting that it is Strouhal dependent.

As the velocity ratio drops to 0.79, shown in figure (38) b), the spectra of the two jets are seen to approach each other in level, but the frequency shift noted above is still evident. At the lowest velocity ratio, seen in figure (38) c), the overall noise level of the smaller area ratio jet has obviously become greater, although it is clear from the spectral breakdown that the shift in frequency is still present and serves to promote the low frequencies of the area ratio four jet spectrum above those of the area ratio two jet spectrum. These differences are repeated in every detail in the data from jets with hot primary flow, suggesting that aerodynamic adjustments rather than changes in the mode of sound generation are responsible.

Having established the expected changes in the measured coaxial jet noise due to an increase in area ratio, we may proceed to examine how the components of the prediction model adjust to accommodate them.

7.3 The Effect of Area Ratio on the Predictive Model.

The predictive model components are defined for any area ratio due to the inclusion of the area ratio β, but it remains to be seen how the contributing single jets and their combined predicted spectrum will behave at an area ratio other than the one from which the model was developed. By looking at the conditions of the individual equivalent jets as dictated by the equations set out in chapters 4 and 6, the changes in characteristics may be identified and associated with changes in their spectra, which can then be compared with those observed in the experimental domain.

7.3.1 Changes in the Secondary Jet at $\beta = 4$.

In changing from an area ratio of two to four, the diameter is the only characteristic of the secondary jet which is modified, becoming larger by a factor of $\sqrt{5/3}$. The broad effect of this change on the spectrum of the secondary jet is to increase all the levels by around 2dB and to reduce the frequency of the whole spectrum by one third of a third octave, as discussed above. At a velocity ratio of one, this is precisely what is required to match the changes in the measured noise levels. At lower velocity ratios, the secondary jet contribution becomes less and less significant to the total prediction, and it is probable that the errors observed between the measured and predicted spectra are caused by alterations in the other jets comprising the model.

7.3.2 The Fully Mixed Jet at $\beta = 4$.

At the new larger area ratio, the mixed jet diameter varies between the diameter of the primary jet nozzle at $\lambda = 0$ and that of the increased secondary nozzle at $\lambda = 1$, as defined for isothermal jets by equation (4.1.6). On its own this effect would lead to an increase in the noise levels of the mixed jet spectrum at all velocity ratios. However, the velocity of this jet is also dictated by the conservation requirements and is given by equation

(4.1.4). As a consequence of the larger proportion of secondary flow in the mixed jet momentum and mass flow terms at the larger area ratio, the velocity of the mixed jet is diminished at all velocity ratios between zero and one, but most significantly at $\lambda \approx 0.4$. This can be seen in figure (7) which shows the variation of the ratio V_m/V_p with velocity ratio λ at four different area ratios. The resultant effects of these two factors acting on the mixed jet are as follows;

- At a velocity ratio of one, the mixed jet velocity is the same for all area ratios, so the increase in noise associated with the larger diameter is the only change and the mixed jet contribution is about 2dB higher in level, as required;
- At a velocity ratio of say $\lambda = 0.5$ and at isothermal conditions, the reduction in mixed jet velocity is from $0.75V_p$ to only $0.67V_p$, which causes a -4dB reduction on top of the increase due to the diameter increment. The dimension factor at this velocity ratio, given by equation (7.2.1), amounts to +2.3dB, so the net result is a reduction in OASPL from the larger area ratio mixed jet of approximately -1.7dB.
- For all velocity ratios the spectrum of the larger mixed jet will experience a shift to marginally lower frequencies, in the same manner as the secondary jet spectrum.

The general trend of these changes to the mixed jet noise are in complete accord with the differences which are seen to occur in the measured noise spectra as the area ratio is altered.

7.3.3 The Effective Jet at an Area Ratio of 4.

As it stands, the effective jet has a diameter which varies between the primary and secondary nozzles as the velocity ratio increases from zero to one, and a velocity equal to the primary jet velocity. These conditions dictate the principal changes which the effective jet will experience in converting to the larger area ratio, which in turn modify the characteristics of the effective jet spectrum.

At a velocity ratio of $\lambda = 1$, the effective jet at an area ratio of four is larger than it is at area ratio two and so the sound spectrum it produces will be higher by the factor given by (7.2.1). This change is in the same direction as the change in measured data. However, in contrast to the noise from coaxial jets, the increase in effective jet noise is reproduced at all other velocity ratios, since the diameter of the new effective jet is always

greater than it was at an area ratio of two. Now, it will be remembered that the measured spectra for coaxial jets at small velocity ratios have significantly lower noise levels at the larger area ratio. It is therefore clear that the behaviour of the noise from the effective jet in adapting to a larger area ratio is not modelling the changes which occur in the noise from the full coaxial jet at any but the highest velocity ratio. It is also clear that the errors in the effective jet spectrum anticipated above will have the greatest effect on the full predicted spectrum wherever the effective jet is making a significant contribution to it, in other words at the lowest velocity ratios.

The characteristic changes that occur in the spectrum of the effective jet lead us to assume that the over prediction seen in the spectra described in section 7.2 are intimately connected with the use of an effective jet derived at an area ratio of two.

If the model is to predict the noise from area ratios other than $\beta = 2$, it appears that the definition of the effective jet needs to be modified in order to reduce its contribution at larger area ratios as the velocity ratio diminishes. Without the sort of detailed experimental measurements of turbulence intensity at $\beta = 4$ which are provided at $\beta = 2$ by Ko and Kwan, it is difficult to make an adequately supported supposition to explain the aberrant behaviour of the effective jet at the increased area ratio. The remainder of this chapter will deal with the possible mechanisms which would lead to the required reductions in the effective jet spectrum at lower velocity ratios, and attempt to identify the most probable of these. It is to be hoped that this also provides the greatest improvement in the quality of the total prediction.

7.4 Reducing the Effective Jet Spectrum at $\beta = 4$.

To recap, there is a systematic error in the predicted spectra at an area ratio of four which may be attributable to incorrect modelling of the complex mixing region of the coaxial flow. This coincides with undesirable trends in the noise characteristics of the effective jet which represents this zone. In order to overcome these prediction errors, it may be possible to find a parameter of the effective jet which can be assumed to alter in order to improve the fit of this jet's contribution to the total prediction.

There are three characteristics of the effective jet which might justifiably be altered by a change of area ratio to affect the level of its noise emissions;

7.4.1 A Different Effective Jet Diameter.

Firstly, the rate of change of D_e with velocity ratio at an area ratio of four might differ from that derived at an area ratio of two, equation (4.1.5). The measured noise levels for low velocity ratio jets are seen to drop as the area ratio increases, and in order to achieve this the effective jet would actually need to become smaller in diameter as the area ratio increases. This is not an intuitively sound proposition, especially when it is considered that a 37% reduction in diameter is necessary to obtain the drop in OASPL of 4dB observed by Cocking [31]. This is actually smaller than the primary jet nozzle.

7.4.2 A Different Effective Jet Turbulence at $\beta = 4$.

Secondly it might be that the r.m.s. turbulence intensity within the complex region of the jet at $\beta = 4$ is even less than that observed at $\beta = 2$. A decrease from 10% to 9% of V_p would reduce the level of the isothermal effective jet spectrum by 1.8dB. However, the reduction experienced by a hot jet will amount to only half of this, so the optimum turbulence intensity for a good fit to the cold jet data will not provide enough of a reduction to the hot effective jet spectrum, and since the effective jet is more dominant at high temperatures, the accuracy of the full prediction will certainly suffer. Predictions based on these reduced turbulence levels have shown that for cold jets, a reasonable predicted spectrum may be obtained at 90° by adopting a nominal turbulence intensity of 8.5% of V_p, but all the hot jet data is over predicted in the manner described in the previous section, as well as the cold data at small angles. Because of these shortcomings, it will be assumed that the characteristic turbulence levels observed in the complex region of the coaxial flow at an area ratio of two are also to be found at the larger area ratio of four, for the simple reason that they provide a source model which fits the jet noise data measured at the smaller area ratio.

7.4.3 A Modified Effective Jet Velocity at $\beta = 4$.

Finally the velocity of the effective jet at $\beta = 4$ might no longer be equal to that of the primary jet, but to a reduced value. This would

indicate that the measured velocity profiles and turbulence no longer scale on the primary velocity, but on the reduced velocity of a flow field incorporating the extra secondary flow entrained by the inner shear layer, before the two turbulent layers meet and the effective jet commences. Such a phenomenon has been observed at the larger area ratio. The result of adopting a reduced effective jet velocity is to diminish the noise spectrum for the isothermal case by a factor $80\log_{10}(V_p/V_e)$, so a significant change in spectral level may be affected by only a small adjustment to the effective jet velocity. The noise reduction for a hot effective jet will be slightly less due to the different velocity dependence of dipole sources, but not to the extent of halving it, as was seen in the discussion of variable turbulence above. Another advantage of assuming a reduced velocity is that the associated decrease in convective amplification will improve the fit of the prediction at small angles.

7.5 The Application of a Reduced Effective Jet Velocity.

Of the possible alterations described in the previous section, a modified velocity promises to provide a change in effective jet spectrum which most closely matches the measured changes which occur in the data at an increased area ratio. The adoption of a centreline velocity for the effective jet which is less at $\beta = 4$ than it is at $\beta = 2$ is not entirely without merit, since the region being modelled is subtly altered by the change in area ratio. For example the upstream limit of the region modelled by the effective jet, given by equation (4.2.6), now occurs at a lower frequency, corresponding to a position further from the nozzle exit plane, so there is less of the primary potential core contained within it. Secondly, the complex mixing which takes place as the inner and outer shear layers meet must be somewhat diminished at the larger area ratio since there is more distance for the mixing of the individual shear layers before they merge. As a result of this second point, it might be argued that the reduced turbulence intensity argument should be adopted after all, but the effective jet has turbulence intensities which are proportional to V_e so the actual levels of turbulence will be lower as a consequence of reducing the velocity.

In an initial study, optimum values of effective jet velocity were chosen for a selection of isothermal jet test points at 90° in order to obtain the best fit of the prediction to each measured spectrum. It was noted that

the optimum reduction in effective jet spectrum seemed to be independent of velocity ratio as well as absolute jet velocity, and amounted to a 3dB drop in level. This suggests that the effective jet velocity at isothermal conditions and at 90° differs from the primary jet velocity by a constant proportion, given by

$$\frac{V_e^*}{V_p} = \log_{10}{}^{-1}\left(\frac{-3}{80}\right) = 0.917 \qquad (7.1.2)$$

where V_e^* is the new effective jet velocity at area ratio four.

Such a reduction in the velocity of the effective jet was seen to significantly improve the quality of the selected 90° isothermal predictions, so the test domain was extended to include small angles and higher temperature jets. In the latter case, since we are attributing the drop in velocity partly to extra entrainment of cold secondary flow prior to the start of the effective jet zone, we should take account of the change in temperature of the combined flow in some way. If we assume similarity between the velocity and temperature profiles of the jet, then the temperature of a jet which has diminished in primary velocity by 8.3% may be estimated by attributing the same reduction to the primary temperature, as follows;

If we say that

$$V_e^* = xV_p,$$

where x = 0.917 in this case, we can also write the new effective jet velocity relative to the secondary velocity,

$$V_e^* = V_s + \left(\frac{x-\lambda}{1-\lambda}\right).V_{rel} \qquad (7.1.3)$$

so by similarity of profiles the temperature of the new effective jet is given by

$$T_e^* = T_s + \left(\frac{x-\lambda}{1-\lambda}\right).\Delta T \qquad (7.1.4)$$

where ΔT is the difference in temperature between the primary and secondary jets. These two equations clearly become meaningless at the point where $\lambda = x$, which corresponds to the situation of the secondary velocity being equal to the new effective jet velocity. However, due to the low level of the effective jet noise contribution at velocity ratios close to one, the value of x is indeterminate, so it may safely be assumed that V_e^* will always lie somewhere between V_p and V_s.

To recap, it is suggested that a coaxial jet at an area ratio of four has a complex mixing region that differs in certain details from the same region at an area ratio of two. In particular, it is assumed that extra entrainment of secondary flow gases by turbulent processes in the inner shear layer, as well as the postponement of the onset of the effective jet zone due to the larger secondary diameter, cause the turbulence and similarity characteristics of the subsequent region to scale on a velocity which is about 8.5% less than the full centreline velocity employed at the area ratio of two.

7.6 Isothermal Predictions of Jet Noise at $\beta = 4$.

The reduced velocity effective jet may now be incorporated into the model and the full prediction compared with measured spectra. Despite the fact that the experimental database of reference [44] is relatively sparse at the area ratio of four, enough test points are available to give an indication of the influence of the changed effective jet, as well as any other trends which may have developed in the conversion to a larger area ratio.

The following sections deal with the predicted isothermal jet spectra in approximately the order in which they were carried out, starting with two cases at 90° for a velocity ratio of $\lambda = 0.6$ at different absolute velocities, from which the optimum reduction to the effective jet velocity was originally deduced. The fit of these spectra to the data will therefore be the best obtainable, but the subsequent predictions, using the same reduction at other velocity ratios and angles, will demonstrate if the hypothesis has any merit. The following illustrated predictions are only a selection of those carried out, but they have been chosen to best represent the changing qualities of the predictions, as well as any errors which have been identified as the jet conditions vary.

7.6.1 Prediction and Data at 90° and $\lambda = 0.6$

Figure (39) a) illustrates the measured and derived spectra of the noise observed at 90°, from a coaxial jet with a secondary jet exit velocity of 135m/s and a primary jet velocity of 215m/s. It can be seen that the measured data has been predicted to a high level of accuracy, comparable with that of the predictions for the area ratio two cold jet spectra. The low frequency end of the predicted spectrum is made up almost entirely of

mixed jet noise with a marginal addition from the effective jet, but as the data starts to level out at the peak, the mixed jet contribution drops away and it is the increasingly dominant contribution from the effective jet which maintains the full predicted spectrum at the level of the data.

The second figure in this section, (39) b), shows the spectra at all the same conditions as above except for the absolute jet velocities, which are 270m/s and 170m/s for the primary and secondary jets respectively. The quality of agreement is as good as that shown at the lower velocity, although it is noticeable that the balance of contributions is slightly different from the previous case. In particular, the effective jet spectrum is at a higher level and is therefore dominant over a greater range of frequencies, but this extra noise is required by the prediction in order to fit the measured spectrum.

7.6.2 Other 90° Predictions and Data

The agreement between predicted and measured 90° spectra at λ = 0.8 is excellent in both low and high velocity cases, as shown in figures (40) a) and b). The contribution from the effective jet at this velocity ratio is much less significant than at λ = 0.6, but where its effect can be observed the result is certainly not detrimental to the quality of prediction.

Finally at 90°, figure (40) c) shows the data and predictions for a common jet velocity of 170m/s. The predicted spectrum comprises the mixed jet and secondary jet contributions with almost no effective jet noise. The resultant fit is excellent at all frequencies and illustrates nicely the balance between the opposed cut off rates of the two significant model spectra.

7.6.3 Predictions at Other Angles

Moving firstly to the forward arc of observation, figures (41) a), b) and c) show the comparisons between predicted and measured spectra at a measurement angle of 120° for the velocity ratios of λ = 0.63, 0.79 and 1.0 respectively. At λ = 0.63, the fit of the prediction at 120° is not quite as good as it is at 90°, the error appearing as a slight over prediction for the range of frequencies surrounding the data peak. It is difficult to determine whether the fault lies in the contribution from the effective jet or that from the mixed jet, since the error is small, and only occurs where their

contributions are very similar in level. At the intermediate velocity ratio of $\lambda = 0.79$, the quality of prediction is improved, although it could be argued that a small but systematic over prediction may still exist. However, in the third case, shown in figure (41) c), there is no discernible error at $\lambda = 1$, the prediction even reproducing the characteristic step in the low frequency tail of the spectrum.

Moving now to rear arc noise, figures (42) a) and b) show the predicted and measured spectra from the unit velocity ratio isothermal jet received at the downstream angles of 50° and 40° to the jet axis. It is instantly clear that while the fit of the predicted spectrum to the data at 50° is as good as any of the small angle predictions at $\beta = 2$, the 40° prediction is seriously in error. The fault lies in the region of low frequencies dominated by the mixed jet contribution, which appears to be at least 3dB too high in level. This characteristic error is repeated for all the 40° predictions, but at the important velocity ratio of one we can assume that the measured spectrum should be very similar to any of the three unattenuated single equivalent jet spectra, due to the flow field being so similar to that of a single jet. This is clearly not the case at 40° but it is for the 50° spectra.

Because of the relative simplicity of the predictive model at $\lambda = 1$, it has previously been shown to be a reliable indicator of trends in the data, so we will henceforth assume that the discrepancies observed in these area ratio four predictions at small angles are due to a difference between the single jet noise prediction database of ESDU and the measurements of Pyestock. This is not without some merit, since the ESDU method does a lot of interpolation at this sparsely populated region of the database, as indicated by the uneven spectral shapes. Therefore, the subsequent comparisons of area ratio four jets will be at an observation angle of 50°.

The last group of isothermal jet spectra, figures (43) a) to d) show 50° noise predictions at two velocity ratios at each of two absolute velocities. Starting at the lowest of both variables, figure (43) a) illustrates the case for a velocity ratio of $\lambda = 0.63$ at a secondary velocity of 135m/s. It is clear that as before, the dominant contributor at low frequencies is the mixed jet, while the high frequency prediction comprises the effective jet and a minor addition from the secondary jet. At the peak, a good fit is achieved by the combination of a diminishing mixed jet and an ascendant effective jet. Minor low frequency over prediction appears to be caused by an over estimate of the mixed jet contribution, which might be a hint of the

problem encountered at 40°. Figure (43) b) shows spectra at the same velocity ratio but higher overall velocity. The first thing to notice is that the balance of contributions at high frequencies has changed, leaving the effective jet as the principal noise source beyond the peak. The additional contributions from the secondary jet and the rapidly decreasing mixed jet are insufficient to maintain the prediction at the same level as the measured spectrum, leading to systematic under prediction, although the fit is within 1dB for at least two octaves after the peak. Over prediction of the mixed jet spectrum is less apparent in this case.

Despite significant differences in the relative contributions of the single jets to the predictions at a velocity ratio of $\lambda = 0.79$, it is evident from figures (43) c) and d) that the characteristics shown at $\lambda = 0.63$ can be seen again. At the lower absolute velocity, (43) c), the mixed jet is over estimated, leading to over prediction of the low frequency end of the data. In addition, although the measured peak levels and upper end of the spectrum are well predicted, the peak of the predicted spectrum is at too low a frequency. At the higher velocity, (43) d), the only notable errors are seen at the highest and lowest frequencies, due to insufficient effective jet and over prediction of the mixed jet respectively.

7.7 Predictions at $\beta = 4$ for Jets with Hot Primary Flow.

The prediction of the noise spectra from area ratio four jets with high temperature primary flow involves a further alteration to the effective jet conditions, namely a reduction in temperature due to the pre-mixing we have assumed to account for the required reduction in centreline velocity. Now, the temperature of the effective jet is dictated by the optimum reduction in the jet velocity, x in equation (7.1.4), which is in turn obtained from examination of the original predictions based on the full effective jet velocity. Since the levels of the predicted effective jet spectrum now depend on the temperature of the jet, it appears that the process of optimisation may be complicated. However, it will be remembered that in chapter 6 it was argued that the temperature has no significant effect on the physical characteristics of the flow field, in which case it is reasonable to assume that the degree of pre-mixing at an area ratio of four is unaffected by temperature, and the optimum effective jet velocity for cold jets may also be used for hot jets.

It will be shown in the following sets of predictions that a reasonable quality of prediction may be achieved over a reduced range of hot jet conditions at an area ratio of four, although certain characteristics of low velocity ratio hot jet noise are not modelled very well by the present scheme.

7.7.1 Hot Jet Predictions at 90°

Starting at a velocity ratio of one, figure (44) a) shows a high quality of prediction, with all the model components making some contribution to the final predicted spectrum. Despite the effective jet spectrum being low compared to the other two spectra, its contribution is significant in improving the low frequency prediction by enhancing the mixed jet noise.

Two predictions at $\lambda = 0.8$ are shown by figures (44) b) and c), illustrating high and low speed cases. The first, at a secondary velocity of 267m/s, has a similar level of accuracy to the unit velocity ratio example above, even though the effective jet contribution is more significant at all frequencies. The slower condition, at $V_s = 170$m/s, has not been predicted as successfully, showing a mismatch of spectrum shape at the low frequencies and insufficient levels at the predicted peak. At the high frequency end of the spectra, the fit has improved, indicating that the secondary jet contribution at least is behaving like the true sound sources found near the coaxial nozzle.

The last three predictions at 90° are for the velocity ratio of $\lambda = 0.63$, at the secondary velocities of 267m/s, 170m/s and 132m/s respectively. In a similar manner to that shown by the $\lambda = 0.8$ predictions, the quality of these predictions deteriorates as the absolute velocity decreases, due apparently to an over estimate of the effective jet spectrum. It is clear that for frequencies where either the mixed or the secondary jet spectra dominate, the fit is excellent. Even for the worst case shown by figure (44) f), although the effective jet dominates the low frequency end of the predicted spectrum, the quality is satisfactory. However, over estimates of the peak levels of the effective jet contribution are significant, amounting to 2dB more than the data for the slowest jet, with a resultant over prediction of 3dB two octaves beyond the peak of the data. These same cases will now be presented at other angles.

7.7.2 Hot, $\beta = 4$ Predictions at 50° and 120°

Firstly, figure (45) a) shows the prediction at 50° for the unit velocity ratio case. Although the low frequency end of the data is well predicted by the mixed jet spectrum, its contribution at the data peak is insufficient and a slight under prediction results. As the secondary jet spectrum rises to dominance, the fit improves again.

The peak levels are again under predicted at different $\lambda = 0.8$ cases. In the faster example shown by figure (45) b), the predicted peak consists of a slightly dominant mixed jet and a significant addition from the effective jet which, due to its temperature, emits less noise at high velocities than the slower mixed jet. The relative contributions are reversed at lower speed, figure (45) c), because the hot effective jet now emits enough noise to dominate the mixed jet, but in neither case can their combined noise level match the measured noise from the coaxial jet. The highest and lowest frequencies are predicted with improving accuracy, particularly in the former case where the secondary jet becomes dominant. The prediction for the slower jet at 120° is also illustrated, as representative of the accuracy obtained in the forward arc. A good agreement is observed over the majority of the data, although a slight secondary peak appears in the predicted spectrum at precisely the point where the three single jet contributions are at the same level.

The three cases of $\lambda = 0.63$ jets with decreasing overall velocities are shown again at 50°, in figures (45) e), f) and g). In complete contrast to their behaviour at 90°, the quality of predictions improves as the velocity diminishes. The spectrum of the fastest jet, with a secondary velocity of 267m/s, suffers serious under prediction at the peak and for at least two octaves beyond. The mixed and secondary jets appear to be contributing suitably to the prediction at low and high frequencies respectively, but the central region of the very pointed spectrum is only supported by the effective jet spectrum, which is significantly too low to maintain the fit. The intermediate secondary velocity of 170m/s shows a vastly improved fit to the data, principally due to the shape and level of the effective jet spectrum which now match the characteristics of the measured spectrum. A marginal under prediction is still evident, but to each side of the peak the data has been well matched, with small but useful additional noise contributions from the mixed and secondary jets. The slowest of the $\lambda = 0.63$ cases is shown in figure (45) g), and it is clear that the effective jet

constitutes the majority of the predicted spectrum at this condition, yet the quality of prediction is as good as any to be seen in previous chapters. Where the effective jet spectrum does move away from the data, the quality of prediction is maintained by precisely the correct contributions from the mixed and secondary jets as they become significant.

Finally, the lowest velocity ratio at the intermediate velocity is shown in figure (45) h) for 120°. The overall fit is within 0.5dB except for a two octave region of over prediction just above the peak frequency. A very similar characteristic was seen in the same jet at 90°, figure (44) e).

7.8 Observations and Conclusions.

The application of the predictive model to coaxial jets of area ratio four has not been straightforward, due to problems associated with the noise attributed to the effective jet. By assuming that the flow field at $\beta = 4$ is significantly different from that at $\beta = 2$, a reduced effective jet velocity has been adopted. This has been attributed to a greater degree of turbulent mixing before the beginning of the effective jet region. When empirically determined, the optimum velocity of the effective jet at an area ratio of four for cold jets appears to be independent of the velocity ratio, and amounts to just over 90% of the primary velocity. This reduction causes the effective jet noise contribution to be modified, thus greatly improving the agreement between predicted and measured spectra. There are no obvious systematic errors in the cold jet predictions, although the measured levels of low frequency noise at 40° were considered to be at variance with the predicted spectrum at a velocity ratio of one, and were thus rejected in favour of comparisons at 50°.

In further extending the model to jets with high temperature primary flow, account has been taken of the extra mixing and its effect on the temperature of the new slower effective jet. It was assumed at this point that the effective jet temperature would be reduced due to entrainment of air from the secondary jet stream, the extent of reduction being ascertained from the similarity between temperature and velocity profiles.

It is immediately clear from some of the figures illustrating the data and corresponding predictions that the model can no longer predict all the changes that occur in the radiated mixing noise as the temperature of the primary flow of this larger jet is increased. In particular, it appears that the

contribution of the effective jet is at fault. At all conditions and angles it is notable that where the mixed or secondary jet contributions are dominant, the fit of the prediction to the measured spectrum is relatively good, whereas the greatest errors occur when the effective jet spectrum is dominant. In essence, although the significant errors in the predicted spectra all occur at low velocity ratios, they are concentrated at small angles in jets of high overall velocity, and at roughly perpendicular angles for slow jets. This phenomenon cannot be explained in terms of a single directivity problem, and further progress is unlikely before more detailed information on the flow field and turbulence structure at different area ratios becomes available. In absolute terms it can be argued that the prediction method still provides a useful estimate of spectral levels and shape in the forward arc and at 90°, and the degree of error never amounts to more than ±3dB as the angle of observation moves around the rear arc to 50°.

In conclusion, the noise from isothermal coaxial jets of area ratio four at a selection of angles and velocity ratios has been successfully predicted by empirically adjusting the velocity of one component of the flow model.

Unfortunately, the limits of this model have been over stretched by trying to predict the noise from coaxial jets with high temperature primary flow. The resultant errors are evident at low velocity ratios and exhibit unexplained directional characteristics.

Chapter 8

The Model in a Flightstream.

The need to predict accurately the noise generated by the exhaust of jet engines is as important when the engine is in flight as when it is in a stationary ambient medium. This thesis puts forward a method of modelling three dominant and spatially distinct sound source regions within the exhaust flows of stationary coaxial jets. The model was used initially to re-predict the isothermal measured spectra from which it was developed, and has been extended to successfully predict the noise spectra from jets of the same size but with hot primary flow. At a larger area ratio, the sound emissions of isothermal jets have been predicted with qualified success, but the hot jet predictions were less satisfactory. It remains to be seen if the stationary model can be utilised to predict the far field noise of a coaxial jet in a simulated flight stream.

8.1 Introduction

The problems of in-flight prediction have been approached from a number of directions, the primary requirement being to reproduce noise data from engines moving forwards relative to a surrounding medium. Measurements from moving jet engines include full scale flight testing, a method used by Michel and Bottcher [45]; carriage on ground based vehicles, for example the Bertin Aerotrain; and spinning rig configurations such as that used by Rolls Royce and reported by Cocking [57]. An alternative method involves placing a stationary jet within a larger jet stream to simulate forward motion. This was the method chosen by the experimental team at Pyestock which provided the noise data we are trying to predict. The method involves some different considerations from those for a moving nozzle, and they can be summarised as follows; Propagation effects at the flight stream shear layer, and the absence of relative movement between nozzle and observer. As a test of the present prediction model, a scheme which converts static jet noise spectra to in-flight data has some practical benefits, especially when it is considered that the data for jet noise in flight has been obtained using a static jet nozzle in

simulated flight. If we can successfully apply a static to flight correction scheme to the present model of discrete sound sources, then it could be argued that we are correctly modelling those aspects of the stationary coaxial jet exhaust which change in flight.

A number of works have been published describing the changes required to convert simulated flight data to actual in flight or flyover data, notably by Cocking and Bryce [58] and Morfey and Tester [59], which demonstrate that satisfactory conversion can be achieved as long as the flight stream to jet area ratio is large, specifically greater than forty. The specific problem of differences between simulation and true flight will therefore not be dealt with in this work.

8.2 The Experimental Test Regime

Because the primary objective of the experimental studies was to measure and examine jet noise sources, the flight simulation was limited to only one simulation velocity of $V_f = 55m/s$, at the secondary jet velocity of $V_s = 170m/s$. The area ratio two case is well represented, with data from jets at eight velocity ratios between 0.56 and 1.24. For hot jets and jets at the larger area ratio, the two extremes of 0.63 and 1.24 have been tested.

The diameter of the flight simulation nozzle was a constant 0.54m, which provides flight to jet area ratios of 75 and 46 for the coaxial jet area ratios of $\beta = 2$ and 4 respectively. As for the previous sets of measurements, the data is presented in the form of third octave spectra received at every ten degrees of jet axis to microphone angle θ_m between 30° and 130°.

For each measurement position, the in flight emission angle θ_f has subsequently been calculated, and corrections for shear layer refraction and background noise due to the flight stream have been applied to the raw data. The flight data also incorporate a Doppler frequency correction. These corrections were derived by Bryce and Pinker [60], based on earlier experiments in the anechoic facility at DRA Pyestock. In the form presented in the Pyestock reports [44] and [61], the results are those which would be obtained if the jet were actually in flight. The data and corresponding predictions of this chapter are all presented in terms of the flight angle θ_f, but this is only a change of labels, the data is unaltered.

8.3 The Static to Flight Correction Method

The static coaxial jet prediction model is made up of three equivalent single jets, parts of whose spectra combine to form the predicted spectrum of the coaxial jet. A straightforward test of the validity of this model would be to apply a single jet static to flight correction to each of the components and compare the final spectrum with the simulated flight data from Pyestock. It was considered sensible to adopt the scheme developed by ESDU in reference [62] for the reasons described at the end of section 4.2, as well as for the sake of consistency. It must be stressed that this correction scheme was derived entirely from single jet data and is only designed for the conversion of single static jets to the flight situation.

The conversion to flight is achieved through three different empirically derived adjustments which are applied to stationary jet data. These are provided in the form of a FORTRAN program which predicts the in flight spectrum of a single jet whose stationary noise spectra over a range of angles are available to the program, as outlined below.

- The first correction is a transposition of the static emission angle θ_m to the flight emission angle θ_f, as shown in figures (46) a) and b), so that the spectrum measured at the former angle is now seen at the latter. The flight emission angle, from Bryce [63], is given by

$$\cos\theta_f = \frac{\cos\theta_m}{1-0.65M_a\cos\theta_m} \tag{8.3.1}$$

where M_a is the flight Mach number V_a/a_o. The factor of 0.65 is included to account for the fact that the ambient medium is now moving, which reduces the shear between the jet and its surroundings.

- The second change is a shift in spectral levels due to the effects of movement on the source, which takes the familiar form

$$\Delta SPL = 10\log_{10}\left(\frac{V_j}{V_{rel}}\right)^m \tag{8.3.2}$$

and which constitutes the most significant adjustment to the noise spectrum.

In the ESDU scheme, the velocity exponent m has been derived using empirical correlations of experimental data and is given by

$$m = 5.4 + 4.2\left[1 - 0.5\left(\frac{V_f}{V_j}\right)\right]\left(\frac{V_j}{a_o}\right)\cos\theta_f + \left(\frac{V_j}{a_o}\right)^{1.3}(0.5\cos\theta_f - 1)\sin 2\theta_f$$

$$+\tau\left[\left(\frac{V_j}{a_o}\right)\left[1 - 2\left(\frac{V_j}{a_o}\right)\cos^2\theta_f\right]\cos\theta_f - 1\right] \qquad (8.3.3)$$

where the temperature function τ is given by

$$\tau = \frac{1.2\left[\left(T_j/T_o\right) - 1\right]^2}{\left[\left(T_j/T_o\right) - 1\right]^2 + 0.05\left[\left(T_j/T_o\right) + 0.7\right]\left(V_j/a_o\right)^2} \qquad (8.3.4)$$

The rather complicated expressions above, from the flight prediction work of Bryce [63], serve to slightly alter the velocity exponent from its normalised value of m = 5.4 due to a dependence on jet velocity, angle of measurement and jet to ambient temperature ratio.

As an example of the reduction we might expect to see in the spectral levels of a typical jet in flight, a cold single jet (τ = 0) of exit velocity 170m/s surrounded by a flightstream of 55m/s will experience a correction of approximately -9dB. If the temperature of this jet is increased from the ambient condition so that $T_j/T_o = 3$, the value of the temperature factor at 90° becomes τ = 1.2, changing the velocity exponent to m = 4.0. The resultant flight reduction is therefore reduced to -6.8dB, a change of +2.4dB.

The reduction factor given by (8.3.2) can be rewritten thus;

$$\Delta SPL = -10\log_{10}\left(1 - \frac{V_f}{V_j}\right)^m \qquad (8.3.5)$$

From this expression it is clear that the reduction in spectral level due to flight actually becomes smaller as the jet velocity increases, despite the position of the jet velocity as numerator in the initial formula.

- Thirdly, a Doppler shift is applied to the measured static jet frequencies in order to correctly model the change due to enhanced source convection. The ratio of flight to stationary frequencies is given by

$$\frac{f_f}{f_s} = \left[1-\left(\frac{V_f}{V_j}\right)\right]\left[1+1.2\tau\left(\frac{V_f}{V_j}\right)\sin\theta_f\right]\left[1+0.2\sin^2 2\theta_f \cos^2\theta_f - 0.08\tau\right]$$

(8.3.6)

8.4 Extension of Flight Correction to Coaxial Jets

The predicted stationary coaxial jet spectrum comprises noise spectra from three independent, isolated single equivalent jets which model the sound sources within the more complicated mixing of the coaxial jet exhaust. It is now proposed that the effect of flight on the noise of coaxial jets may be reproduced by applying a single jet flight correction scheme to each of the single jets comprising the model. It is therefore being assumed that the predictive model, originally developed to predict the acoustic behaviour of coaxial jets, will also mirror the physical changes which lead to the noise differences in flight. By using the static to flight correction scheme outlined above, it becomes a straightforward exercise to convert each stationary equivalent jet spectrum measured at a microphone angle θ_m to an in-flight spectrum at the corresponding flight angle θ_f.

The effect of a simulated flightstream on the noise spectrum of coaxial jets is well illustrated in the Pyestock report [44], of which two representative examples are shown in figures (47) a) and b). They show static and in-flight spectra for a coaxial jet of area ratio of $\beta = 2$ at the two velocity ratios of $\lambda = 0.8$ and 0.56 respectively. It is clear that significant changes do occur in the spectrum of coaxial jets in changing from static to simulated flight conditions, and that these changes are dependent not only upon the absolute velocities, but also on the velocity ratio of the coaxial flow.

As mentioned above, the ESDU static to flight correction scheme requires a database of static noise data for a range of measurement angles, from which it interpolates to the flight angle specified by the user. In order to predict the effect of flight at various angles on each of the three contributing jets independently, it is therefore necessary to provide sets of static spectra for the secondary, effective and fully mixed jets over a wide range of static angles for every different jet condition. Since the final predictive model comprises three single jets at different velocities, the coaxial jet flight correction actually consists of three corrections which depend on the conditions of these jets. Now the most significant part of the

ESDU flight correction is the reduction in spectral level, which is dependent upon the jet velocity. Since the effective jet is always the fastest of the three components, it will suffer the least flight reduction, and similarly the secondary jet will be reduced the most. This will exacerbate the differences between the contributing spectra at low velocity ratios, and certainly lead to predicted changes in flight which are velocity ratio dependent, but it remains to be seen if these are in sympathy with the changes in the measured data.

8.5 Predictions of Simulated Flight Data

In this section, selected simulated flight data will be presented alongside the corresponding predicted spectra, starting with isothermal jets at $\beta = 2$, then hot examples with the same geometry, followed by cold and hot jets at $\beta = 4$.

An example of the magnitude of the correction in noise level due to flight is illustrated by the isothermal jet at $\beta = 2$ and $\lambda = 0.63$. The measured spectrum in the flight case, illustrated in figure (51) c), differs in level from that of the stationary jet shown in figure (18) b) by about -7dB, while the corresponding single jets comprising the predictive model are each reduced by different amounts due to their different velocities. The secondary jet, at a velocity of 168m/s, suffers an overall flight reduction of -9.3dB, the mixed jet at 215m/s is reduced by -7.0dB and the effective jet at 266m/s is reduced by only -5.4dB. Despite this disparity in the flight factors for the three component jets the final prediction, which comprises these apparently divergent contributions, is within 1dB of the data over the vast majority of the spectral range.

8.5.1 Isothermal Jets of Area Ratio $\beta = 2$ in Flight

Figures (48) a) to d) illustrate the predicted spectra and the data for the case where the primary velocity is equal to the secondary velocity, at flight angles of 29.6°, 57.5°, 90.2° and 118.0°. The predictions at all angles are excellent, exhibiting scatter in the order of 0.5dB across the spectrum and only showing systematic error in the form of slight underprediction for the smallest angle at high frequencies.

The successful prediction of this particular jet condition in flight demonstrates only that the static to flight correction scheme can be relied

upon to predict the flight changes observed in single jets, since the coaxial jet at the velocity ratio of one is equivalent to the single jet case. The three single jets of the present model are all the same at $\lambda = 1$, so the same correction factors are applied to each one. The only difference between the predicted noise from this coaxial jet and that predicted for a single jet is due to the presence of the effective jet contribution which, as in the static case, affords a small but useful addition to the predicted spectrum.

As the primary velocity is increased the velocity ratio becomes less than one, and the noise from the coaxial jet increases. In terms of the current model, the interaction region of the jet becomes more and more dominant. Now the principal effect of flight on a jet is to reduce the noise by an amount proportional to $(V_j/V_{rel})^m$, so at a constant flight speed, the noise reduction gets less as the jet velocity increases. It is therefore fair to say that as the primary jet velocity increases, the increasingly dominant effective jet contribution will be even more relevant in flight as it will not be reduced by as much as the other contributing spectra.

The next velocity ratio is $\lambda = 0.79$, shown in figures (49) a) to d) at similar flight angles to above. The smallest angle predicted is 29.2°, which again shows excellent fit to the data, but as the observer position moves through 57.3° to 90.2° and 118.2°, a systematic over prediction develops. This directivity error is seen at frequencies above the peak of the data and is greatest in the forward arc position, amounting to +1.5dB. It should be noted that the predicted spectrum at this velocity ratio comprises significant noise contributions only from the mixed and effective jets, of which the former is always dominant.

Figures (50) a) to d) illustrate the velocity ratio of $\lambda = 0.70$. Again the frequencies beyond the peak of the data are suspect, but now it is evident that the directivity effect is greater, causing under prediction for the smallest angle as well as over prediction of the measured noise at 90.2° and 118.3°. It is noticeable that the mixed and effective jets are much closer in level at this velocity ratio, but their combined spectrum exhibits similar errors to the $\lambda = 0.79$ case which was dominated by the mixed jet spectrum. Despite these discrepancies the general quality of prediction is good, fitting the measured spectrum within 1dB for the majority of the frequency range and matching the spectral shape well.

Finally in this section, predicted and measured spectra at the lowest velocity ratio of $\lambda = 0.63$ are illustrated by figures (51) a) to d). The directivity problem is still evident at the smallest and largest angles, but

the over prediction seen at 90.2° and 118.0° are not as bad as those observed above, at $\lambda = 0.7$. The contribution of the effective jet is at least as significant as the mixed jet spectrum at all angles for this velocity ratio. It is interesting to note that the errors in prediction do not increase substantially as one or other of the contributing jets becomes dominant, suggesting that the problem lies not with any single component but rather with the directivity of the whole model in flight. It is possible that the flight stream surrounding the coaxial jet flow subtly alters the directivity of some or all of the modelled regions, but without detailed velocity and turbulence measurements in simulated flight conditions, it is impossible to estimate the validity of such an idea.

8.5.2 Hot Jets at $\beta = 2$ in Flight

Turning now to coaxial jets of area ratio two in flight but with heated primary flow, the experimental tests only include jets with a velocity ratio of $\lambda = 0.63$ at primary jet temperatures of 600K and 800K. The first group of figures, (52) a) to d), show data and prediction for a secondary jet velocity of 134.6m/s and a primary jet with a velocity of 212.5m/s and a temperature of 600K. It should be noted that this is a particularly slow jet when compared with either previous examples or with the single jets in the predictive database of ESDU.

It can immediately be seen that the secondary jet has no significant influence on the predicted spectrum due to its extremely low level of noise, and that the prediction therefore consists of the combined noise contributions of the mixed and effective jets. It is also evident that the overall quality of prediction is not as good as that for isothermal jets seen above. Apart from the prediction at 30.5°, the model under predicts the low frequencies and over predicts the high frequencies due to a poor approximation of the spectral shape, although the error is never more than ±1.2dB. The lowest angle appears to reverse this pattern, although the error in this case is best described as a shift in frequency of the whole spectrum by one third octave.

Figures (53) a) to d) show the flight spectra for another jet of velocity ratio $\lambda = 0.63$, but at a secondary velocity of 266.7m/s with a primary jet of velocity 423.2m/s and a temperature of 800K. Similar characteristics are observed, but not to such an exaggerated degree as the slower jet at 600K. The only significant deterioration in predictive quality

is for the smallest angle, which is now under predicted at the peak of the data by 3dB.

The conditions of this jet are more typical of the single jet noise database, which is evident from the relatively smooth appearance of the contributing spectra due to reduced dependence on interpolation by the ESDU scheme. The resultant predictions, with the exception of that at 30.7° are all within 1dB of the measured spectrum.

It should be pointed out that in general, the quality of these particular simulated flight predictions is commensurate with that for the equivalent stationary jets described in section 6.3.3, although there are individual points where the fit is significantly worse, and it can be argued that the process of converting to flight at these conditions is not the primary cause of inaccuracy. In particular, a comparison of the static and flight predictions for $\beta = 2$ jets at 800K, shown in figures (36) a), b) and c) and (53) a), c) and d) respectively, show significant similarity in both the frequency and magnitude of the prediction errors.

8.5.3 Cold and Hot Jets at $\beta = 4$ in Flight

The last two sets of diagrams in this chapter illustrate the measured and predicted spectra for jets of area ratio four in simulated flight conditions, with the optimised effective jet velocity of section 7.5 incorporated into the model. Firstly, (54) a) to d) show isothermal jet spectra at four flight emission angles. This is another very slow jet, with characteristically flat spectral shapes even at 30.5°, but it is evident that the predicted spectra are generally poorer in quality than any at $\beta = 2$. This appears due to errors in the prediction of spectral level and shape, leading to noise level discrepancies of up to ±3dB although the 57.3° prediction is surprisingly good. It is not possible to identify the principal source of error, because the spectral contributions from the effective and mixed jets are so similar. It is again interesting to compare predictions of the same jet at static and in-flight conditions, shown for example by (43) a) with (54) a), or (41) a) with (54) d). The errors are certainly not similar in magnitude, but some of the qualities exhibited by the predicted spectrum as it diverges from the static data can be identified to a greater extent in the flight predictions, suggesting that some of the predictive error may already be present in the static area ratio four prediction. If the principal fault involves an over prediction of the high velocity effective jet for example,

then this will certainly be aggravated in the process of converting from a stationary spectrum to one in flight because of the reduced flight effect on fast jets.

Finally, hot jet spectra at the same angles are shown in (55) a) to d). These jets are truly as far from the stationary, isothermal $\beta = 2$ jets as the data goes, and some significant errors are starting to appear. At 31.0°, the measured peak is under predicted by 2dB, although the predicted shape is representative of the data. At 90.0° the over prediction amounts to 2dB for nearly three octaves around the measured peak, corresponding to a very dominant and sustained effective jet contribution. Very similar behaviour is observed in the prediction for 117.8°. Only the data measured at a flight angle of 57.4° has been well predicted, for no explicable reason; the effective jet contribution is equally dominant, but in combination with the mixed and secondary jets, the final prediction is absolutely perfect.

Corresponding static jet spectra are shown in figures (44) e) and (45) d) and e), and it is again argued that some qualitative aspects of the in-flight prediction errors may be seen in these static jet spectra.

8.6 Observations and Conclusions

The purpose of this chapter was to investigate the effect of a flightstream on the noise emitted from a coaxial jet, with the objectives of firstly providing a test of the physical basis of the stationary jet noise model, and secondly producing a viable prediction scheme for coaxial jet noise in flight. Empirically derived single jet static to flight corrections have been applied to each of the three contributing equivalent single jets before summation and hence the coaxial jet simulated flight data have been predicted.

The static to flight corrections are in three parts; a sound level reduction based on the relative jet velocity ($V_j - V_f$), the flight angle and a function of the jet temperature; an angular transposition; a Doppler shift.

The prediction of noise from isothermal jets of area ratio two in flight has been carried out with notable success over a range of velocity ratios and flight angles, showing a degree of accuracy comparable with the same jets in stationary conditions.

Jets of area ratio two with hot primary flow have been predicted in flight with qualified success; the predictions deviate from measured spectra at small and large angles and at the limits of the frequency range, although the shapes and overall levels are in reasonable agreement. Similarity between these flight predictions and equivalent static examples suggests that prediction errors are not due principally to the process of flight conversion but were already present in the prediction of the static hot jet, and have been exacerbated by the adjustments necessary for flight prediction.

At an area ratio of four, cold and hot jet spectra have been predicted which exhibit small but systematic errors. However, some of the deviations of the predicted spectra from measured data are similar in character to the discrepancies observed in the corresponding static cases, suggesting that a proportion of the error lies in the static jet prediction.

Until detailed turbulence and velocity information for the interaction region of jets of area ratio four is obtained, the present model represents a useful tool for the prediction of coaxial jet noise, although there is a limit to the extent the static prediction can be used to predict in-flight jet noise.

Summary and Conclusions.

A predictive model has been developed from a limited coaxial, isothermal, jet noise database which has subsequently been shown to predict the noise spectra measured from jets at a wide range of velocity, area and temperature ratios. It is believed that in many important ways the model reflects the aerodynamic behaviour of coaxial jet exhaust mixing processes.

The true coaxial flow has been divided into three regions within which the velocity and turbulence characteristics are largely consistent with those of a single jet, and it is the contention of this thesis that the noise issuing from the mixing regions of the coaxial flow can be approximated by the incoherent sum of the noise contributions from the parts of the equivalent single jets which represent the true flow field. The principal strength of this method lies in its use of straightforward single jet third octave band spectra as provided for example by the standard SAE Aerospace Recommended Practice ARP 876C [46].

Estimation of the noise spectra of the single jets may be achieved by any means, but for the sake of simplicity and ease of use, an interpolative database method produced by the Engineering Science Data Unit (ESDU) was employed.

The three single equivalent jets represent the following identifiably different regions of the coaxial flow;

- The outer or secondary to ambient shear layer, modelled by a jet with the same diameter as the outer nozzle of the coaxial jet, running at the secondary flow velocity. This jet contributes to the noise generated between the nozzle exit plane and the end of the secondary potential core.
- The complex mixing zone characterised by non-similarity of velocity and turbulence profiles which is found at the coincidence of the inner and outer shear layers. This is modelled by a single jet operating at the primary jet velocity which provides the same thrust as the full coaxial jet, but with a peak turbulence level of 10% rather than 15%.
- The fully merged jet found downstrean of the end of the primary potential core, which is modelled by a single jet providing the same thrust and mass flow as the coaxial jet.

Since only part of each of these jets is employed to represent the spectral contribution of a corresponding part of the coaxial jet, their spectra are subsequently curtailed in accordance with carefully argued analysis of source location data.

The resultant noise prediction scheme has been shown firstly to repredict the measured third octave band noise spectra emitted by model scale, isothermal, subsonic, coaxial flow from nozzles with an outer to inner area ratio of two, at a wide range of velocity ratios. The overall quality of fit between measured and calculated spectra is excellent, remaining within a decibel for the majority of the spectral range over a wide arc of observation, at velocity ratios between 0.56 and 1.24.

The model has then been shown to predict the noise from jets with heated primary flow very successfully, and further development has led to modifications enabling jets of different area ratio to be accommodated, albeit with an empirically derived velocity adjustment.

The application of static-to-flight corrections to the component single jets produces changes commensurate with noise measurements taken from coaxial nozzles in simulated flight. In other words, a flightstream has the same effect on the predicted noise as it does on the noise from the true coaxial flow, suggesting that the aspects of coaxial flow which are changed in flight are being correctly modelled.

In conclusion, the present model, developed from limited data, has been shown to reflect large and small scale changes in coaxial jet mixing noise due to different operating conditions with a useful degree of success.

It is recommended that similar success may be achieved for equivalent scale model jets provided that the following constraints are observed;

$$135\text{m/s} \leq V_s \leq 270\text{m/s}$$
$$0.5 \leq \lambda \leq 1.24$$
$$T_o \leq T_p \leq 800\text{K}$$
$$T_s = T_o$$
$$\beta = 2 \text{ or } 4$$

These are dictated partly by the extent of the original database, partly by the extended database used to develop the hot jet model, and also by the limits of Ko and Kwan's experiments at the single area ratio of $\beta = 2$. If the arguments of chapter 7 are correct, then it can be assumed that jets with area ratios between two and four may be predicted successfully by

adopting some interpolated value for the effective jet velocity, and similarly an extrapolation to values below 92% of V_p will provide the effective jet velocity for larger area ratios.

Confirmation of the validity of the model can only be achieved by continued testing. In particular, it would be useful to predict the noise from nozzles with geometries closer to those of working jet engines, such as $^3/_4$ cowl and pre-mix configurations. The most immediate improvement would be achieved by experimental measurement of mean velocity profiles across the jet at positions between three and eight primary diameters downstream of a coaxial nozzle, with area ratios of three, four and five in order to uncover the velocity dependence of the effective jet with area ratio. A more extended study which would be of great value would be the measurement of local turbulence intensity levels at these same conditions in order to more closely pinpoint the characteristics of the effective jet region, and to determine more clearly how the single jet characteristics seen at a velocity ratio of one alter to those so plainly demonstrated at the lower velocity ratios.

References.

[1] Smith M J T (1989)
'Aircraft Noise.' Cambridge University Press

[2] Ko N W M, Kwan A S H (1976)
'The initial region of subsonic coaxial jets.' J.Fluid Mech. **73** 2, pp 305-332

[3] Lighthill M J (1952)
'On sound generated aerodynamically. I. General theory.'
Proc. Roy. Soc., Series A, vol. **211**, pp 564-578

[4] Lighthill M J (1954)
'On sound generated aerodynamically. II. Turbulence as a source of sound.' Series A, vol. **222**, pp 1-32

[5] Phillips O M (1960)
'On the generation of sound by supersonic turbulent shear layers.'
J. Fluid Mech. **9**, pp 1-28

[6] Ribner H S (1964)
'The generation of sound by turbulent jets.' Advances in Applied Mechanics **8**, pp 103-182

[7] Ffowcs Williams J E (1963)
'The noise convected from turbulence at high speed.'
Phil. Trans. Roy. Soc. A **255**, pp 469-503

[8] Lush P A (1970)
'Measurement of subsonic jet noise and comparison with theory.'
J. Fluid Mech. **46** (3), pp 477-500

[9] Tanna H K (1976)
'An experimental study of jet noise. Part I: Turbulent mixing noise.'
J. Sound Vib. **50**, pp 405-428

[10] Lilley G M (1972)
'The generation and radiation of supersonic jet noise. Part IV: Theory of turbulence generated jet noise, noise radiation from upstream sources and combustion noise.' AFAPL-TR-72-53, vol. IV.

[11] Lilley G M, Morris P J, Tester B J (1973)
'On the theory of jet noise and its applications.'
AIAA Paper No. 73-987

[12] Mani R (1976)
'The influence of jet flow on jet noise.
Part 1. The noise of unheated jets.' J. Fluid Mech. **73**, pp 753-778
'Part 2. The noise of heated jets.' " " " pp 779-793

[13] Ribner H S (1969)
'Quadrupole correlations governing the pattern of jet noise.'
J. Fluid Mech. **38**, pp 1-24

[14] Laufer J, Kaplan R E, Chu W T (1973)
'Acoustic modelling of the jet noise abatement problem.'
Proceedings of the Interagency Symposium in Transportation Noise,
Stanford University, March 28th - 30th, 1973

[15] Hoch R G, Duponchel J P, Cocking B J, Bryce W D (1973)
'Studies on the influence of density on jet noise.'
J. Sound Vib. **28**, pp 649-668

[16] Lush P A, Fisher M J, Ahuja K (1973)
'Noise from hot jets.' Proc. British Acoust. Soc. Spring Meeting

[17] Tanna H K, Fisher M J, Dean P D (1973)
'Effect of temperature on supersonic jet noise.'
AIAA Paper No. 73-991

[18] Morfey C L (1973)
'Amplification of aerodynamic noise by convected flow
inhomogeneities.' J. Sound Vib. **31**(4), pp 391-397

[19] Fisher M J, Lush P A, Harper Bourne M (1973)
'Jet noise.' J. Sound Vib. **28**, pp 563-585

[20] Tester B J, Morfey C L (1976)
'Developments in jet noise modelling - Theoretical predictions and
comparisons with measured data.' J. Sound Vib. **46**, pp 79-103

[21] Morfey C L, Szewczyk V M, Tester B J (1978)
'New scaling laws for hot and cold jet mixing noise based on a
Geometric Acoustic model.' J. Sound Vib. **61**, pp 255-292

[22] Morfey C L M, Szewczyk V (1977)
'Jet noise modelling by geometric acoustics.
Part I: Theory and prediction outside the cone of silence.'
ISVR Tech. Report 77-91
also: 'Part II: Theory and prediction inside the cone of silence.'
ISVR Tech. Report 77-92
and: ' Part III: A computer program for the prediction of jet mixing noise.'
ISVR Tech. Report 77-93

[23] Ribner H S (1981)
'Perspectives on jet noise.' AIAA paper No. 81-0428

[24] Forstall W, Shapiro H H (1950)
'Momentum and mass transfer in coaxial gas jets.' Trans. A.S.M.E., J. Applied Mech. **10**, pp 399-408

[25] Greatrex F B (1961)
'Bypass engine noise.'
Trans. Soc. Automot. Engrs. Vol. **69**, pp 312-323

[26] Chigier N A, Beer J M (1964)
'The flow region near the nozzle in double concentric jets.'
Trans. A.S.M.E., J. Basic Eng. **86**, pp 797-804

[27] Williams T J, Ali M R M H, Anderson J S (1969)
'Noise and flow characteristics of coaxial jets.' J. Mech. Eng. Sci. **11**, pp 133-142

[28] Eldred K M. (1971)
'Far field noise generation by coaxial flow jet exhausts.'
Wyle Lab. Report, FAA-RD-71-101, 1.

[29] Pau S P, Lowson M V (1970)
'Some applications of jet noise theory.' AIAA paper No. 70-233

[30] Olsen W, Friedman R (1974)
'Jet noise from coaxial nozzles over a wide range of geometric and flow parameters.' AIAA paper No. 74-0043

[31] Cocking B J (1976)
'An experimental study of jet noise.'
National Gas Turbine Establishment (NGTE) Report **333**.

[32] Hammersley R J, Jones B G (1974)
'An experimental investigation of the turbulent characteristics of co-annular jet flows and their role in aerodynamic noise generation.'
2nd Interagency Symposium on Univ. Research in Trans. noise, NCSU, Vol. **I**, pp 36-49

[33] Gliebe P R, Balsa T F (1976)
'The aerodynamics and acoustics of coaxial jet noise.'
AIAA paper No. 76-0492

[34] Tanna H K, Morris P J (1985)
'The noise from normal-velocity-profile coannular jets.'
J. Sound. Vib. **98**(2), pp 213-234.

[35] Stone J R, Groesbeck D E, Zola C L (1981)
'Conventional profile coaxial jet noise prediction.'
AIAA Paper No. 81-1991

[36] Lu H Y (1986)
'An empirical model for prediction of coaxial jet noise
in ambient flow.' AIAA Paper No. 86-1912

[37] Tanna H K (1980)
'Coannular jets - Are they really quiet and why?'
J. Sound Vib. **72**, pp 79-118

[38] Kuznetsov V M, Munin A G (1978)
'Coaxial jet noise and isothermal jets.' Sov. Phys. Acoust. **24**(6),
Nov.-Dec., pp 498-502

[39] Abramovich G N (1963)
'The theory of turbulent jets.' M.I.T. Press.

[40] Fisher M J, Harper-Bourne M, Glegg S A L (1977)
'Jet noise source location: the Polar Correlation Technique.'
J. Sound Vib. **51**, pp 23-54

[41] Strange P J R, Podmore G, Fisher M J, Tester B J (1984)
'Coaxial jet noise source distributions.' AIAA/NASA
9th Aeroacoustics Conference, paper No. AIAA-84-2361.

[42] Lee H S (1984)
'Experimental study on the effects of density, Mach number
and geometry on the large scale structure in a turbulent jet and
its radiated noise.' PhD Thesis, University of Adelaide,
Dept. of Mech. Eng.

[43] Flitcroft E M, Bryce W D (1988)
'A scheme for investigating the basic characteristics of coaxial jet
noise.' Royal Aerospace Establishment, Combustion and Power
plant Noise Division, Noise Note 082/88.

[44] Staff of Noise Section (1991)
'A presentation of the results acquired in the NTF to investigate the
basic characteristics of coaxial jet noise.' RAE Noise Note 116/91.

[45] Michel U, Böttcher J (1992)
'Prediction of jet mixing noise in high-speed flight.'
14th Aeroacoustics Conference, Aachen.
DGLR/AIAA paper No. 92-02-145

[46] Anon. (1985)
'Gas turbine jet exhaust noise prediction.' Society of Automotive Engineers, SAE ARP 867C.

[47] Way D J, Cocking B J (1977)
'The use of co-flowing air streams for the simulation of flight effects on jet noise.' National Gas Turbine Establishment (NGTE) Report **345**.

[48] Davies P O A L, Fisher M J, Barratt M J (1962)
'The characteristics of the turbulence in the mixing region of a round jet.' J. Fluid Mech. **15**, pp 337-367

[49] Brown G L, Roshko A (1974)
'On density effects and large structure in turbulent mixing layers.' J. Fluid Mech. **64** 4, pp 775-816

[50] Panchapakesan N R, Lumley J L (1993)
'Turbulence measurements in axisymmetric jets of air and helium. part 2. Helium jet.' J. Fluid Mech. **246**, pp 225-247

[51] Fisher M J, Harper-Bourne M, Glegg S A L (1977)
'Jet noise source location: The polar correlation technique.' J. Sound Vib. **51**, pp 23-54

[52] Morris P J (1976)
'Turbulence measurements in subsonic and supersonic axisymmetric jets in a parallel stream.' AIAA Journal, **14**, No.10, pp 1468-1475

[53] Powell A (1954)
'The influence of the exit velocity profile on the noise of a jet.' Aero. Quarterly, Vol. **IV**, Feb.

[54] Ribner H S (1958)
'On the strength distribution of noise sources along a jet.' UTIA Report No. **51**.

[55] ESDU Single Jet Noise Prediction Scheme. (E1054)

[56] Tanna H K, Dean P D, Burrin R H (1976)
'The generation and radiation of supersonic jet noise. Vol. III, Turbulent mixing noise data.' AFAPL-TR-76-65 vol. III

[57] Way D J (1976)
'An assessment of the noise from heated and unheated jets measured on the Rolls Royce spinning rig.' N.G.T.E. Internal Report, 1976

[58] Cocking B J, Bryce W D (1975)
'Subsonic jet noise in flight based on some recent wind tunnel tests.'
2nd Aeroacoustics Conference, Hampton, VA.
AIAA paper No. 75-462

[59] Morfey C L, Tester B J (1976)
'Noise measurements in a free jet flight simulation facility: shear layer refraction and facility-to-flight corrections.'
J. Sound Vib. **54**(1), pp 83-106

[60] Bryce W D, Pinker R A (1984)
'Shear layer corrections for flight simulation including flight-stream temperature effects.' Noise Note 002/84, DRA Pyestock.

[61] Mead C J (1993)
'Further model-scale data acquired at higher area and temperature ratio for the study of coaxial jet noise.' Noise Note 129/93,
DRA Pyestock.

[62] ESDU International, plc. (1992)
'Prediction of single-stream jet noise in flight from static circular-nozzle data.' Data Item No. 87011

[63] Bryce W D (1984)
'The prediction of static to flight changes in jet noise.'
AIAA Paper No. 84-2358

[64] Seiner J M, Ponton M K, Jansen B J, Lagen N T (1992)
'The effects of temperature on supersonic jet noise emission.'
14th Aeroacoustics Conference, Aachen.
DGLR/AIAA paper No. 92-02-046

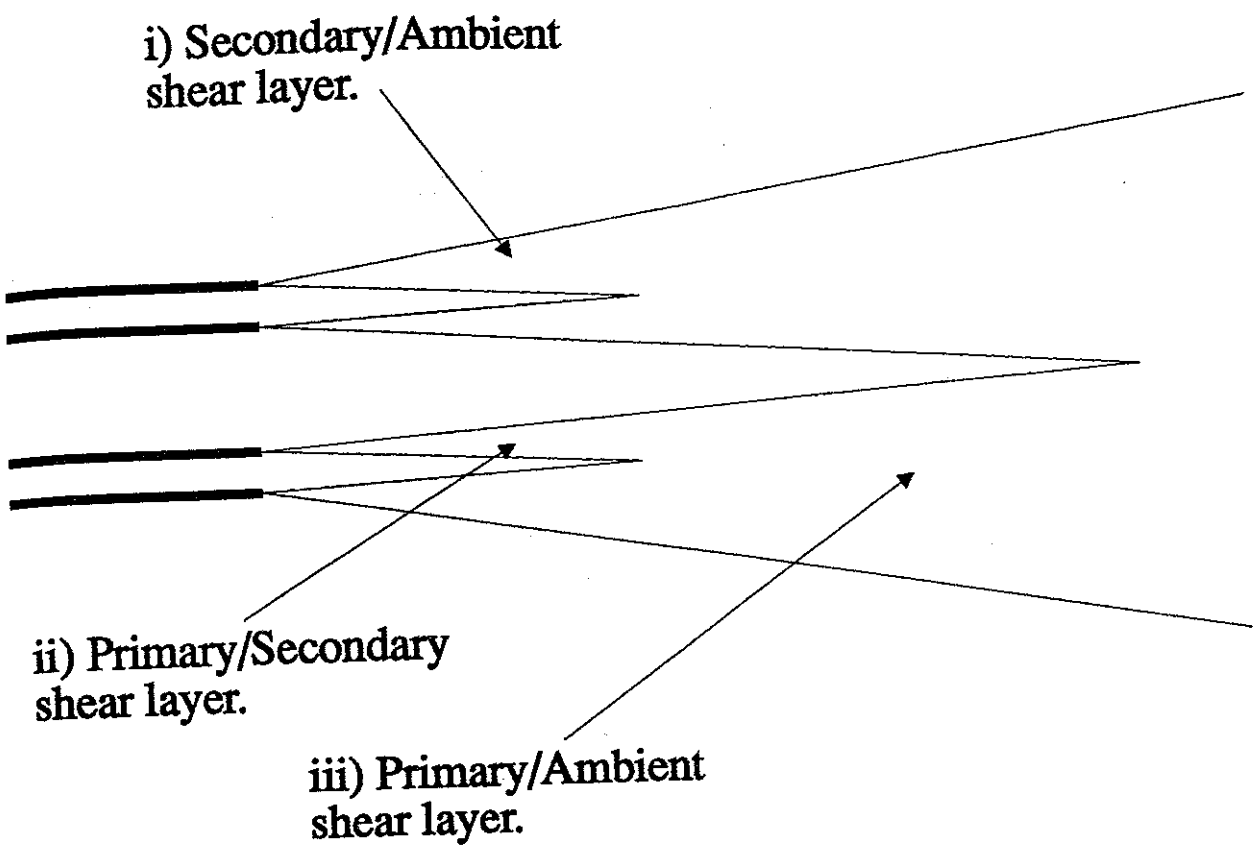

Figure 1. Coaxial jet mixing regions according to Greatrex.

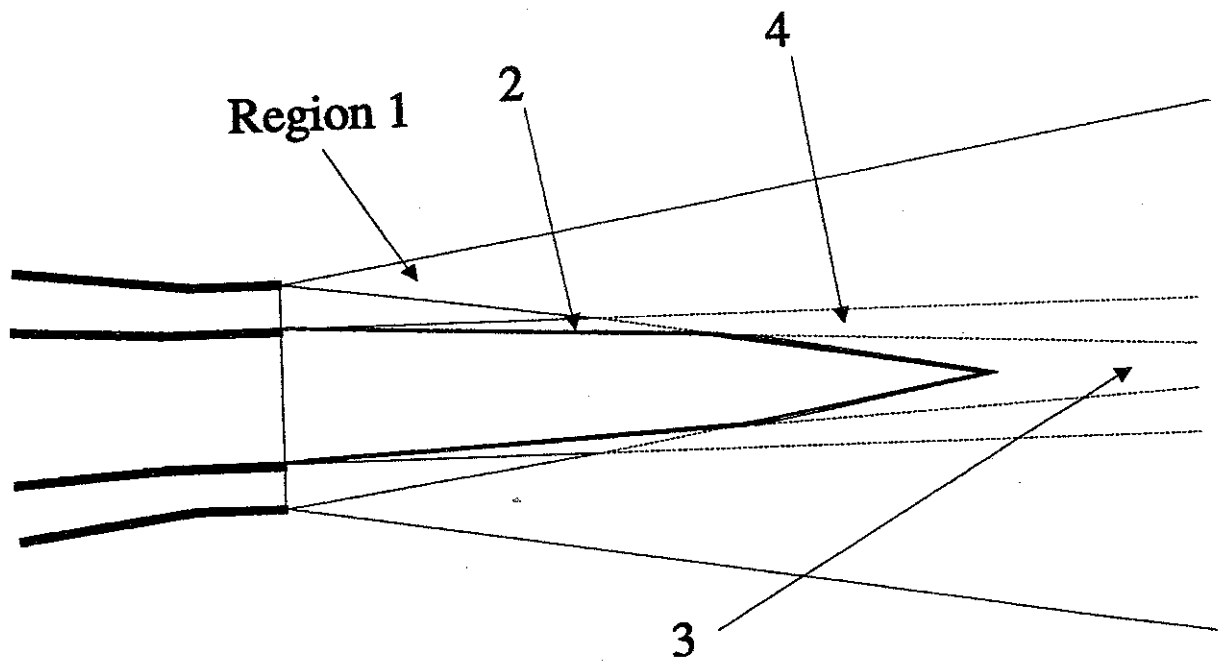

Figure 2. Coaxial jet mixing regions of Flitcroft and Bryce.

Figures 3. Measured spectra from [44]

◇ $\lambda = 0.56$

\$ $\lambda = 0.63$

Z $\lambda = 0.71$

⊠ $\lambda = 0.79$

\# $\lambda = 0.89$

—●— $\lambda = 1.00$

\+ $\lambda = 1.13$

o $\lambda = 1.23$

a) 90°, $V_p = 136$m/s

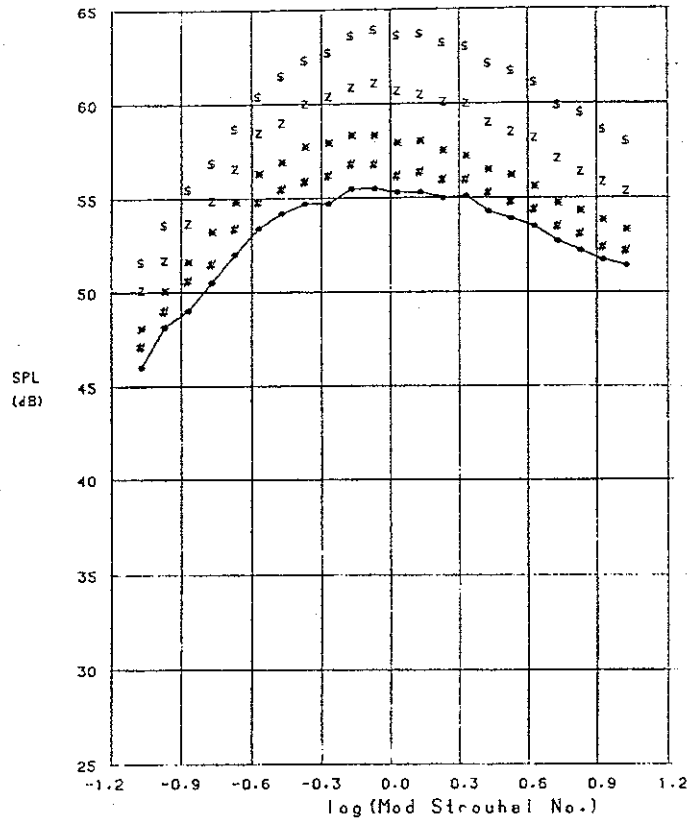

b) 40°, $V_p = 170$m/s

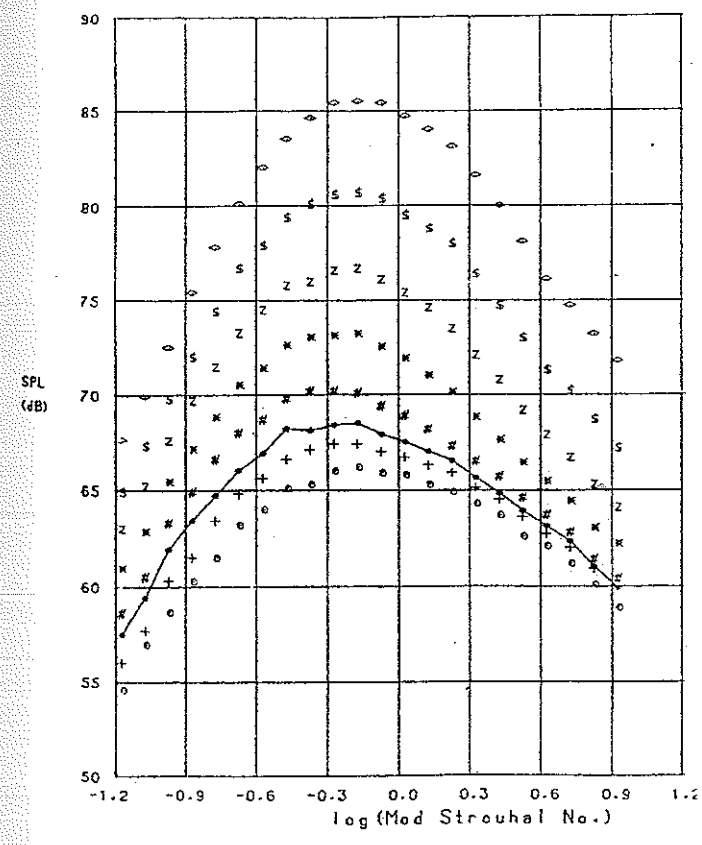

c) 90°, $V_p = 170$m/s

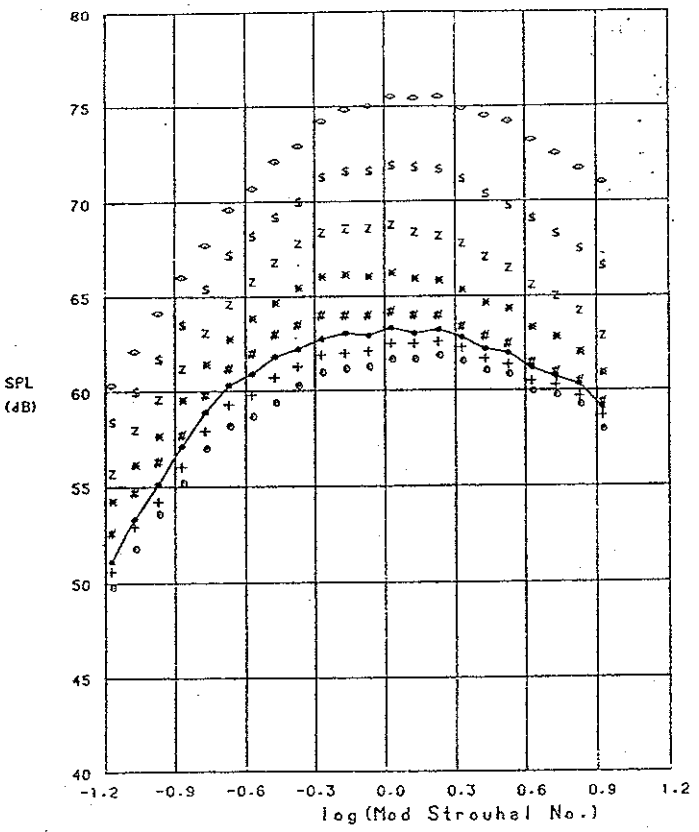

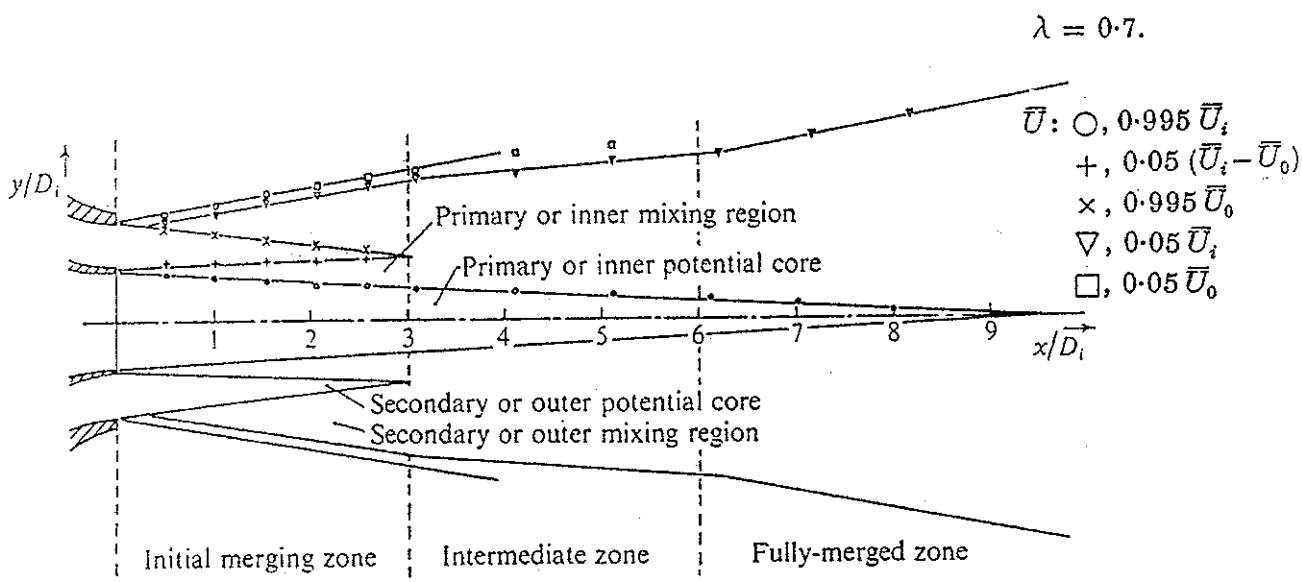

Figure 4. Coaxial jet mixing regions measured by Ko.

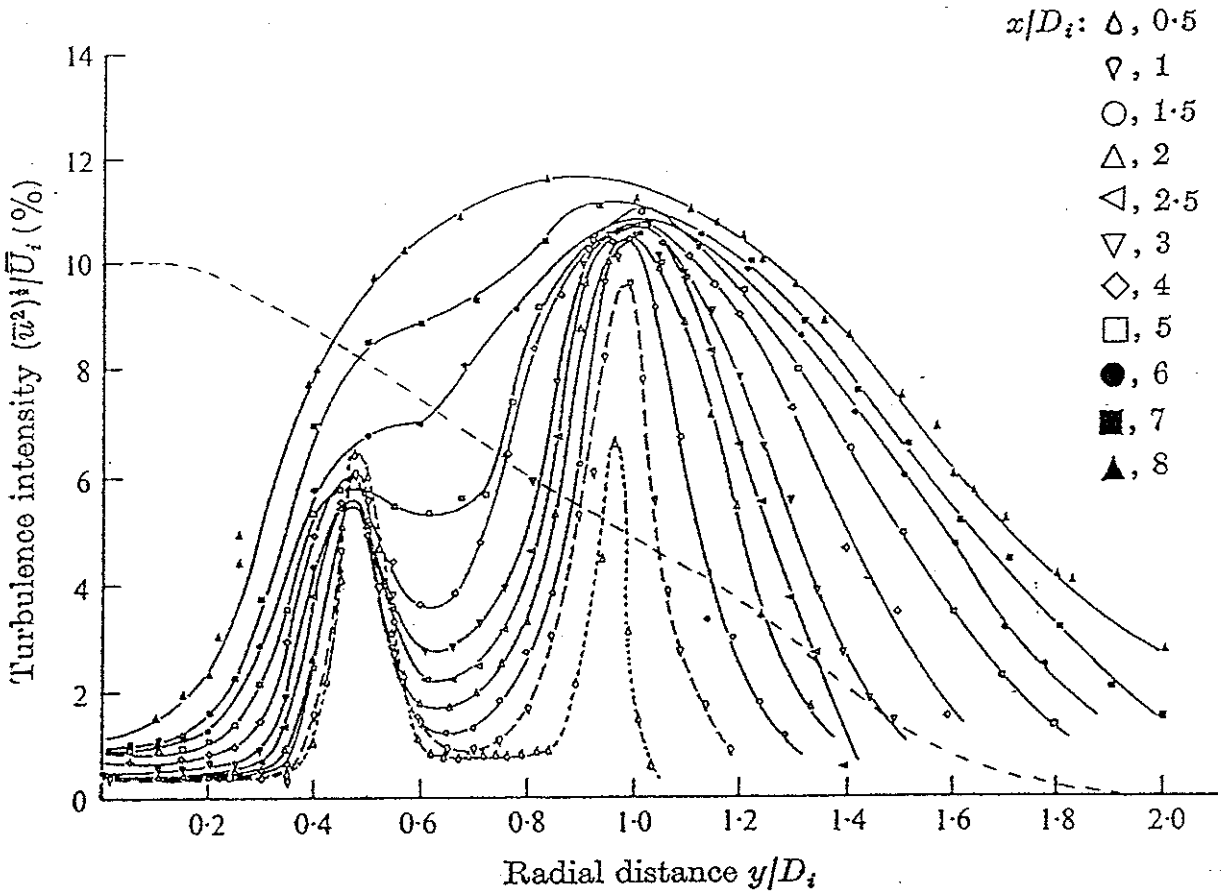

Figure 5. Radial variation of turbulence intensity between 0.5 and 8.0 primary diameters downstream, at a velocity ratio of $\lambda = 0.7$. From Ko.

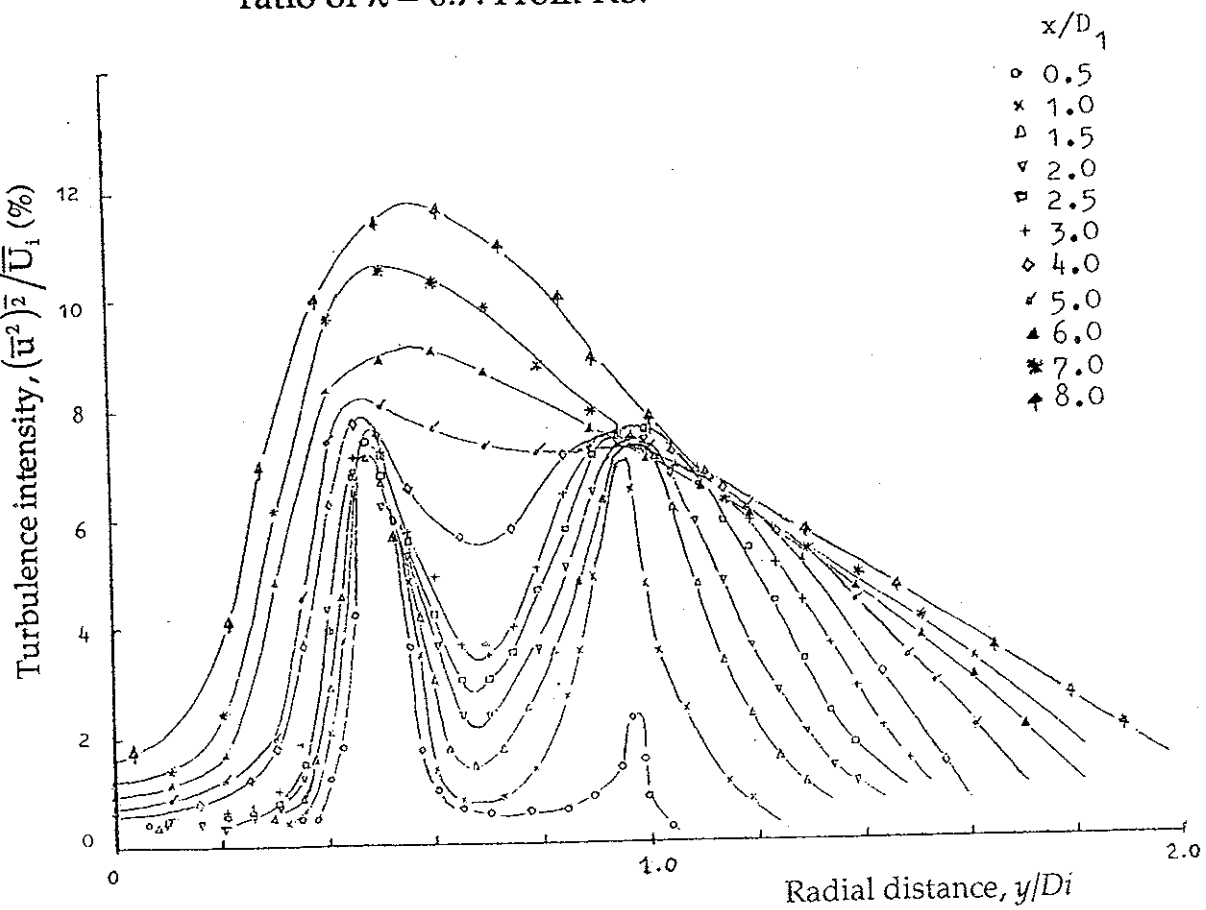

Figure 6. Radial variation of turbulence intensity at a velocity ratio of $\lambda = 0.5$. From Ko.

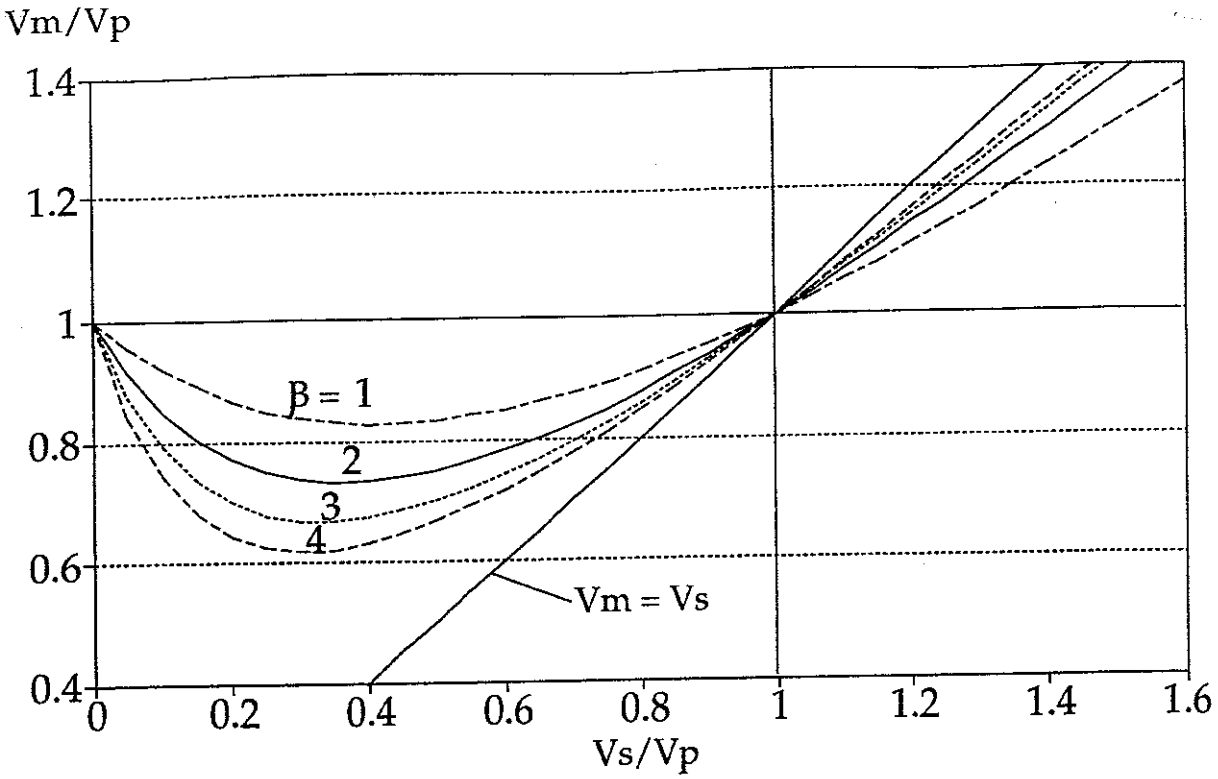

Figure 7. Variation of Vm with velocity ratio at four area ratios.

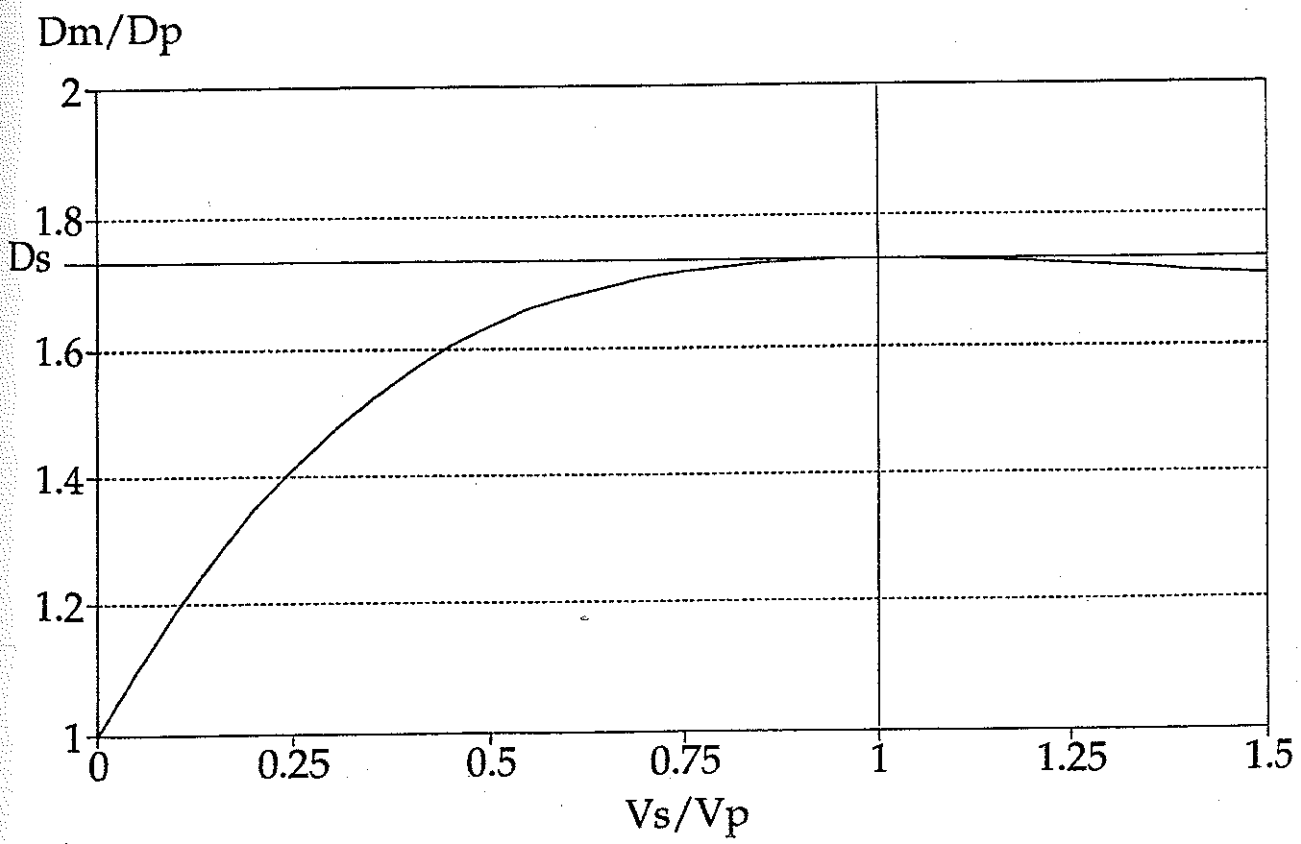

Figure 8. Variation of Mixed jet diameter with velocity ratio at β = 2.

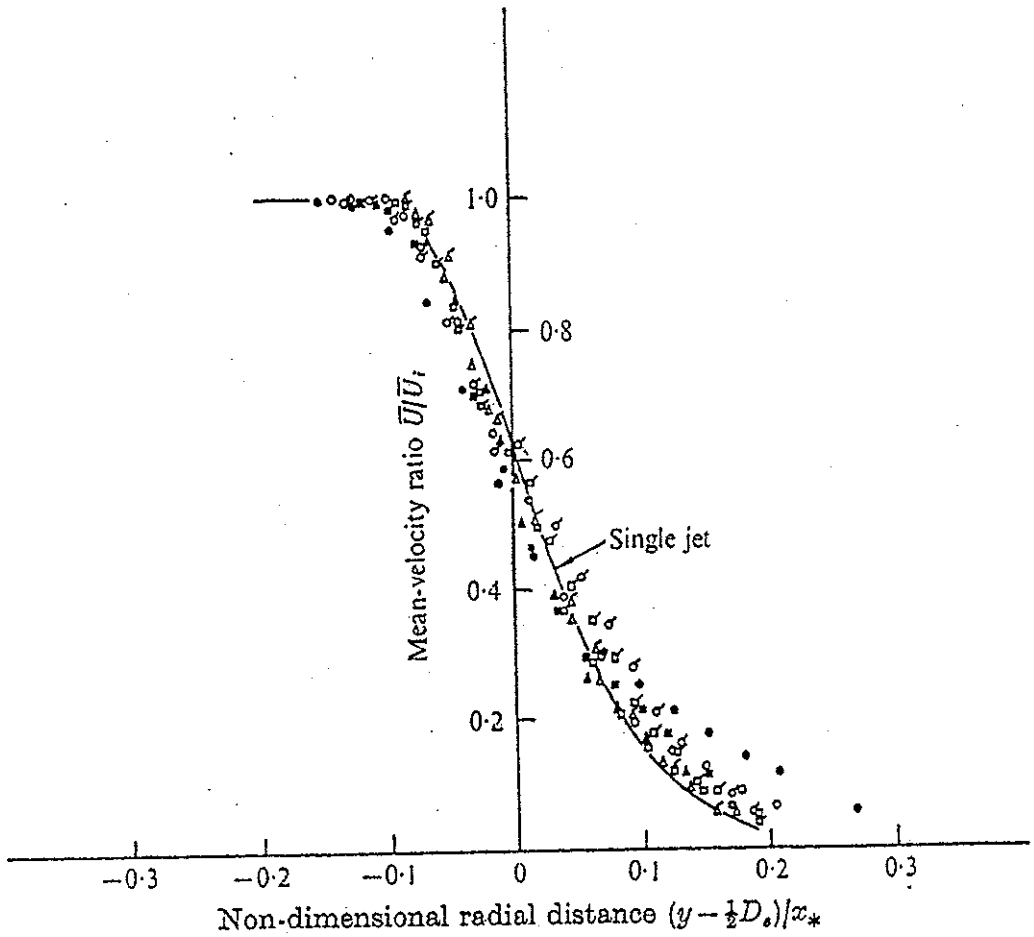

Figure 9. Non-dimensional plot of mean-velocity ratio in the intermediate and fully-merged zones. $\lambda = 0{\cdot}3$. x/D_i: ○, 6; □, 7; △, 8. $\lambda = 0{\cdot}5$. x/D_i: ●, 6; ■, 7; ▲, 8. $\lambda = 0{\cdot}7$. x/D_i: ⊙, 6; ⊡, 7; ◭, 8.

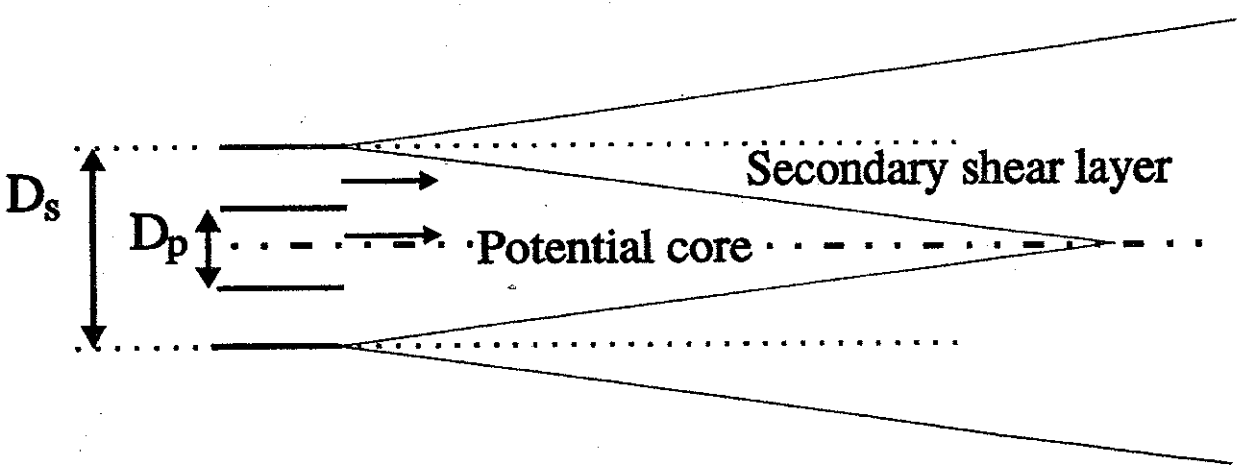

Figure 10. Diagram of flow at $\lambda = 1$: Potential core ends at about 5Ds.

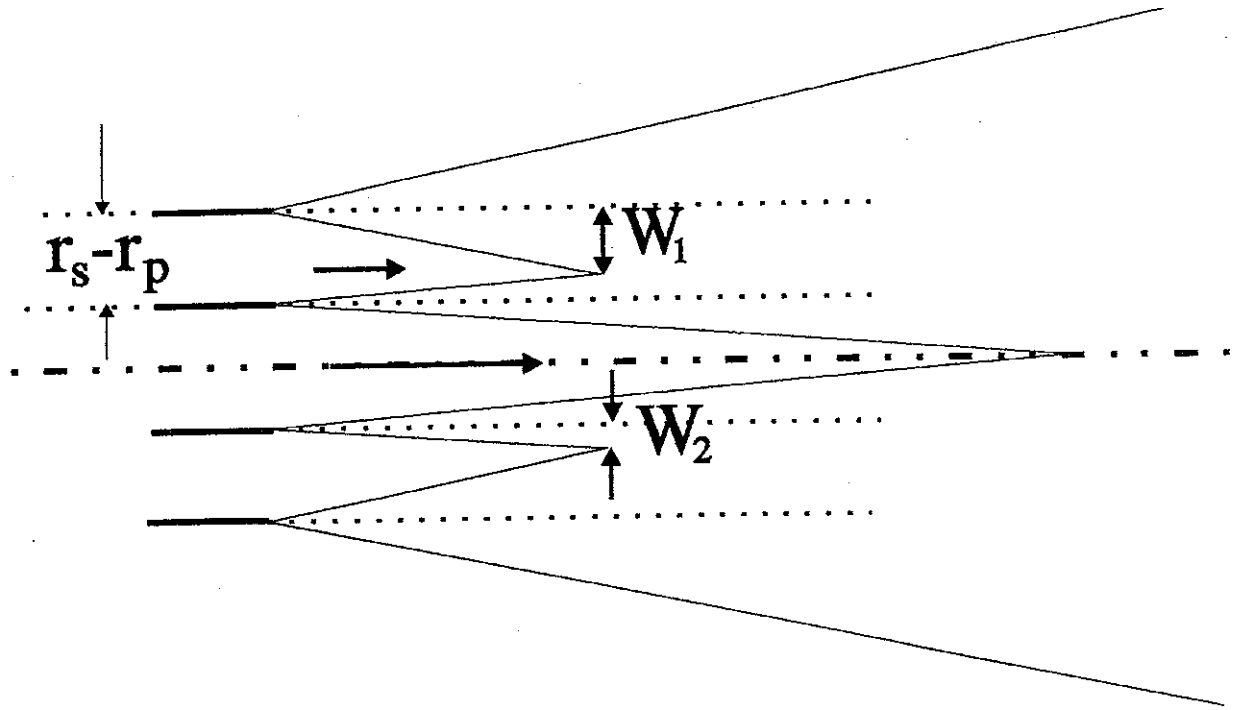

Figure 11. General flow pattern at $\lambda < 1$.

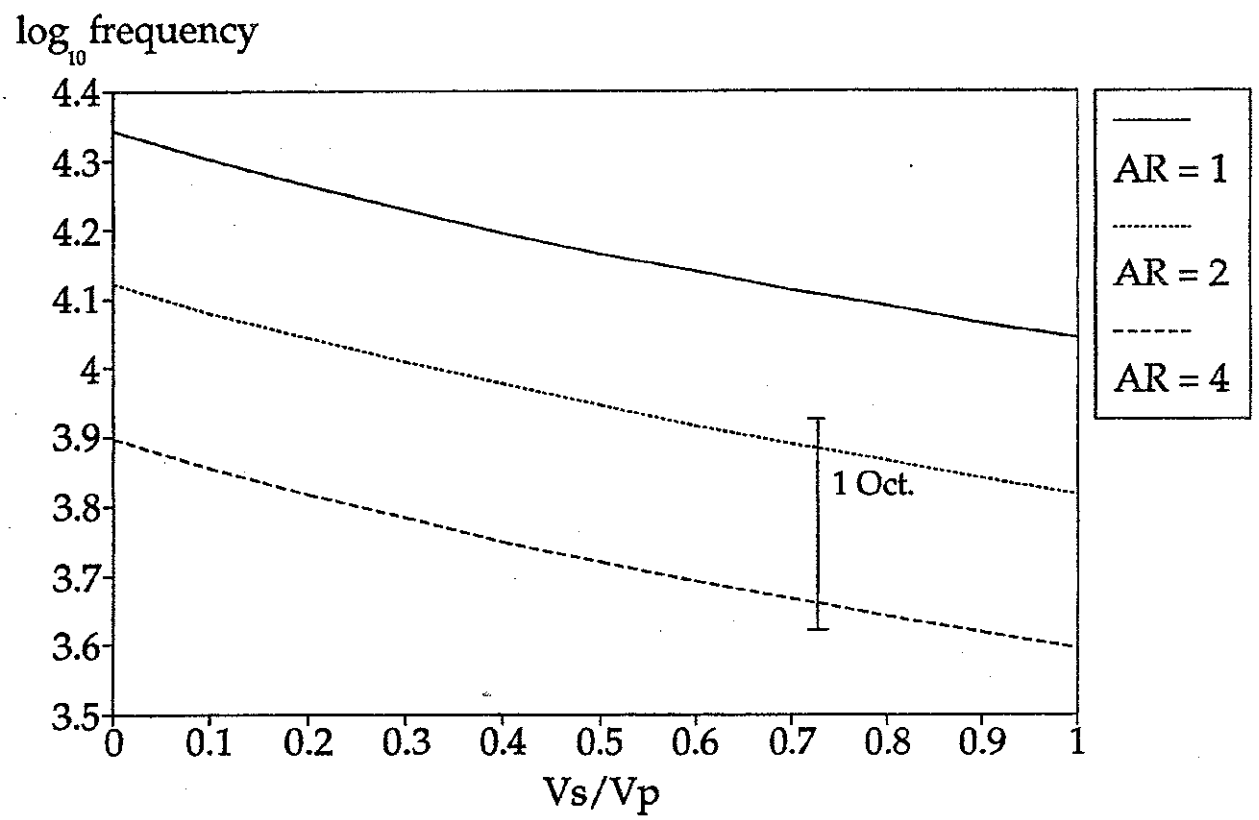

Figure 12. Variation of $\log_{10}$ cutoff frequency with velocity ratio at 3 area ratios.

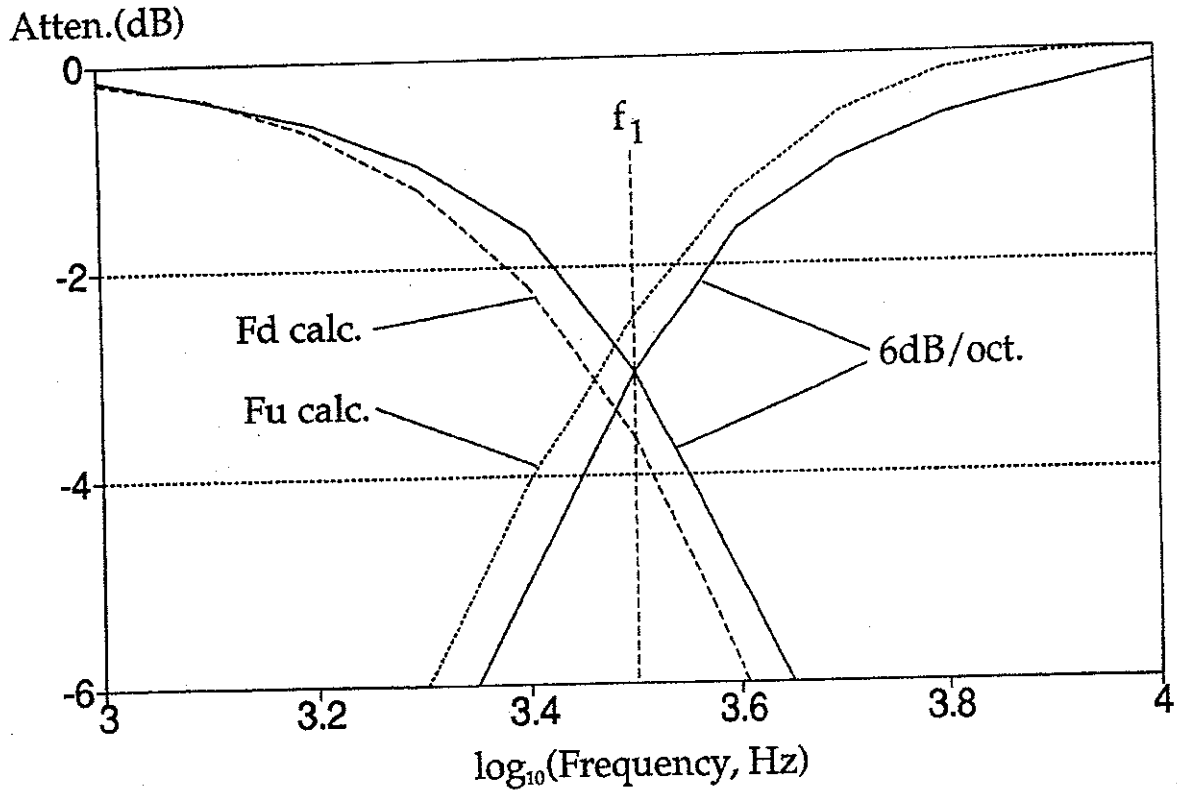

Figure 13. Attenuation rates from source location work for m=4. (6dB/Oct also shown)

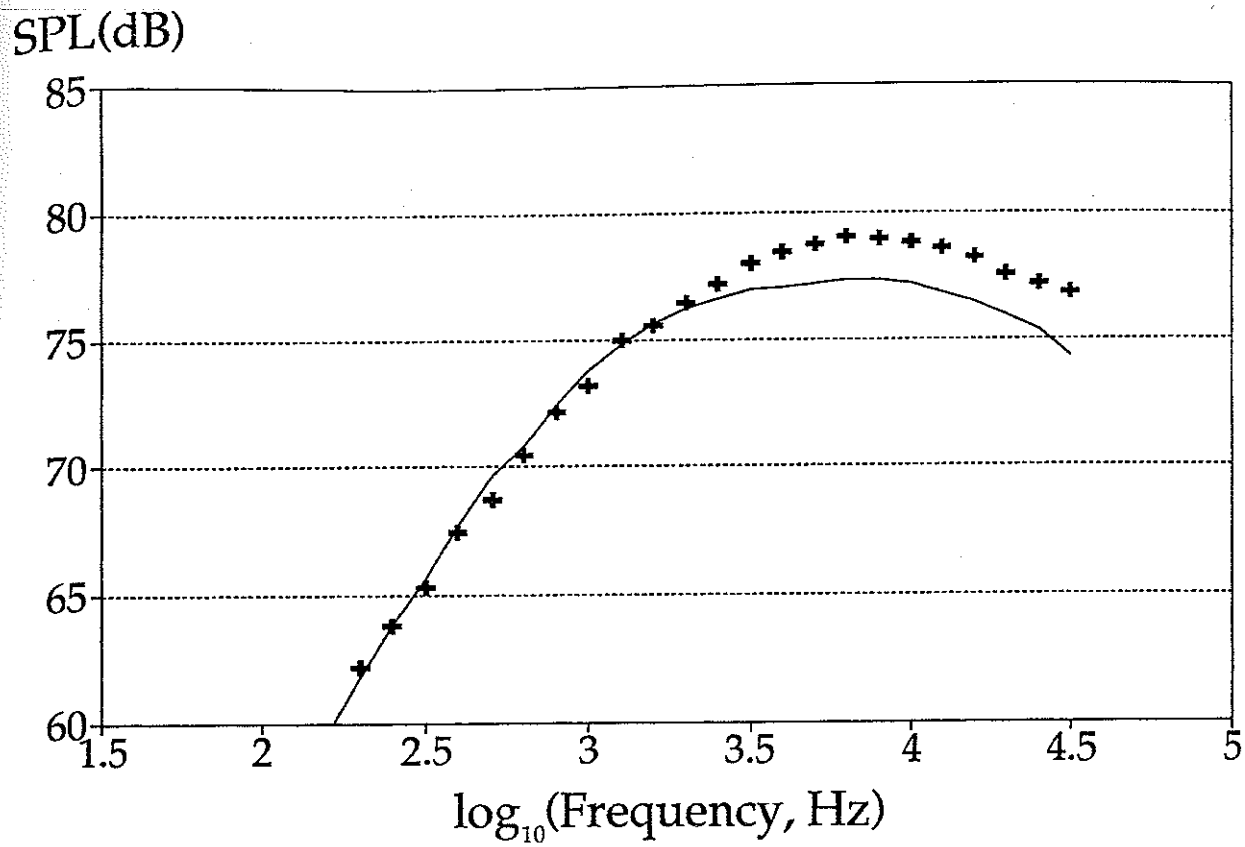

Figure 14 a) Lockheed data. Vj = 241m/s, Tj = 288K, at 90 degrees.

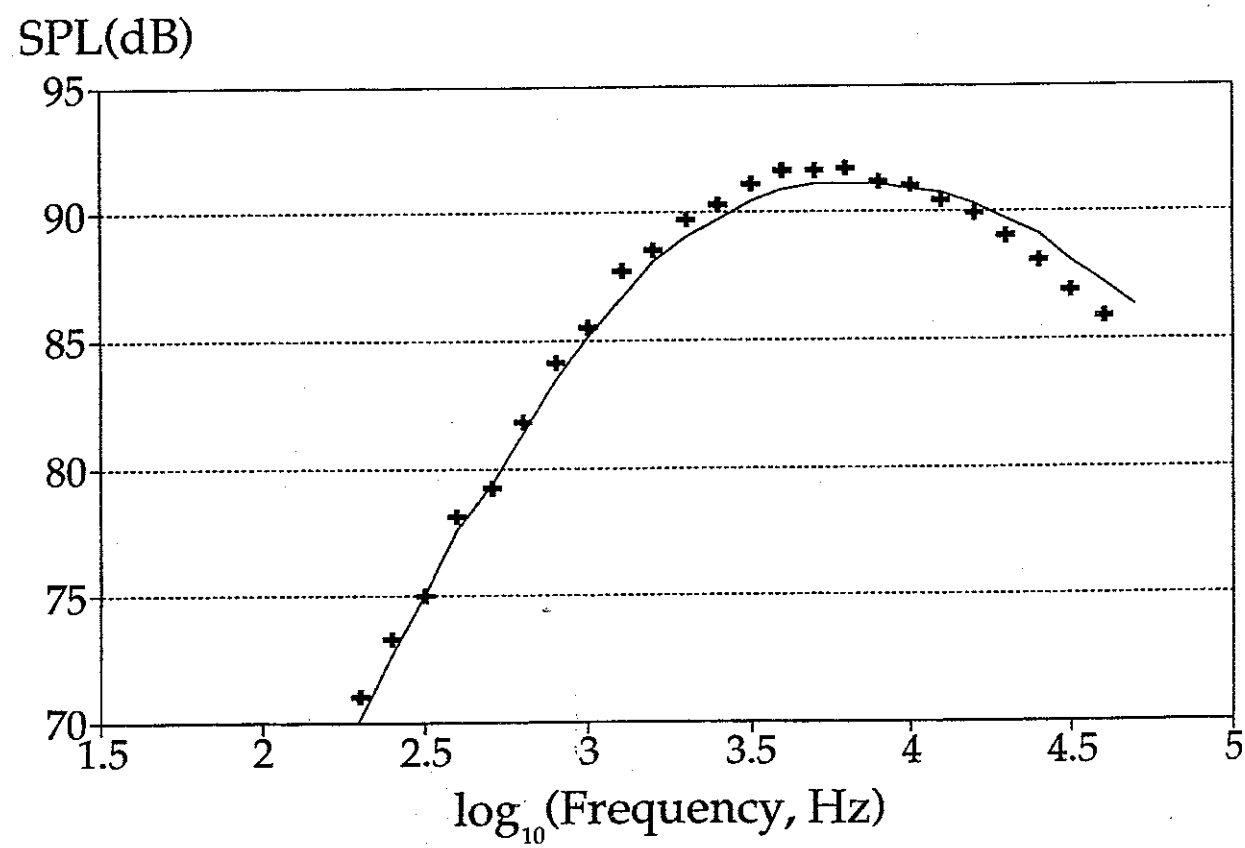

b) Lockheed data. Vj = 410m/s, Tj = 707K, at 90 degrees.

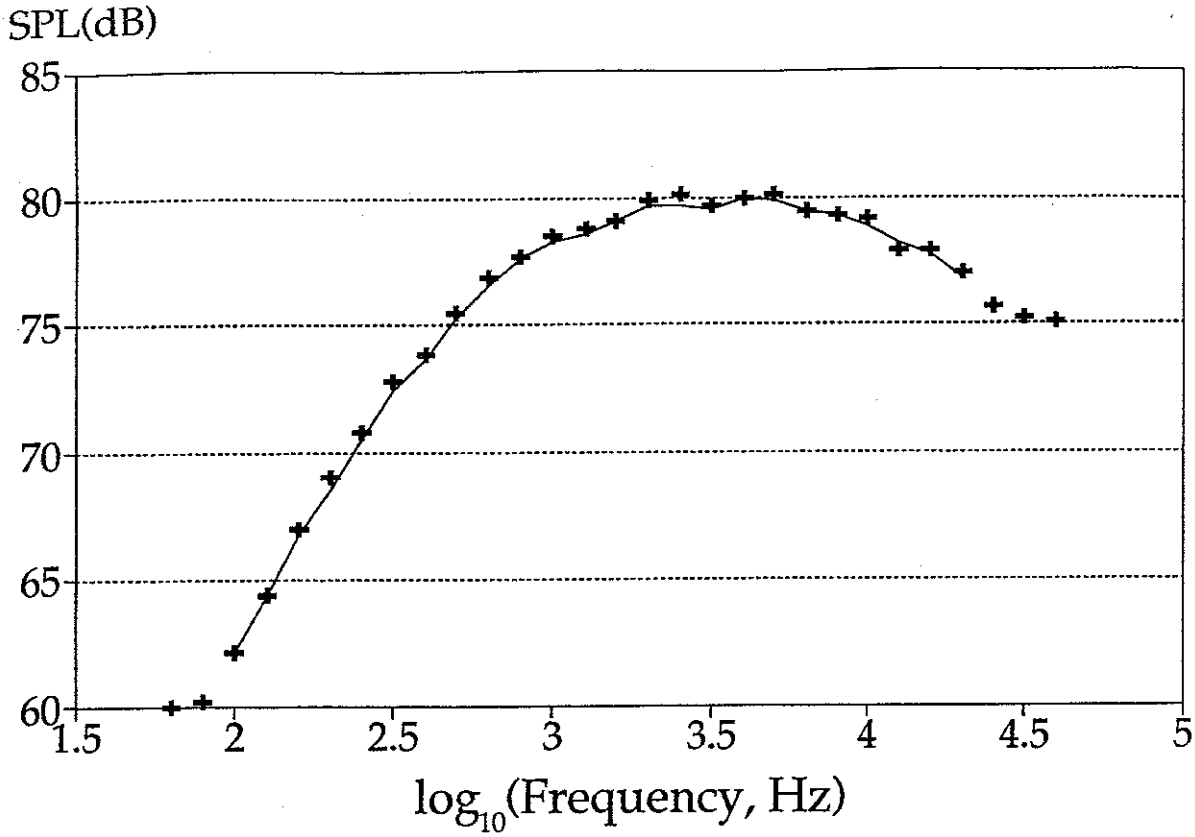

Figure 15 a) Single stream. Vj = 253m/s, Tj = 286.1K, at 90 degrees.

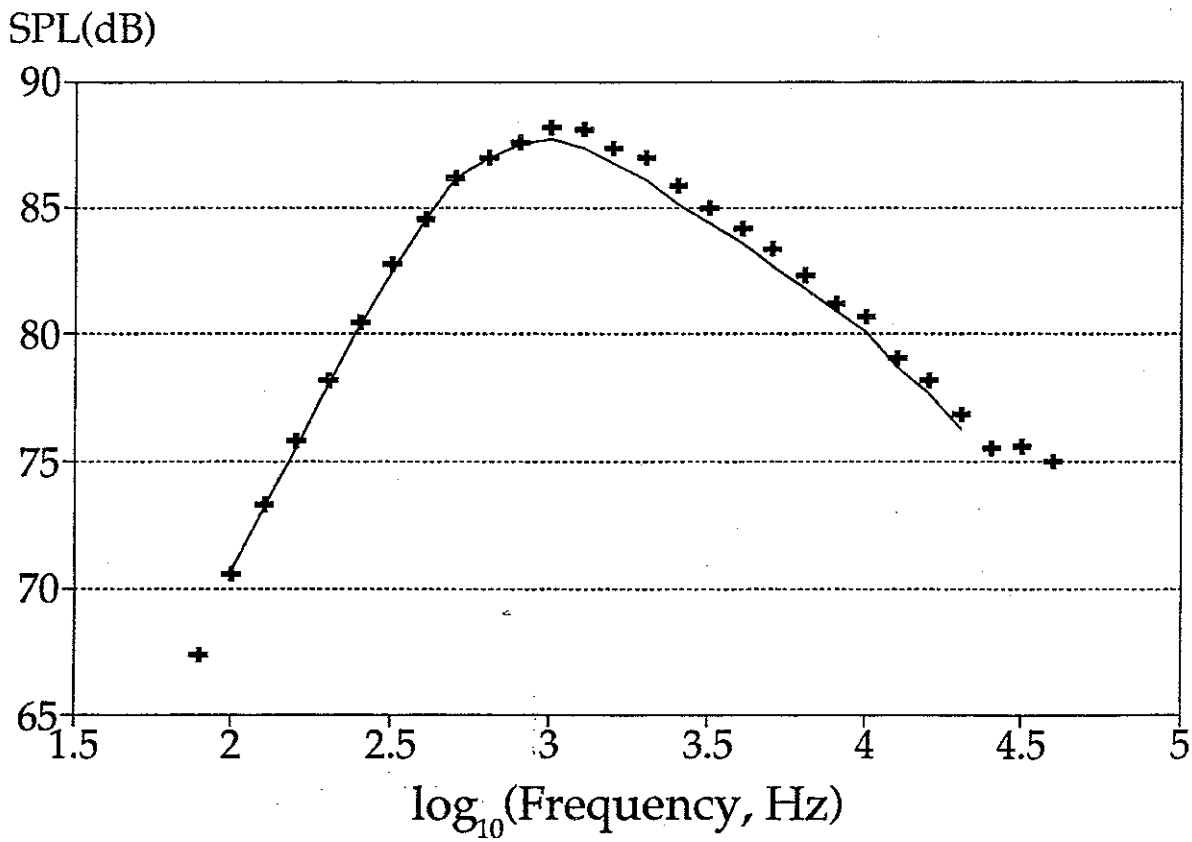

b) Single stream. Vj = 253m/s, Tj = 286.1K, at 40 degrees.

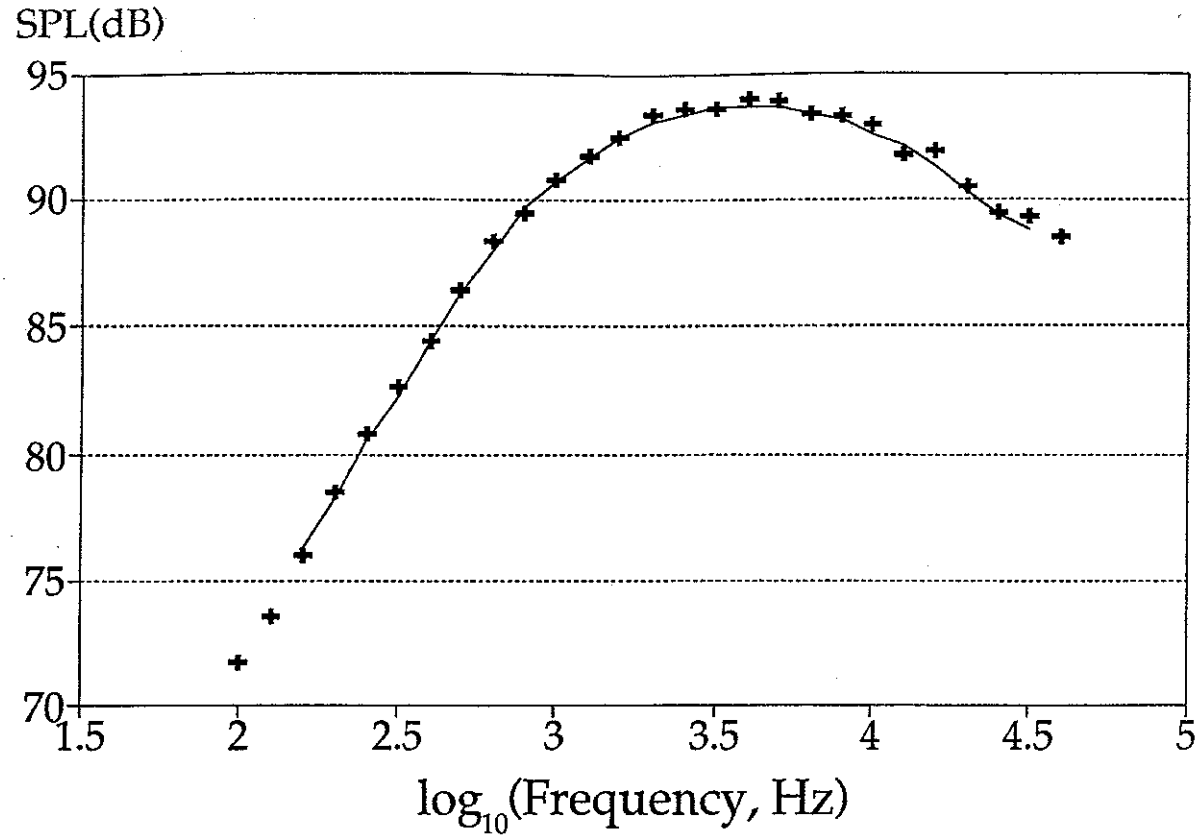

Figure 16 a) Single stream. Vj = 418m/s, Tj = 694K, at 90 degrees.

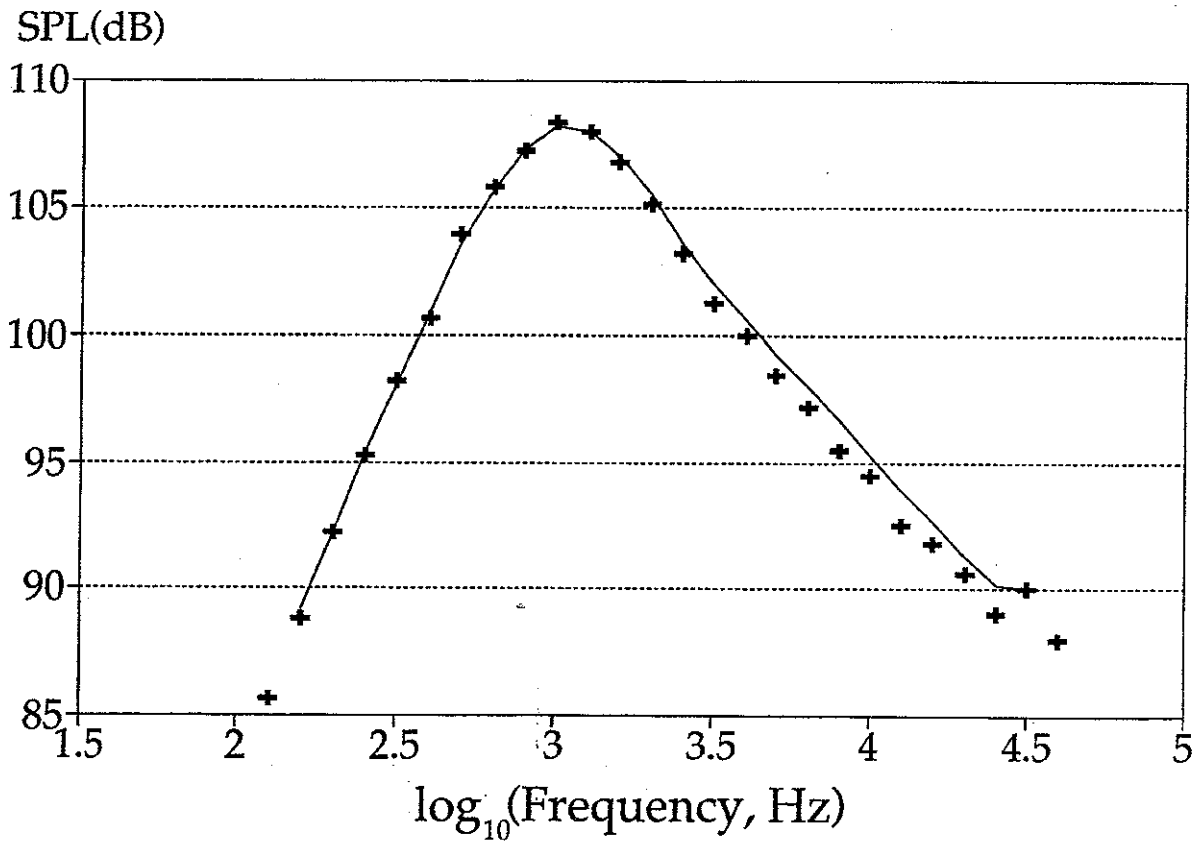

b) Single stream. Vj = 418m/s, Tj = 694K, at 40 degrees.

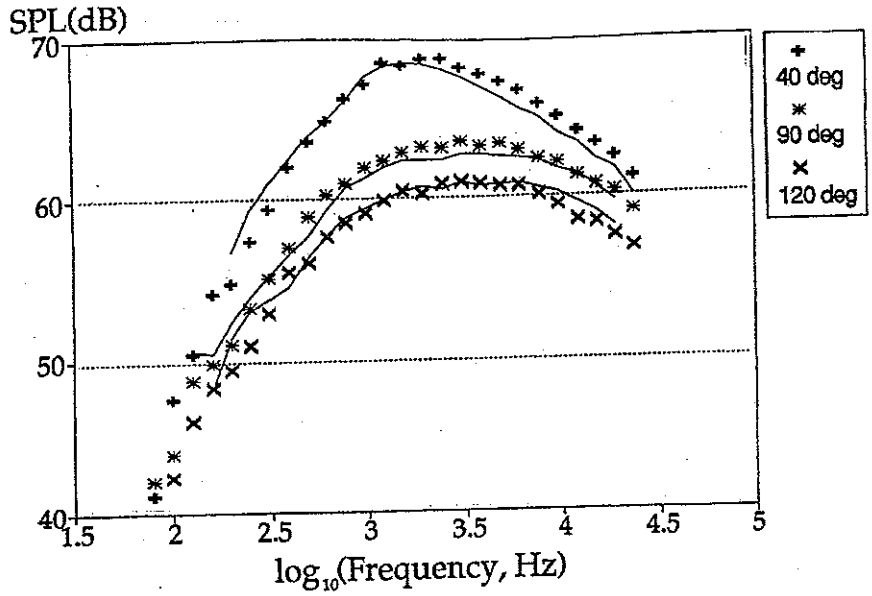

Figure 17. λ = 1.0 spectra at three angles with predictions.

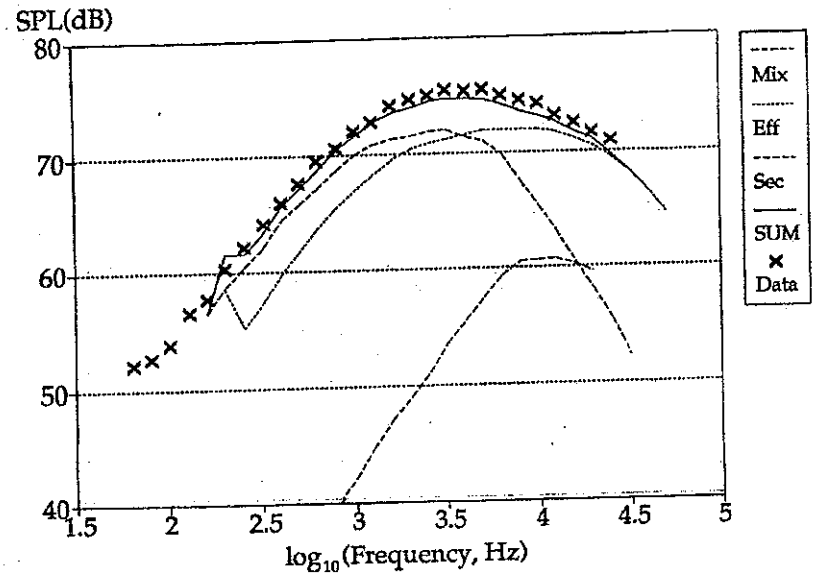

Figure 18 a) 90 degree spectra atλ = 0.563, Vp = 301.9m/s

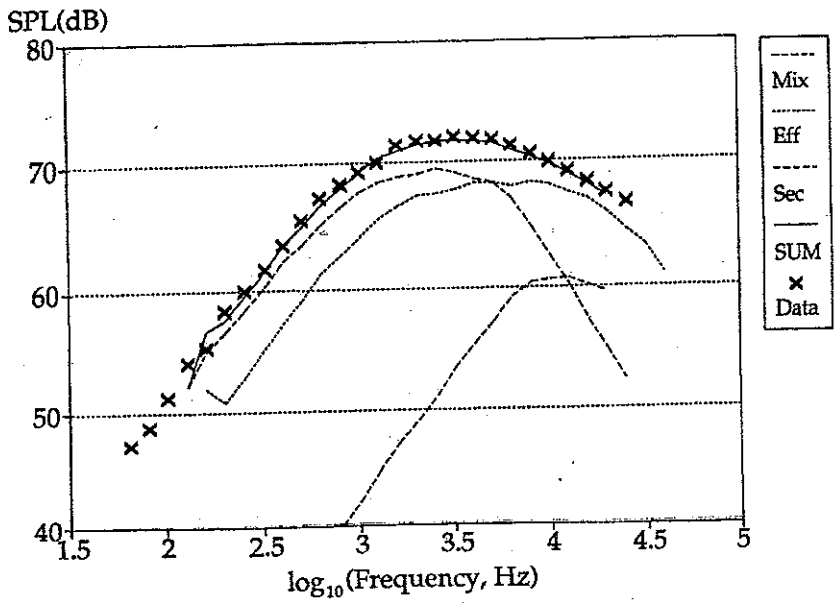

Figure 18 b) 90 degree spectra atλ = 0.632, Vp = 267.2m/s

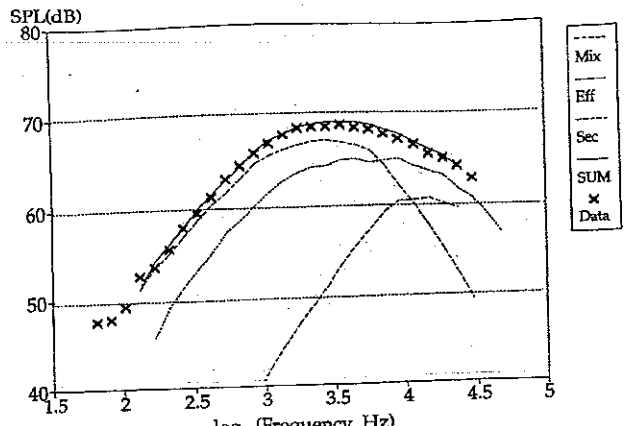

Figure 18 c) 90 degree spectra at $\lambda = 0.708$, Vp = 241.4m/s

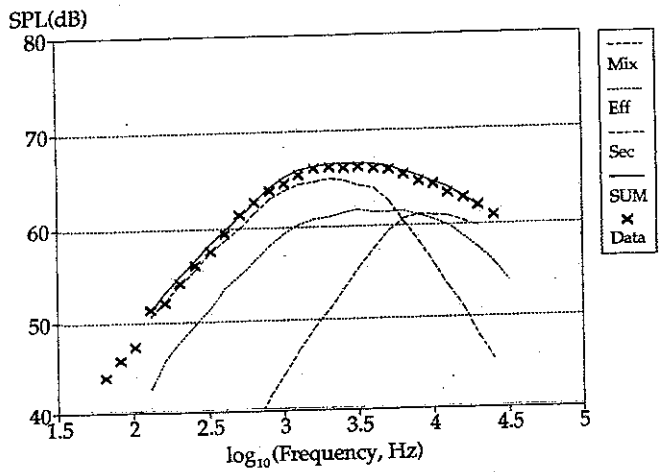

Figure 18 d) 90 degree spectra at $\lambda = 0.791$, Vp = 216.0m/s

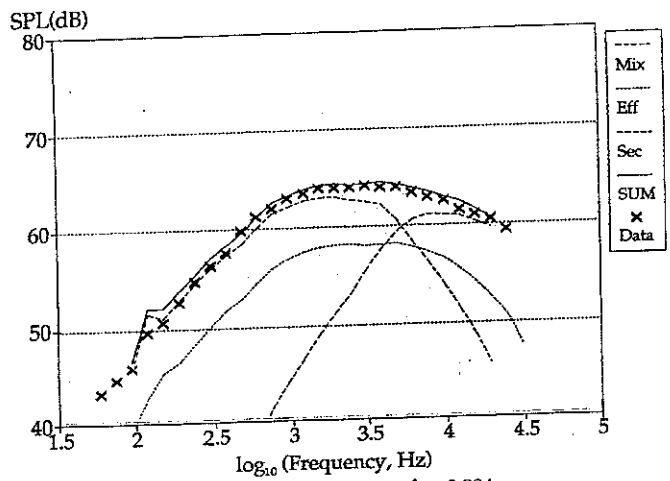

Figure 18 e) 90 degree spectra at $\lambda = 0.894$, Vp = 191.1m/s

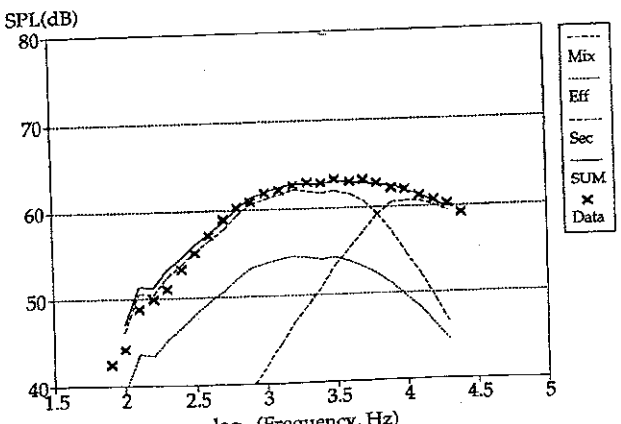

Figure 18 f) 90 degree spectra at $\lambda = 1.00$, Vp = 171.2m/s

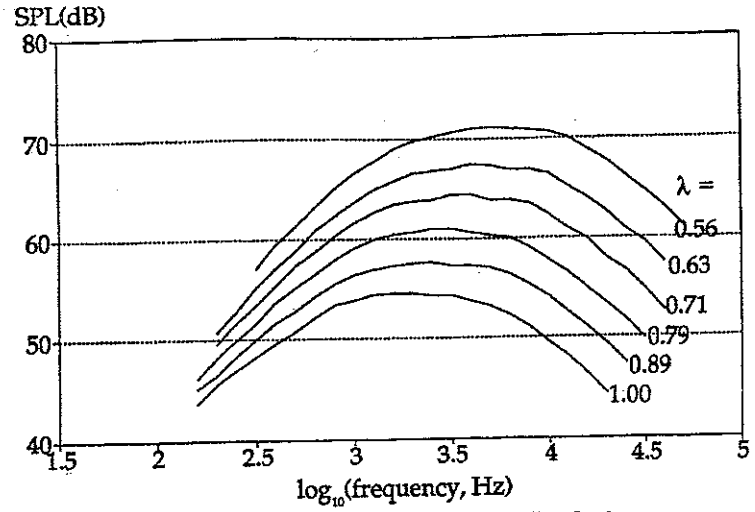

Figure 19. 90° Effective jet spectra at all velocity ratios, for an isothermal jet at AR = 2

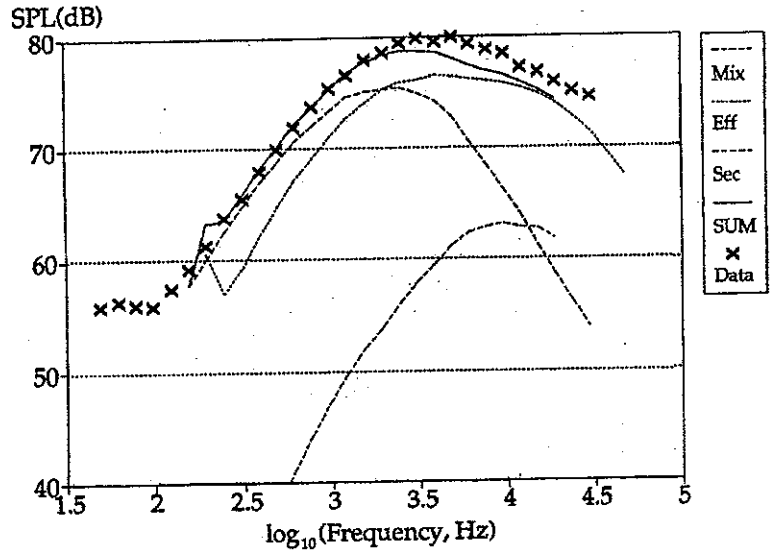

Figure 20 a) 60 degree spectra at $\lambda = 0.563$, Vp = 301.9m/s

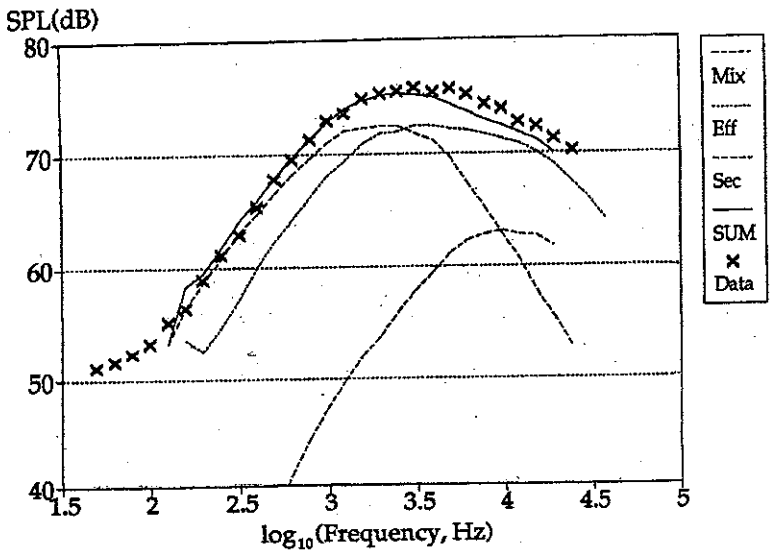

Figure 20 b) 60 degree spectra at $\lambda = 0.632$, Vp = 267.2m/s

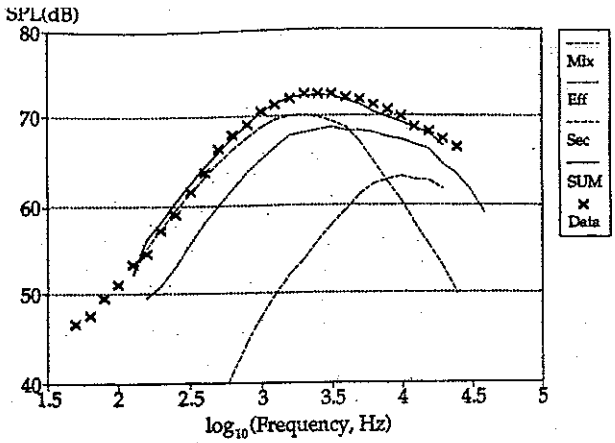

Figure 20 c) 60 degree spectra at $\lambda = 0.708$, Vp = 241.4m/s

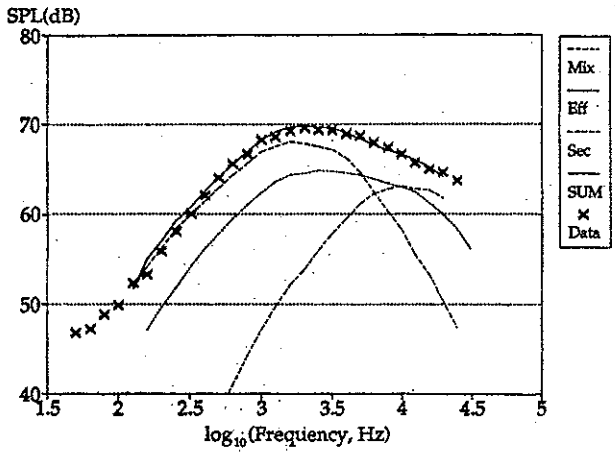

Figure 20 d) 60 degree spectra at $\lambda = 0.791$, Vp = 216.0m/s

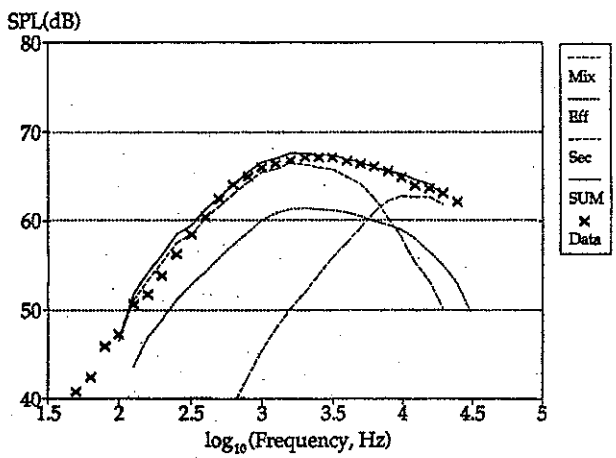

Figure 20 e) 60 degree spectra at $\lambda = 0.894$, Vp = 191.1m/s

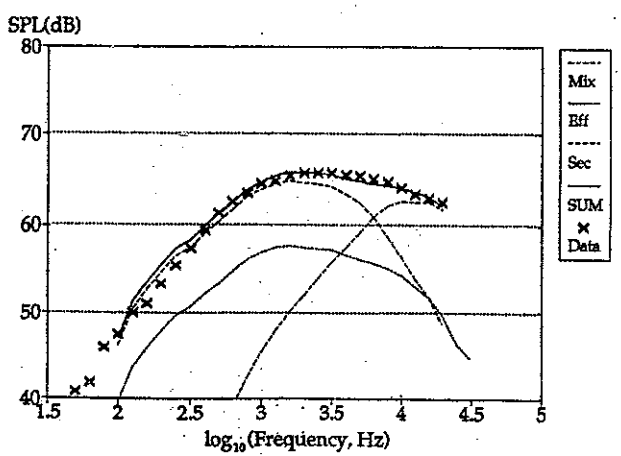

Figure 20 f) 60 degree spectra at $\lambda = 1.003$, Vp = 171.2m/s

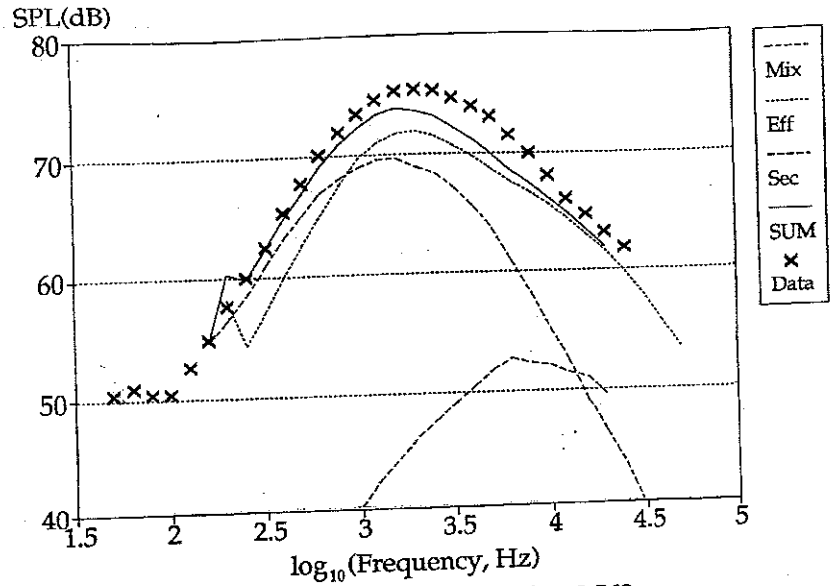

Figure 21 a) 40 degree spectra at $\lambda = 0.563$, Vp = 301.9m/s

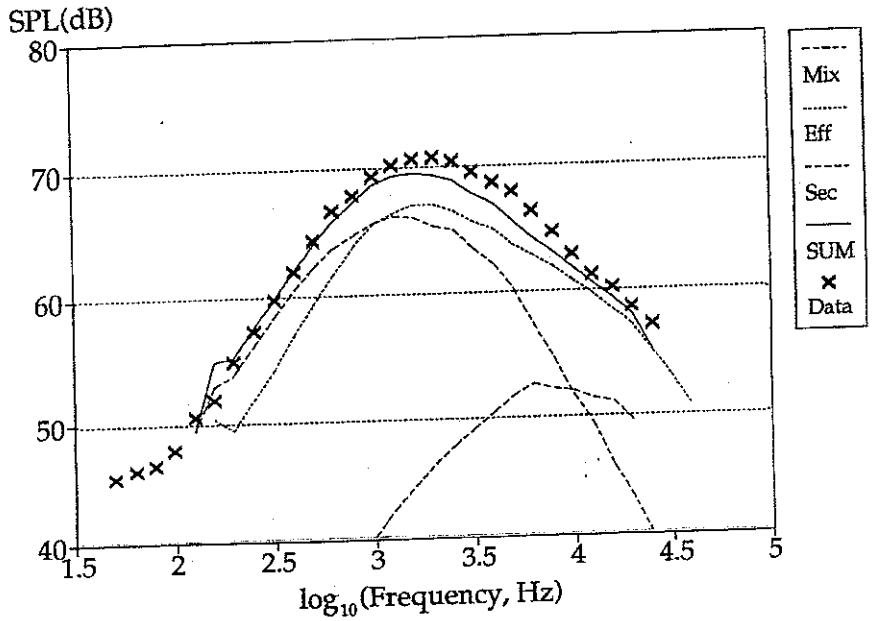

Figure 21 b) 40 degree spectra at $\lambda = 0.632$, Vp = 267.2m/s

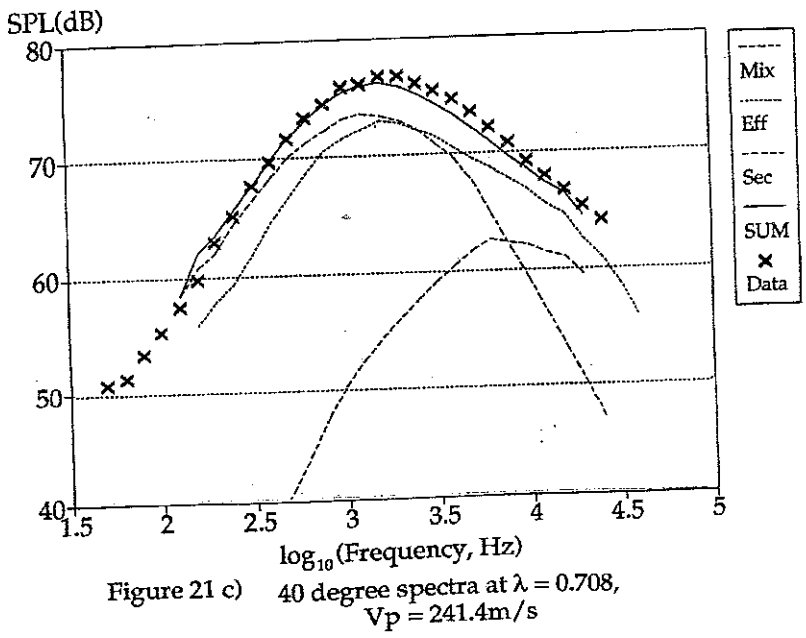

Figure 21 c) 40 degree spectra at $\lambda = 0.708$, Vp = 241.4m/s

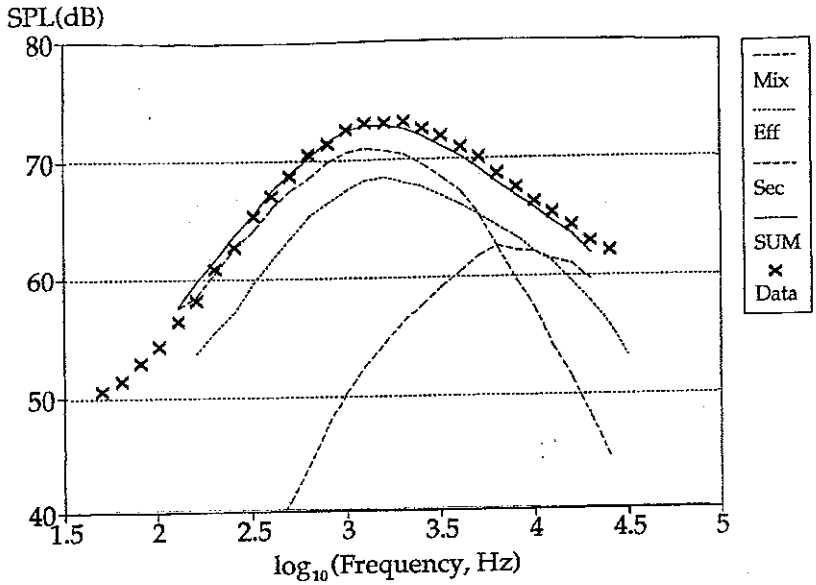

Figure 21 d) 40 degree spectra at $\lambda = 0.791$, Vp = 216.0m/s

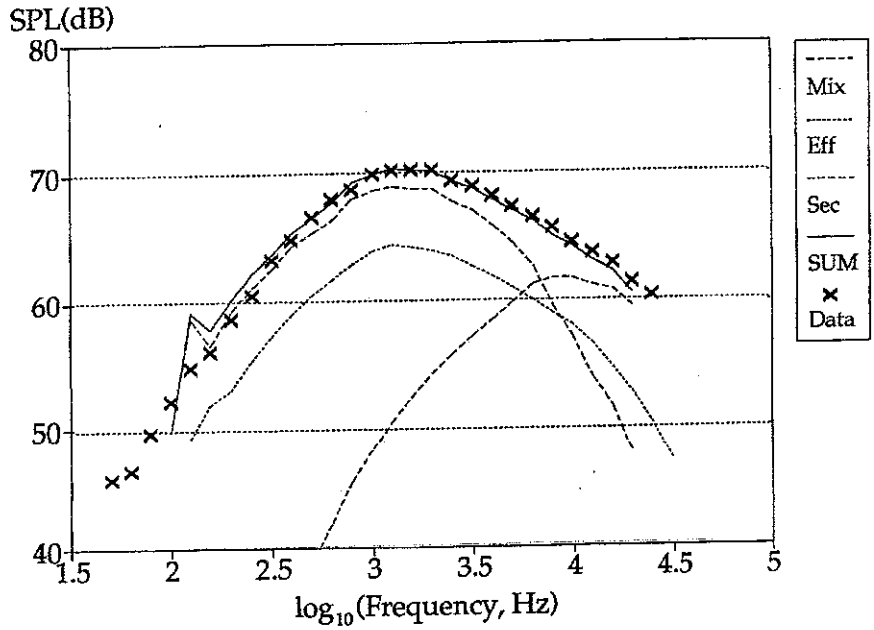

Figure 21 e) 40 degree spectra at $\lambda = 0.894$, Vp = 191.1m/s

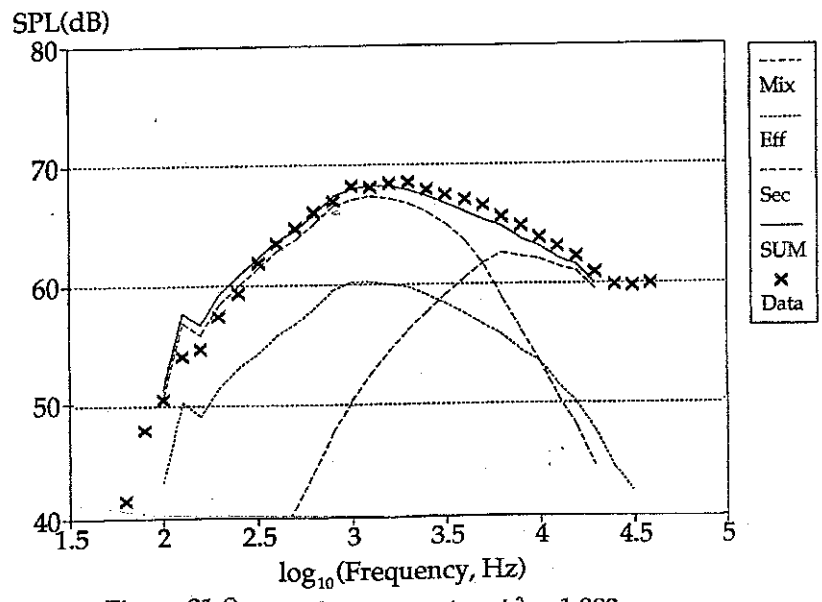

Figure 21 f) 40 degree spectra at $\lambda = 1.003$, Vp = 171.2m/s

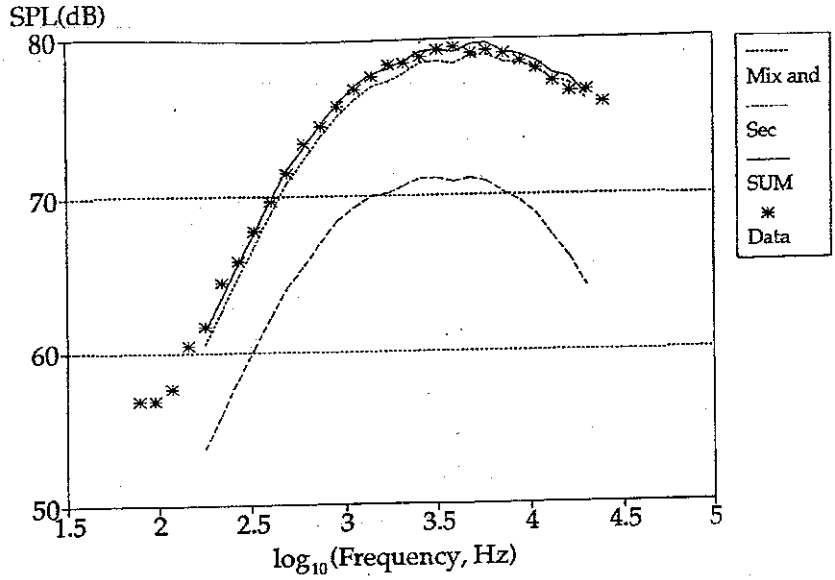

Figure 22. 90 degree spectra at $\lambda = 1.0$, Vp = 268.8m/s

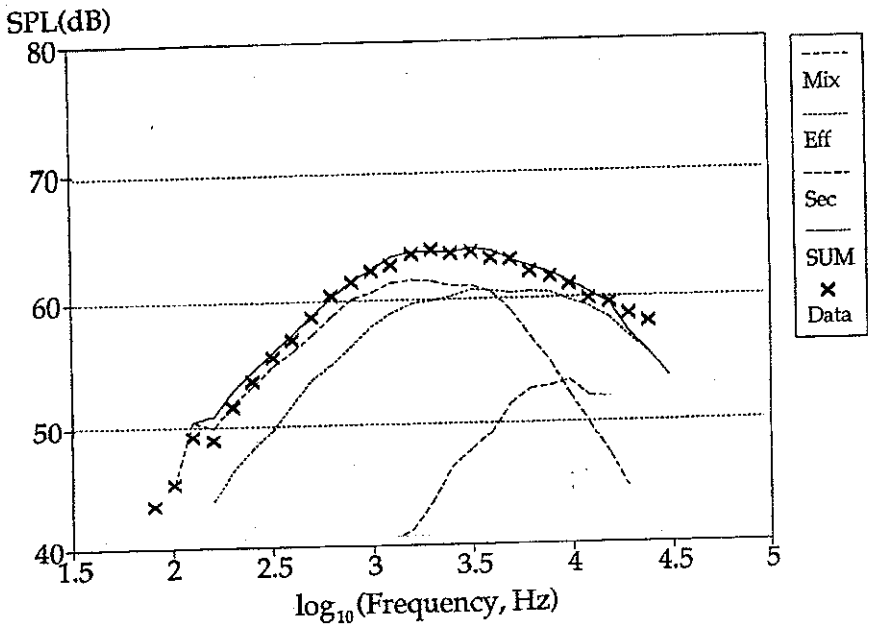

Figure 23. 90 degree spectra at$\lambda = 0.636$, Vp = 213.8m/s

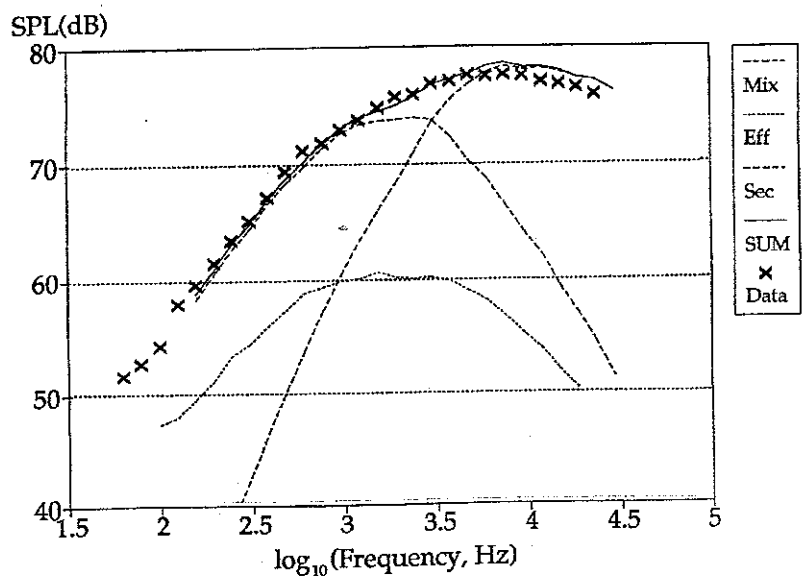

Figure 24. 90 degree spectra at$\lambda = 1.42$, Vp = 190m/s, Vs = 270m/s

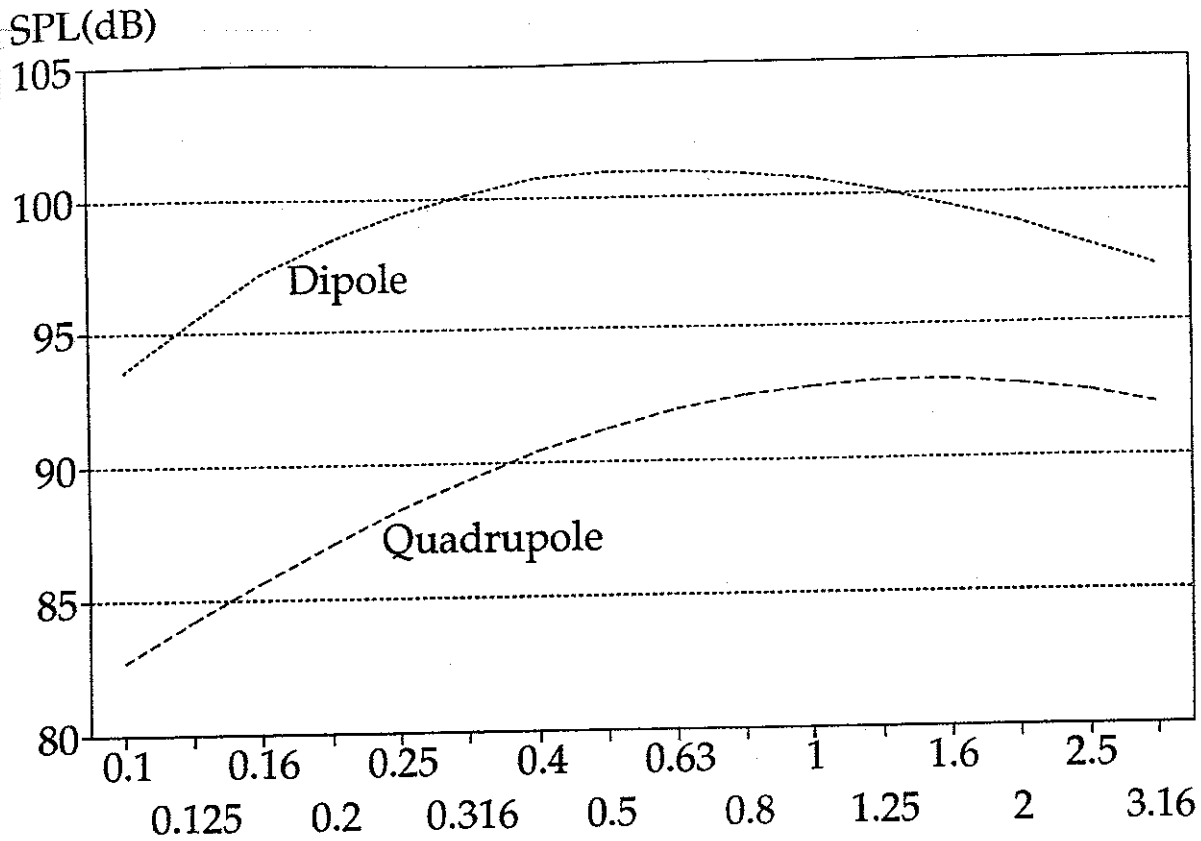

Figure 25. 90° normalised 1/3 octave dipole and quadrupole master spectra at R/d = 72.

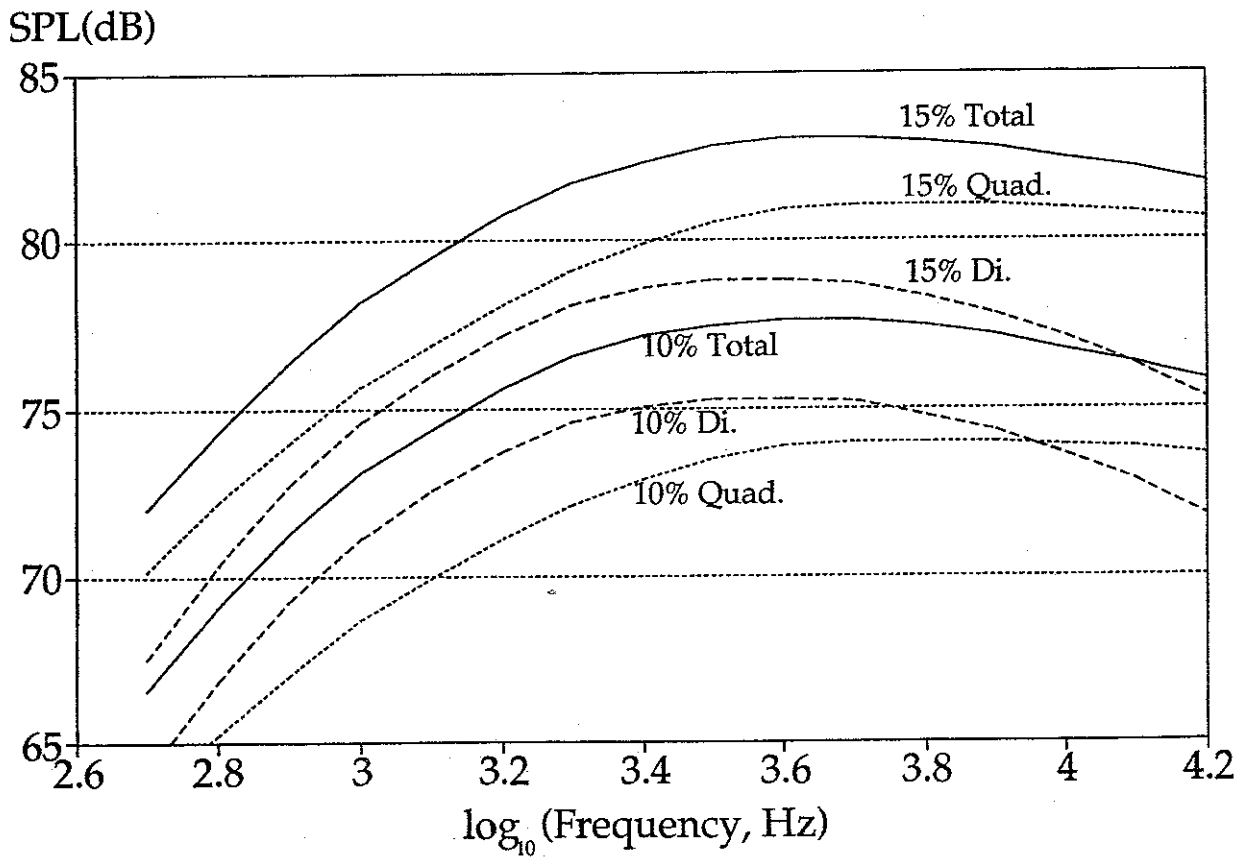

Figure 26. 400K, Mj=0.9, 90 degrees Dipole, Quadrupole and Total spectra.

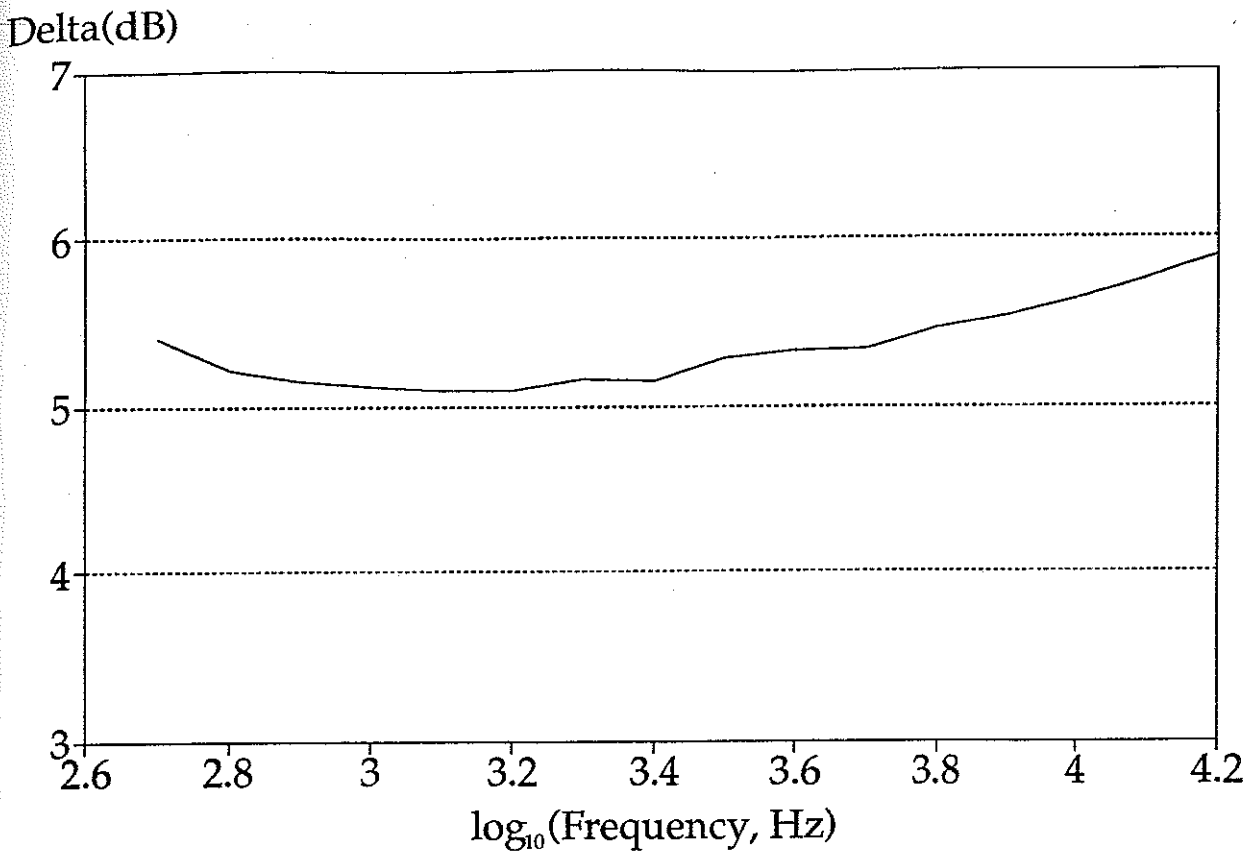

Figure 27. 400K, Mj=0.9, 90°
Difference between 15% and 10% spectra.

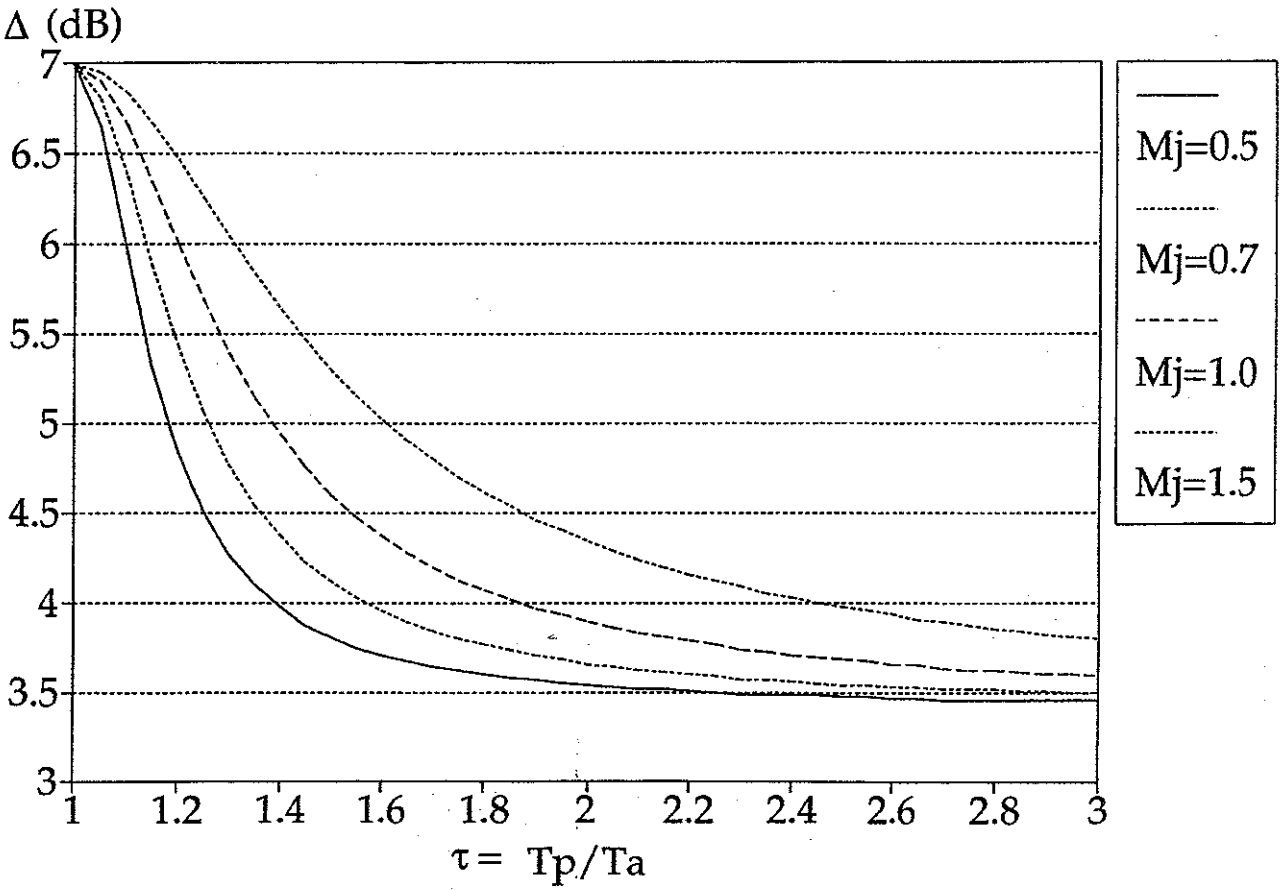

Figure 28. Δ vs. τ at four jet Mach numbers.

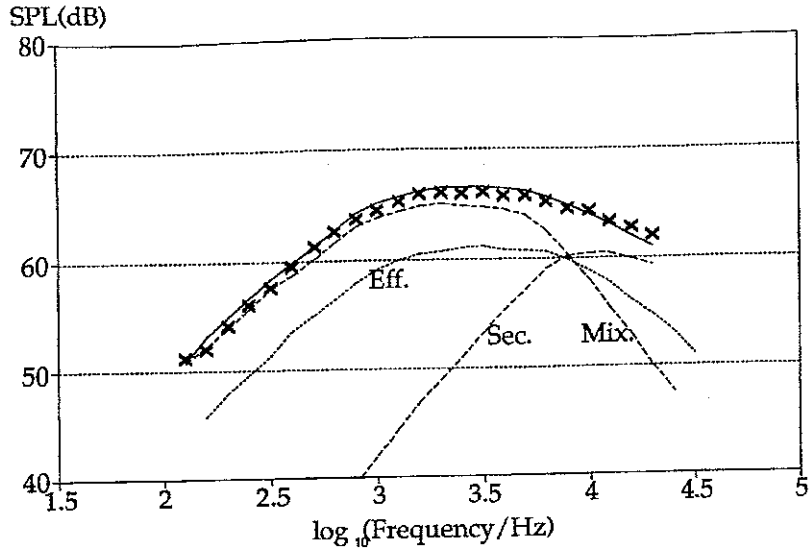

Figure 29 a) 90° prediction at ambient temperature, $\lambda = 0.79$, Vp = 211.3m/s

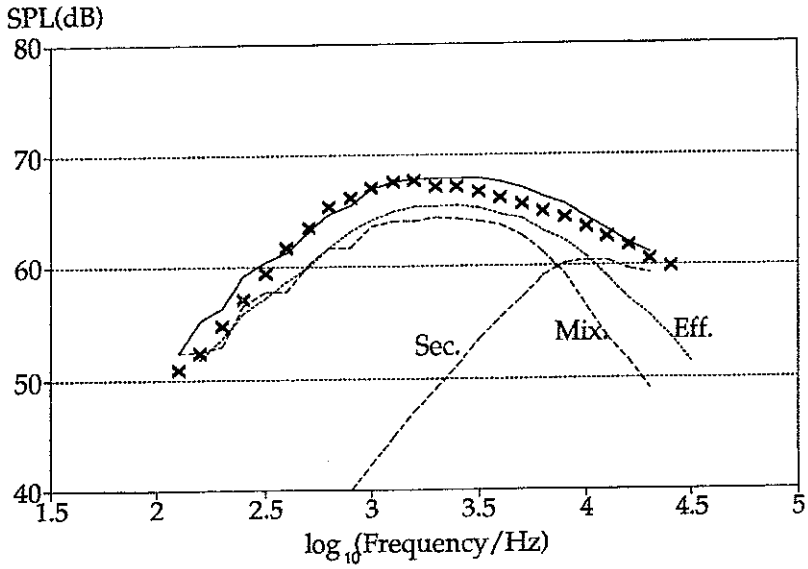

b) 90° prediction at Tp = 600K, $\lambda = 0.79$, Vp = 209.6m/s

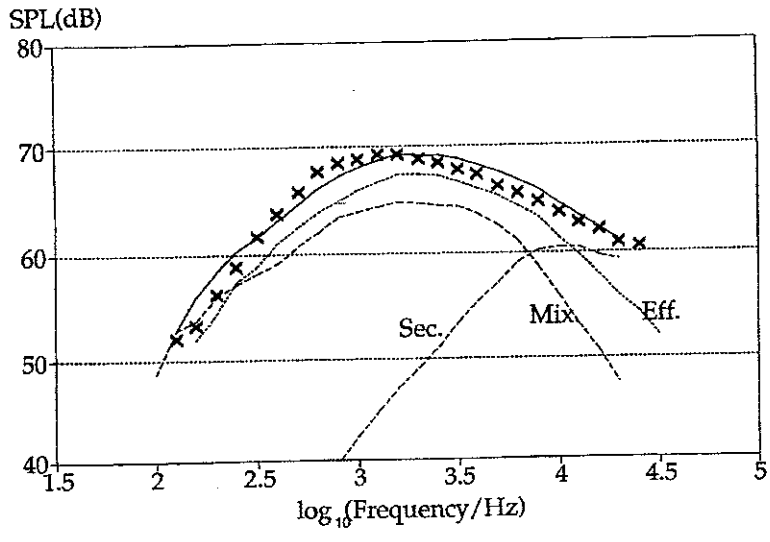

c) 90° prediction at Tp = 800K, $\lambda = 0.79$, Vp = 211.3m/s

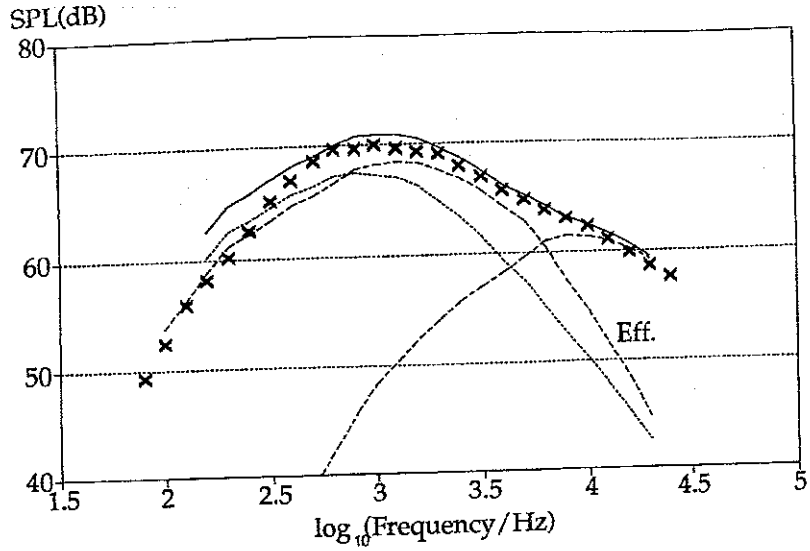

Figure 30 a) 40° prediction at Tp = 600K, λ = 1.00, Vp = 165.4m/s

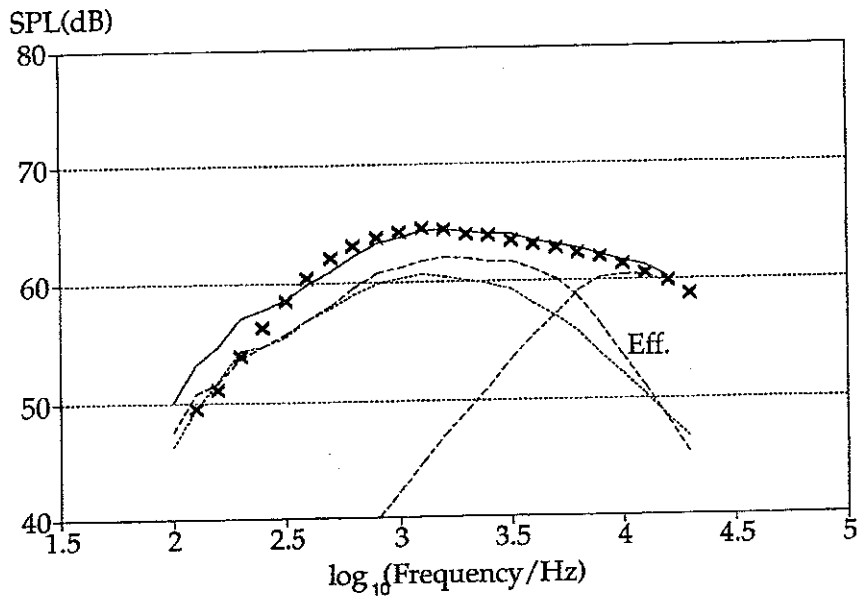

b) 90° prediction at Tp = 600K, λ = 1.00, Vp = 165.4m/s

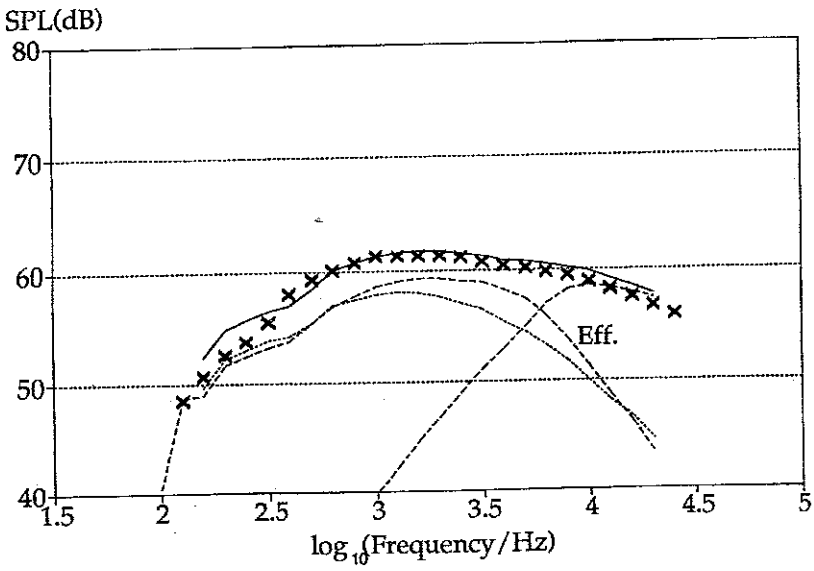

c) 120° prediction at Tp = 600K, λ = 1.00, Vp = 165.4m/s

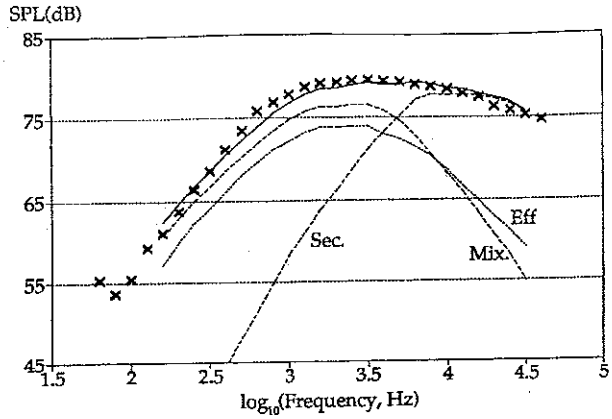

Figure 31. 90° prediction at Tp = 800K, λ = 1.00, Vp = 265.9m/s

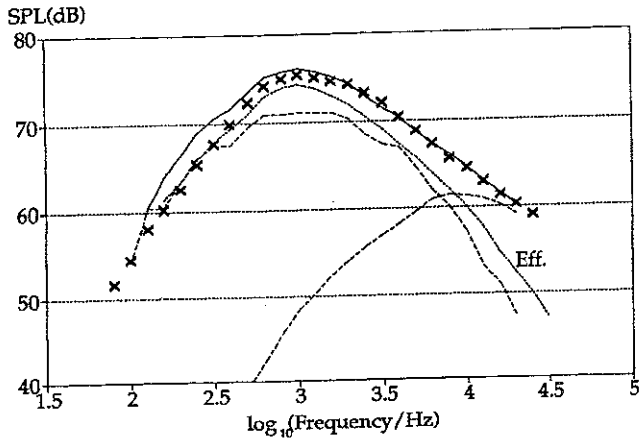

Figure 32 a) 40° prediction at Tp = 600K, λ = 0.79, Vp = 209.6m/s

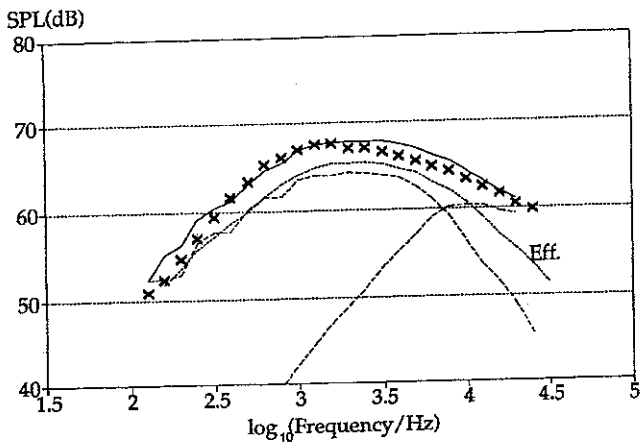

b) 90° prediction at Tp = 600K, λ = 0.79, Vp = 209.6m/s

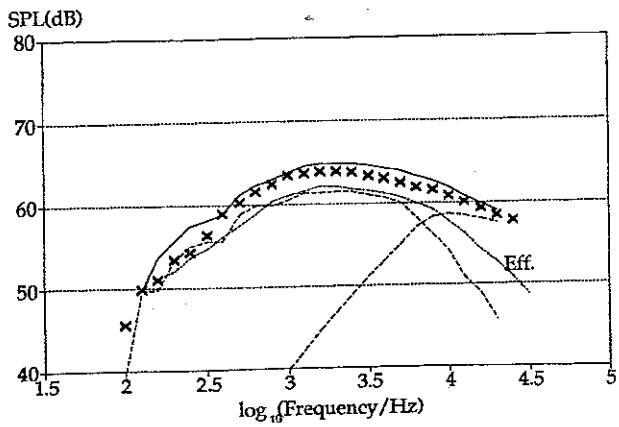

c) 120° prediction at Tp = 600K, λ = 0.79, Vp = 209.6m/s

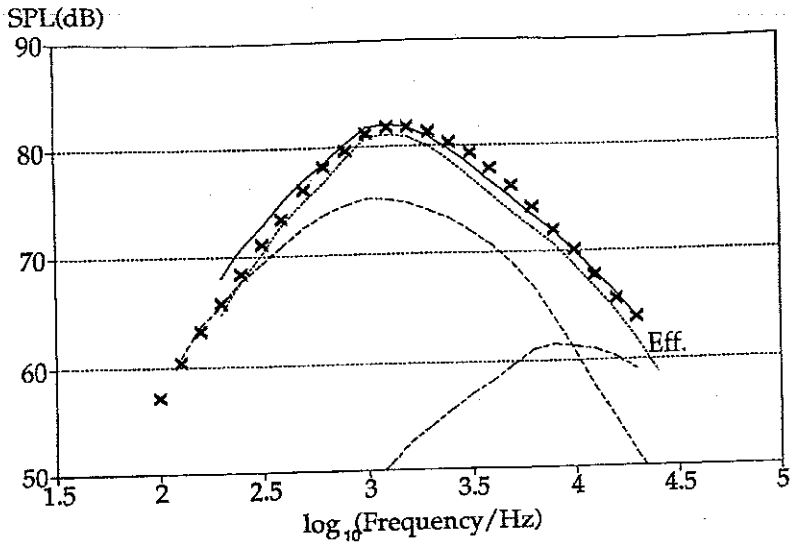

Figure 33 a) 40° prediction at Tp = 600K, λ = 0.63, Vp = 265.3m/s

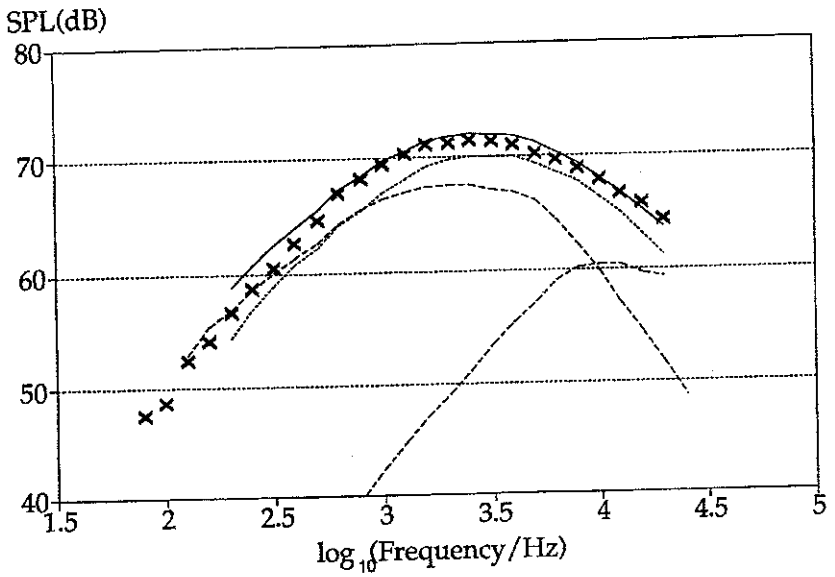

b) 90° prediction at Tp = 600K, λ = 0.63, Vp = 265.3m/s

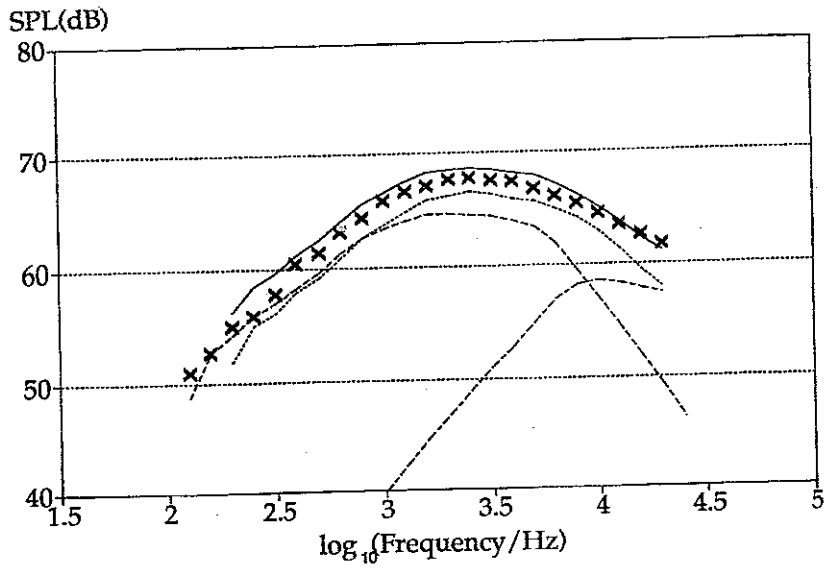

c) 120° prediction at Tp = 600K, λ = 0.63, Vp = 265.3m/s

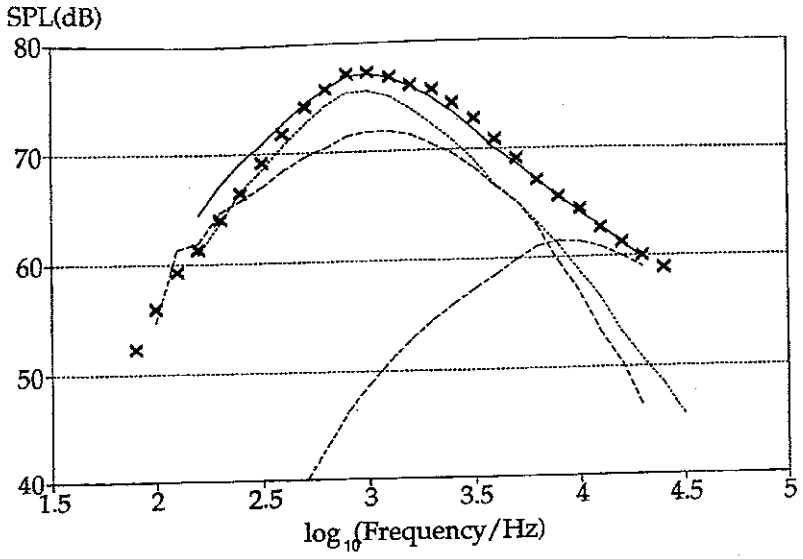

Figure 34 a) 40° prediction at Tp = 800K, λ = 0.79, Vp = 211.3m/s

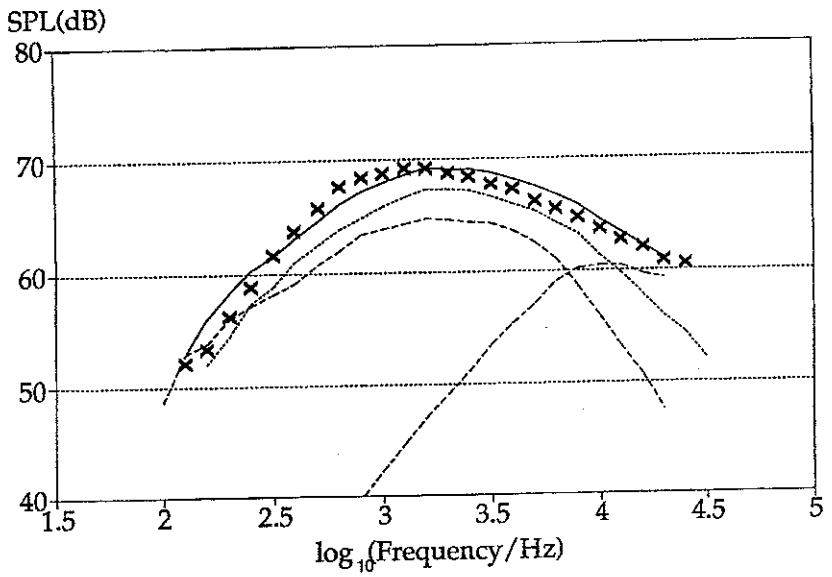

b) 90° prediction at Tp = 800K, λ = 0.79, Vp = 211.3m/s

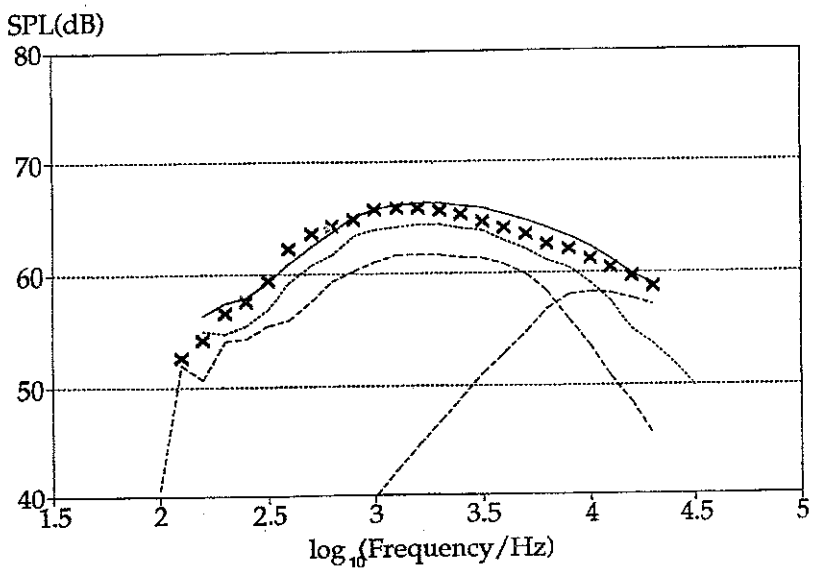

c) 120° prediction at Tp = 800K, λ = 0.79, Vp = 211.3m/s

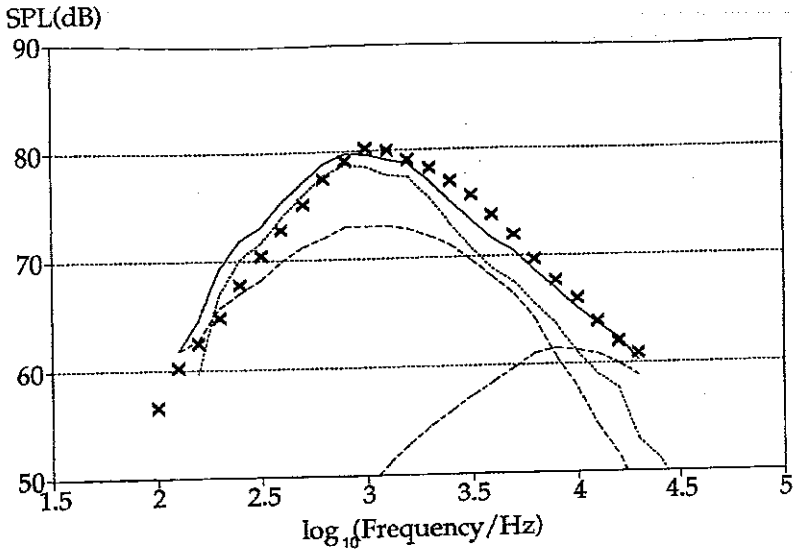

Figure 35 a) 40° prediction at Tp = 800K, λ = 0.71, Vp = 236.9m/s

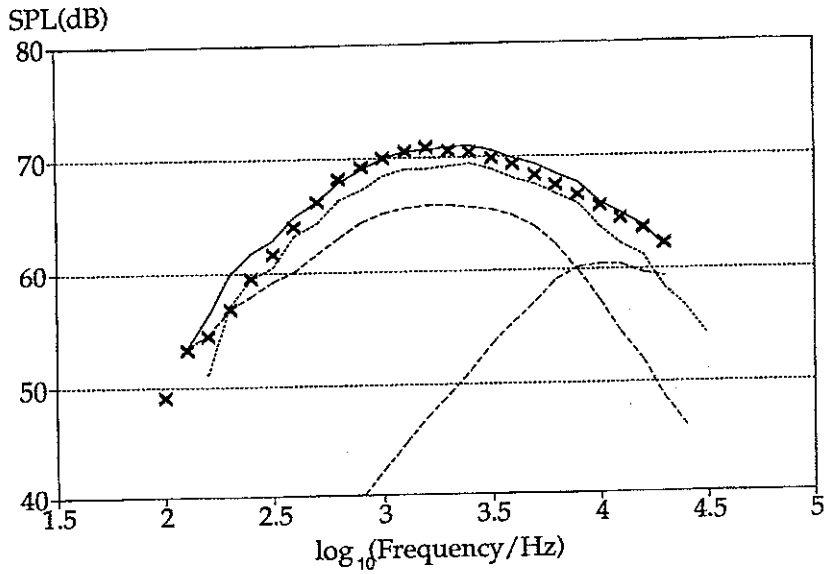

b) 90° prediction at Tp = 800K, λ = 0.71, Vp = 236.9m/s

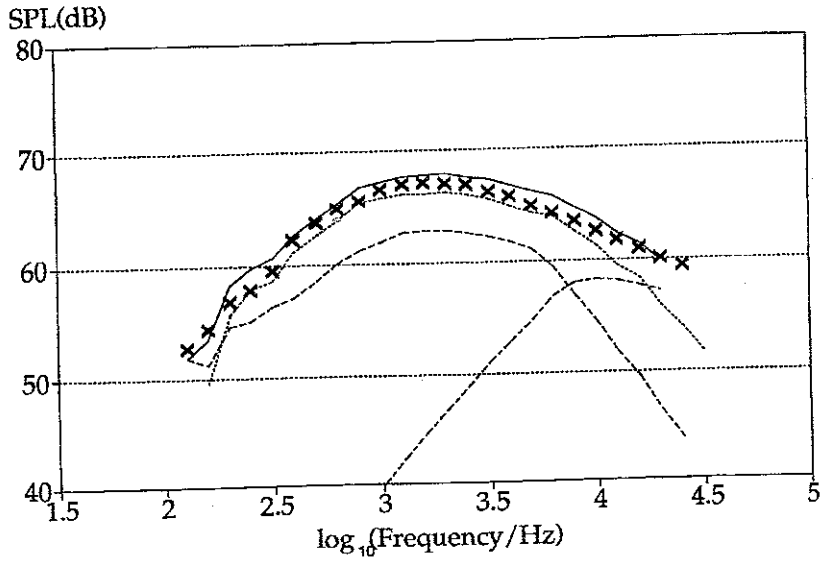

c) 120° prediction at Tp = 800K, λ = 0.71, Vp = 236.9m/s

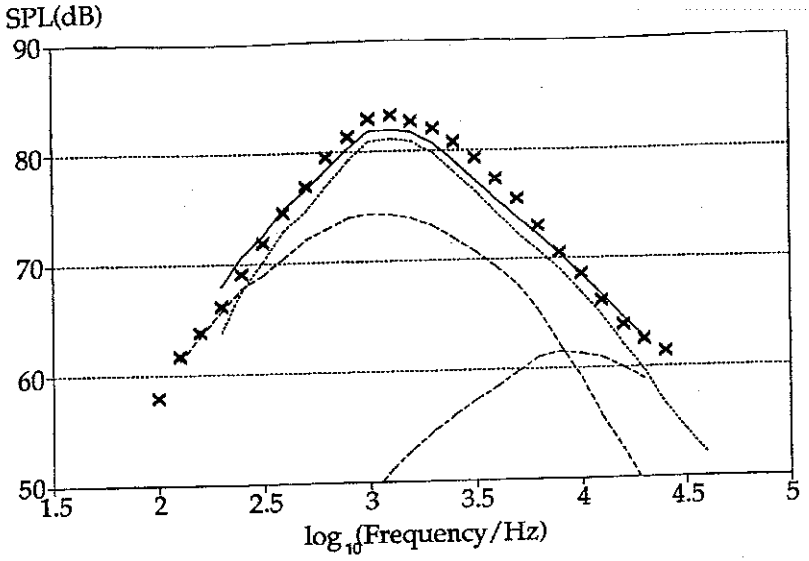

Figure 36 a) 40° prediction at Tp = 800K, λ = 0.63, Vp = 266.3m/s

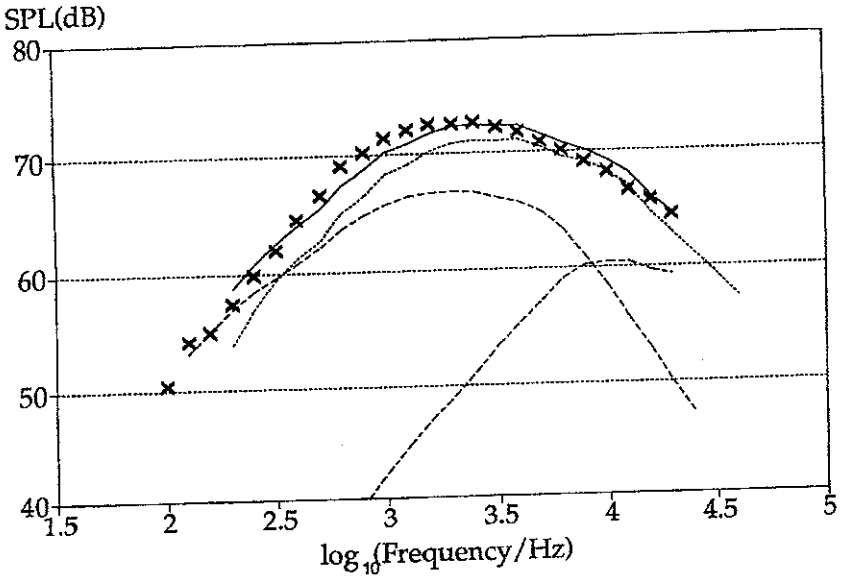

b) 90° prediction at Tp = 800K, λ = 0.63, Vp = 266.3m/s

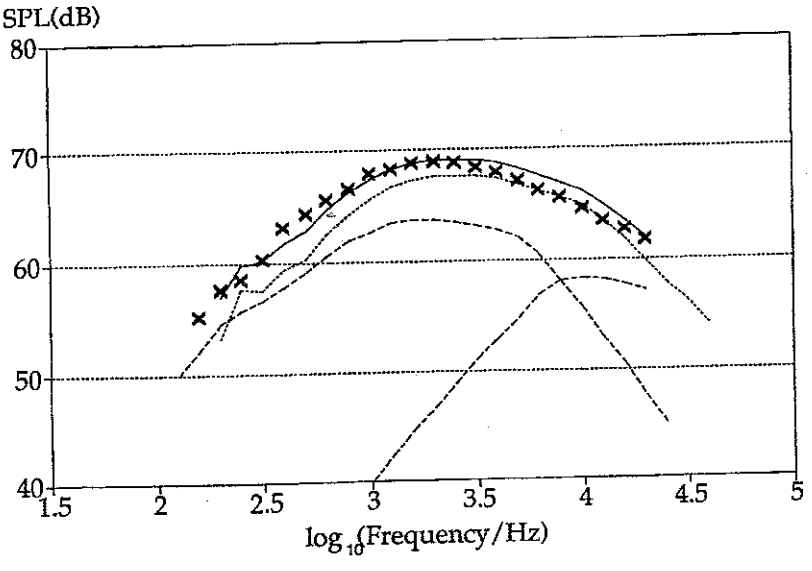

c) 120° prediction at Tp = 800K, λ = 0.63, Vp = 266.3m/s

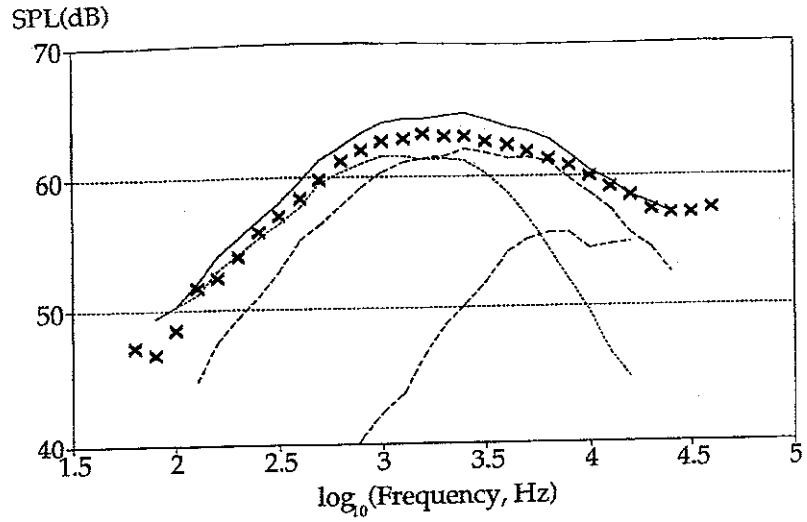

Figure 37 a) 90° ,β = 4, initial prediction at ambient temp., Vp = 215m/s, λ = 0.63

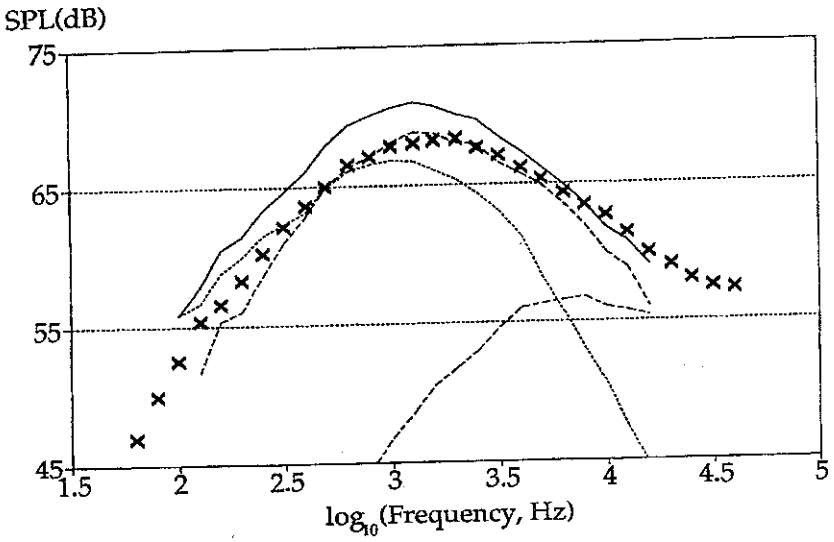

b) 40° ,β = 4, initial prediction at ambient temp., Vp = 215m/s, λ = 0.63

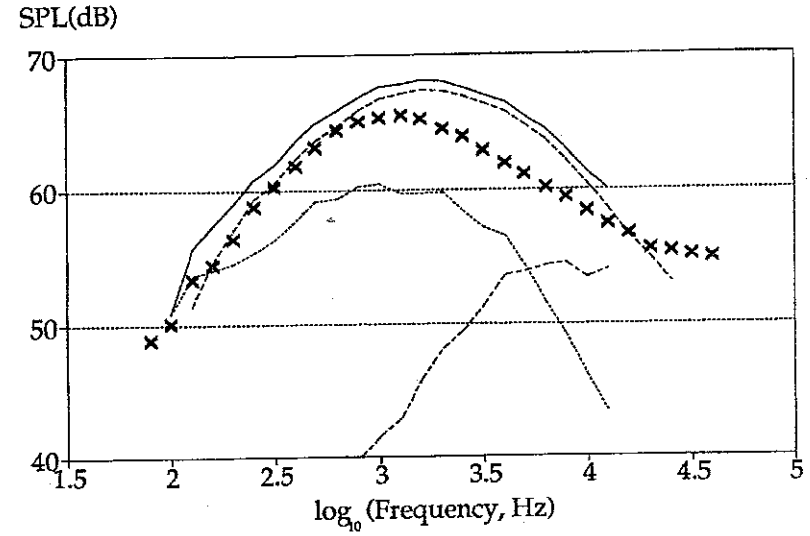

c) 90°, β= 4 initial prediction at Tp = 800K, Vp = 210m/s, λ= 0.63

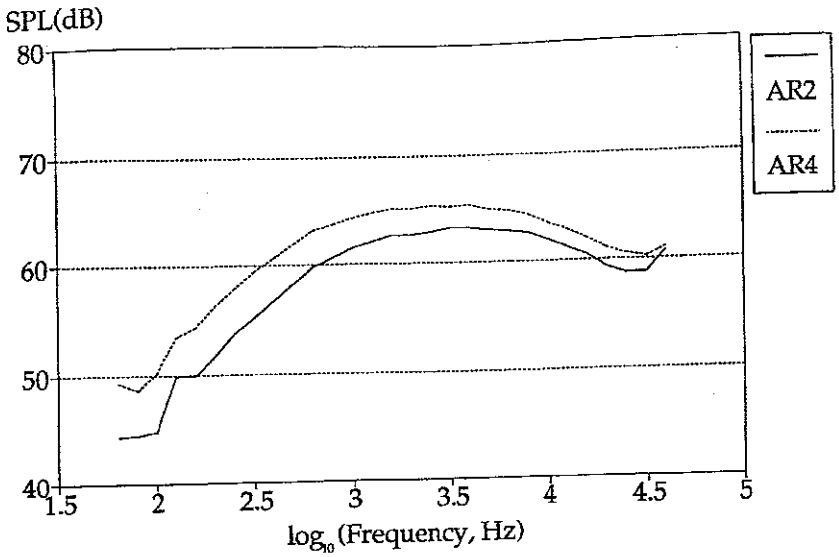

Figure 38 a) 90 °measured spectra for cold jets, Vp = 170m/s, λ = 1.00

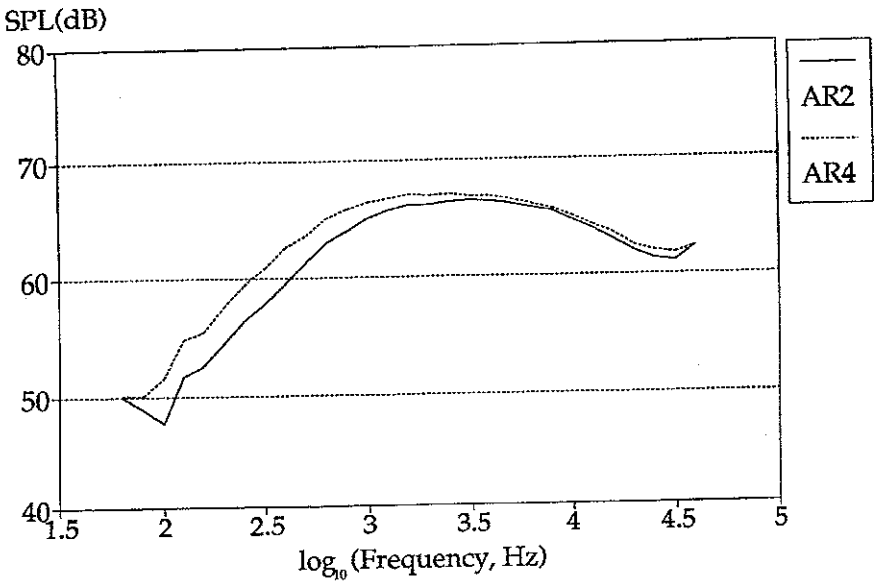

b) 90 °measured spectra for cold jets, Vp = 215m/s, λ = 0.79

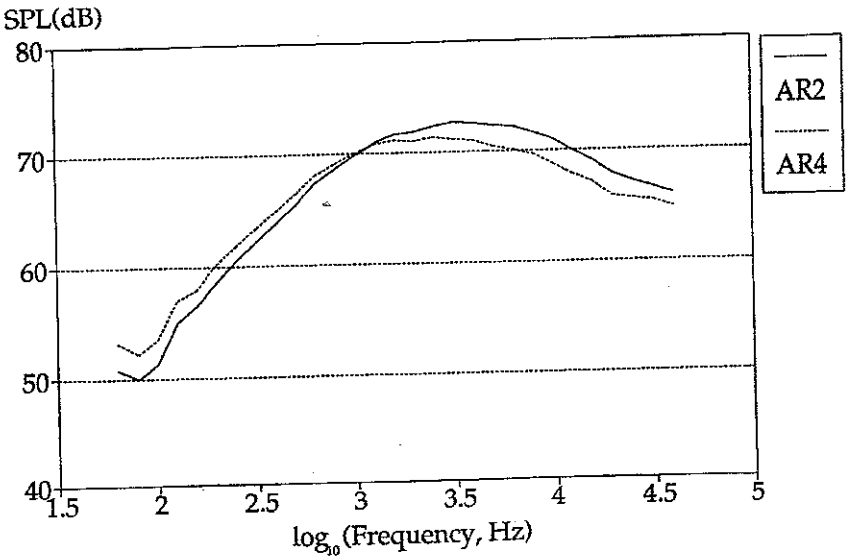

c) 90 °measured spectra for cold jets, Vp = 270m/s, λ = 0.63

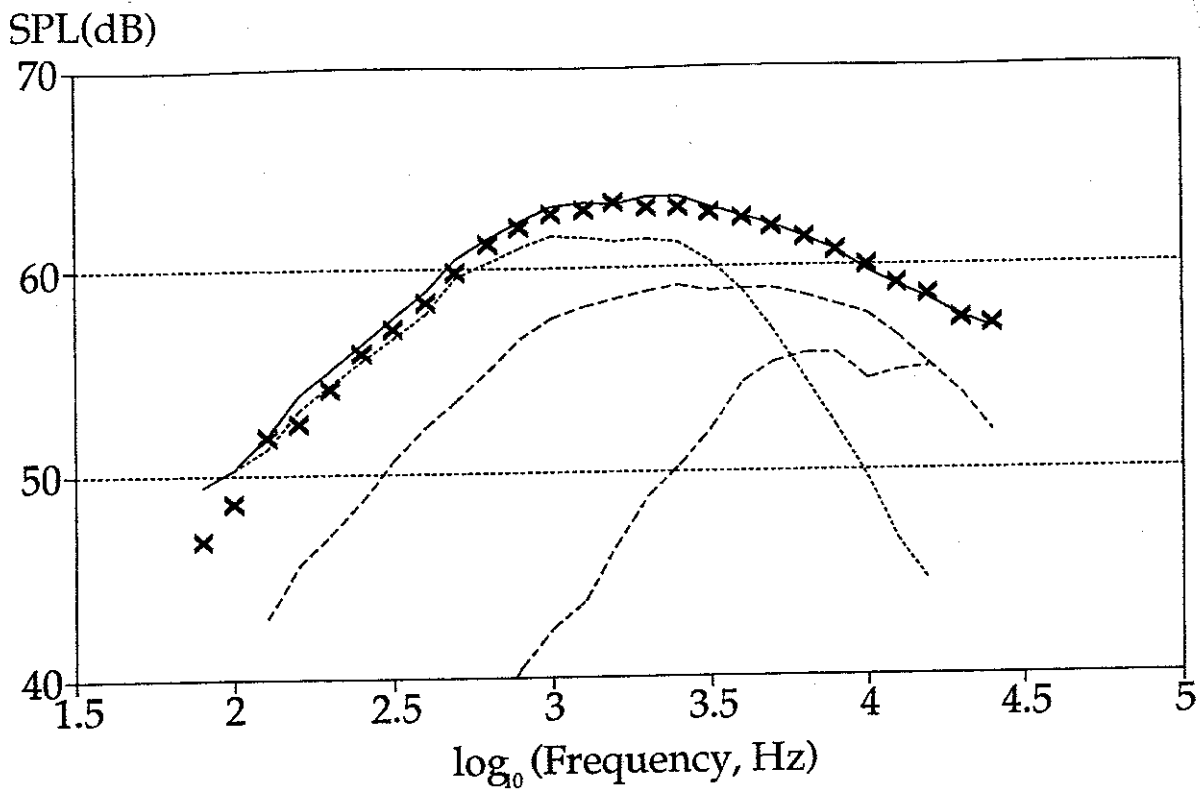

Figure 39 a) 90°, Vp = 215m/s, λ= 0.63
Cold jet.

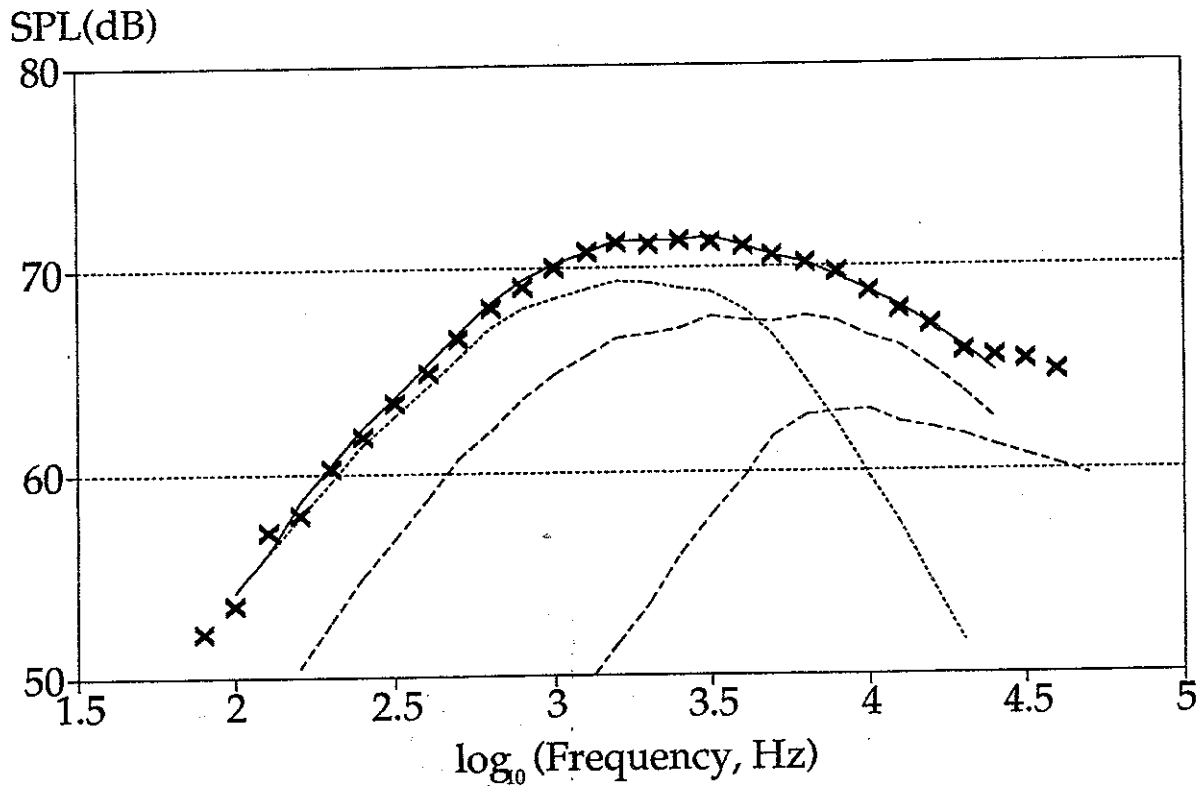

b) 90°, Vp = 270m/s, λ= 0.63
Cold jet.

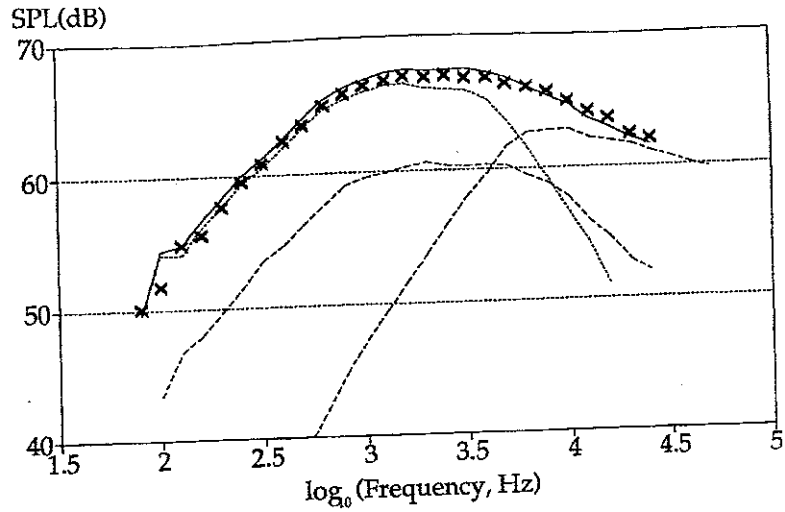

Figure 40 a) 90°, Vp = 215m/s, λ= 0.79
Cold jet.

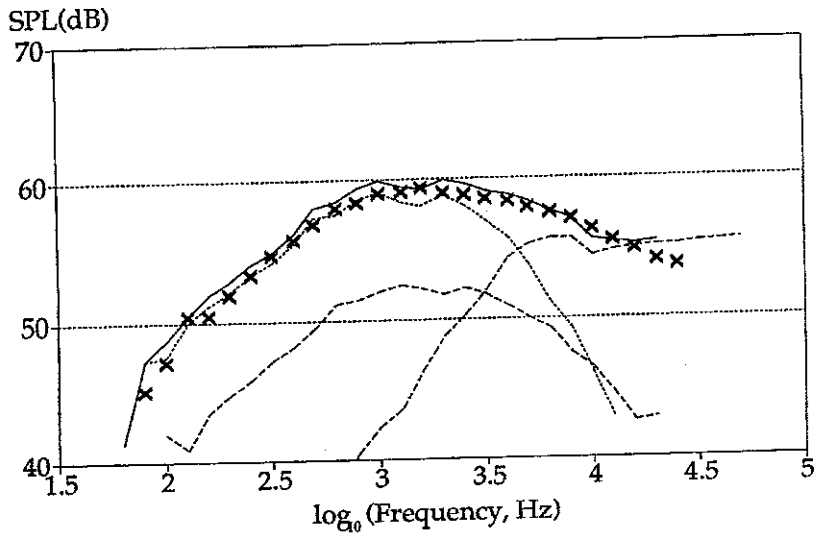

b) 90°, Vp = 170m/s, λ= 0.79
Cold jet.

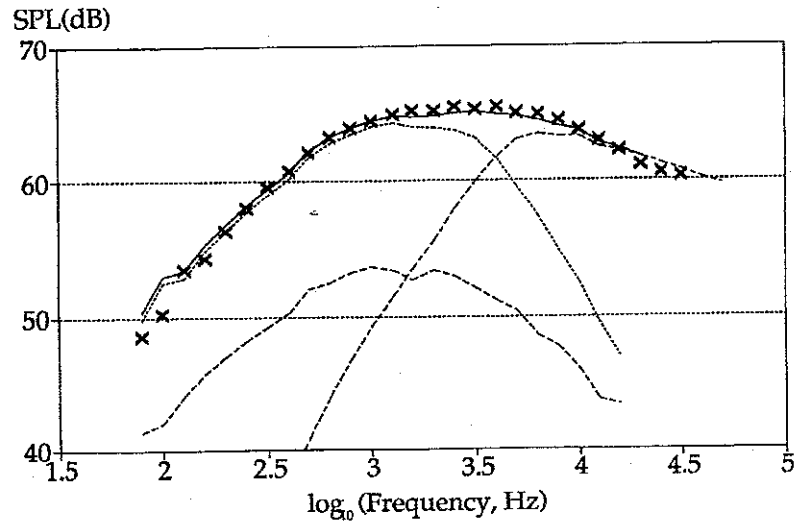

c) 90°, Vp = Vs = 170m/s. λ= 1.00
Cold jet.

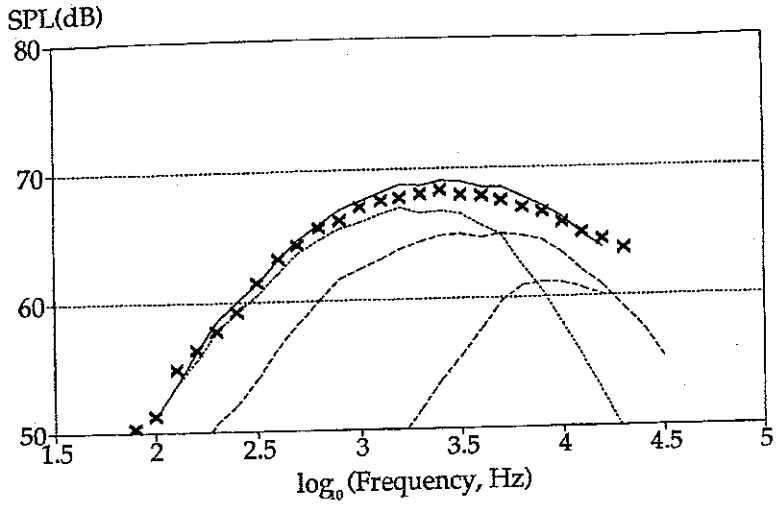

Figure 41 a) 120° , Vp = 270m/s, λ= 0.63
Cold jet.

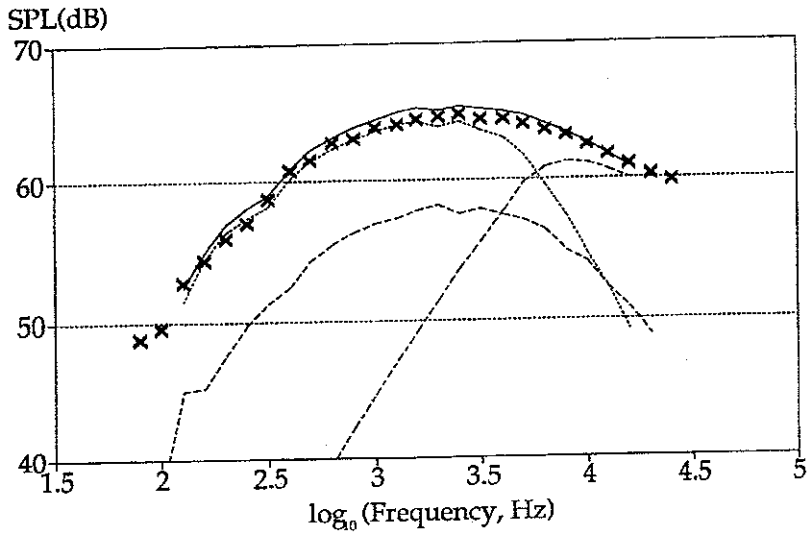

b) 120°, Vp = 215m/s, λ= 0.79
Cold jet.

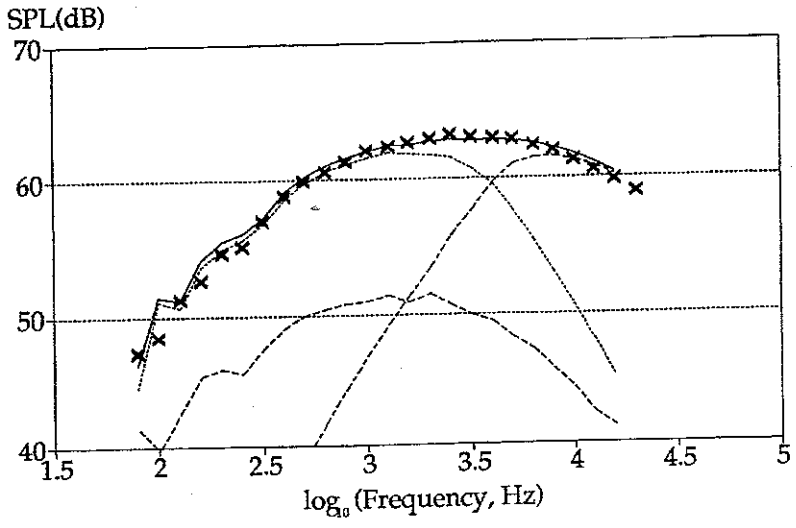

c) 120° , Vp = 170m/s, λ= 1.00
Cold jet.

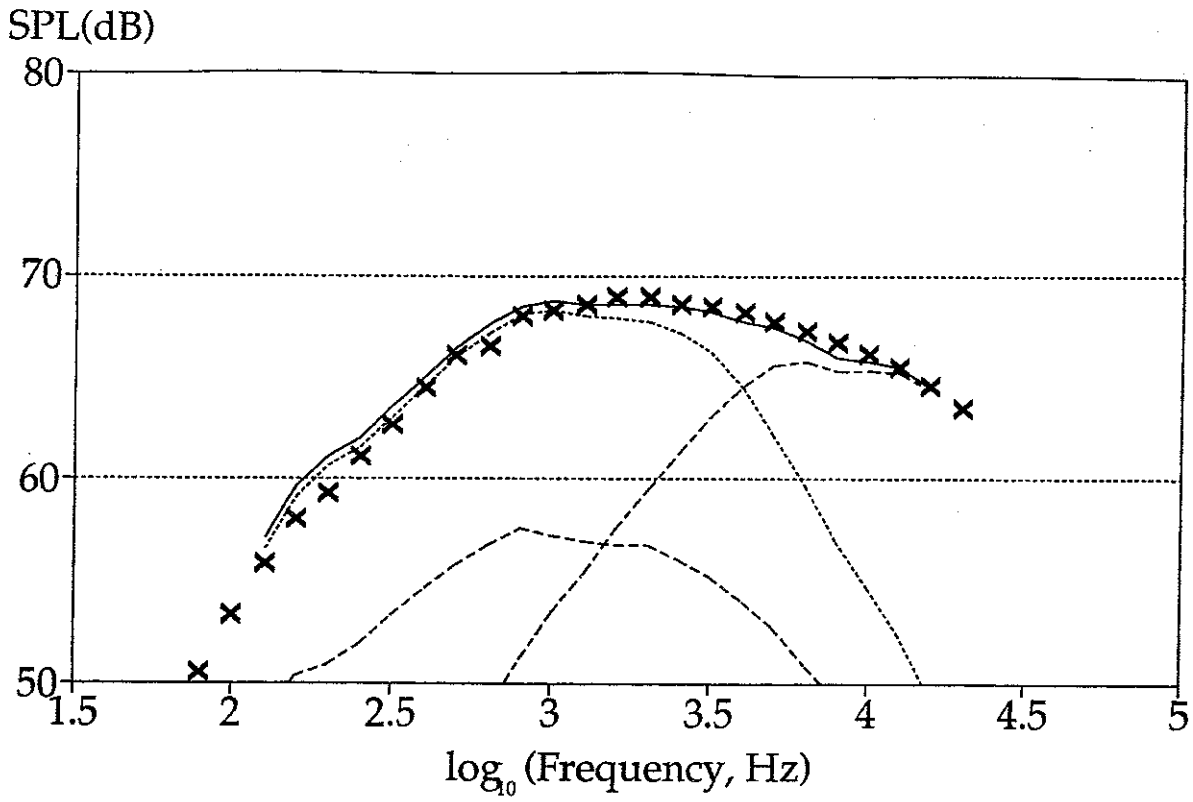

Figure 42 a) 50°, Vp = 170m/s, λ= 1.00
Cold jet

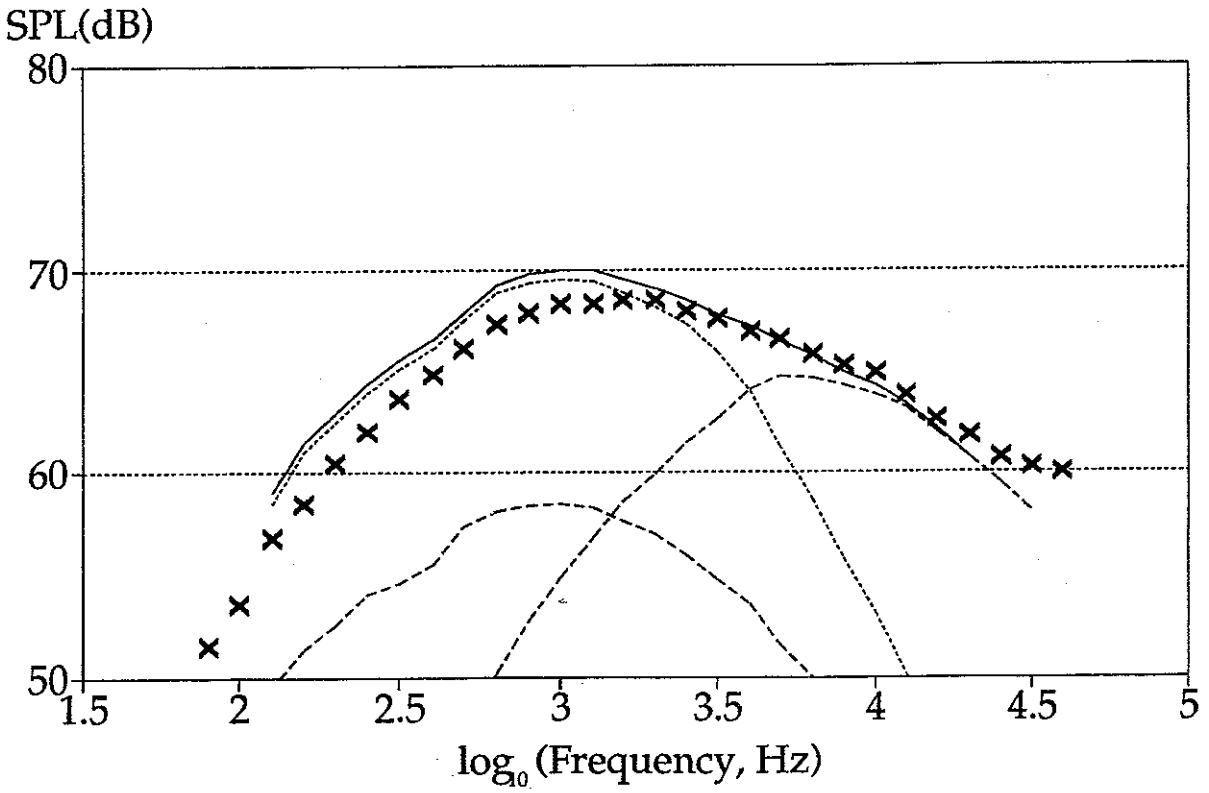

Figure 42 b) 40°, Vp = 170m/s, λ= 1.00
Cold jet

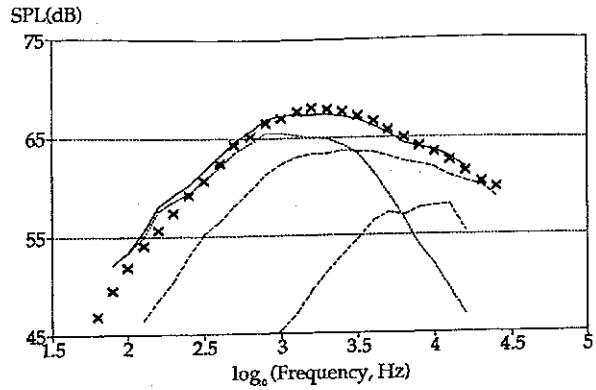

Figure 43 a) 50°, Vp = 215m/s, λ= 0.63
Cold jet

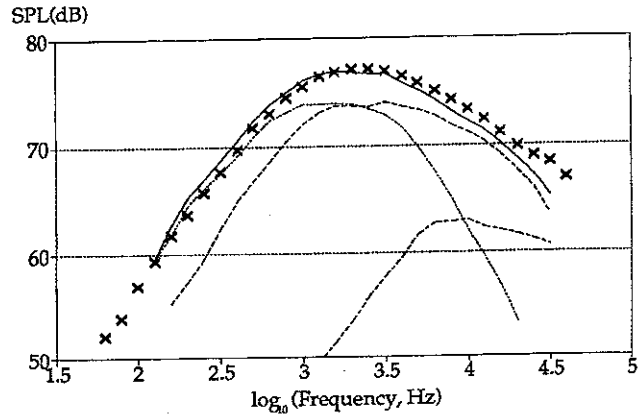

b) 50°, Vp = 270m/s, λ= 0.63
Cold jet

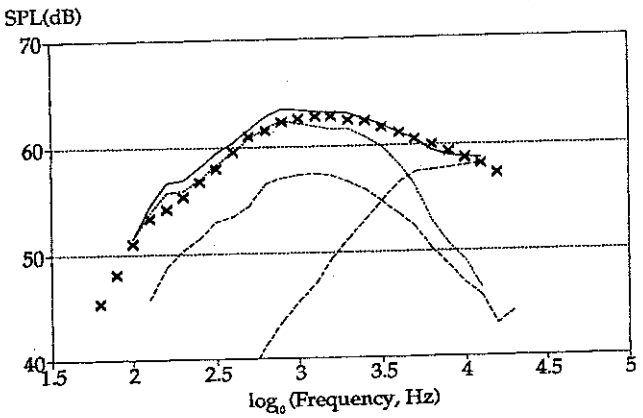

c) 50°, Vp = 170m/s, λ= 0.79
Cold jet

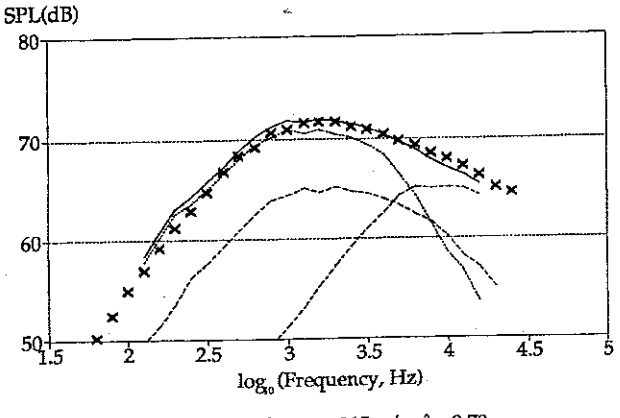

d) 50°, Vp = 215m/s, λ= 0.79
Cold jet

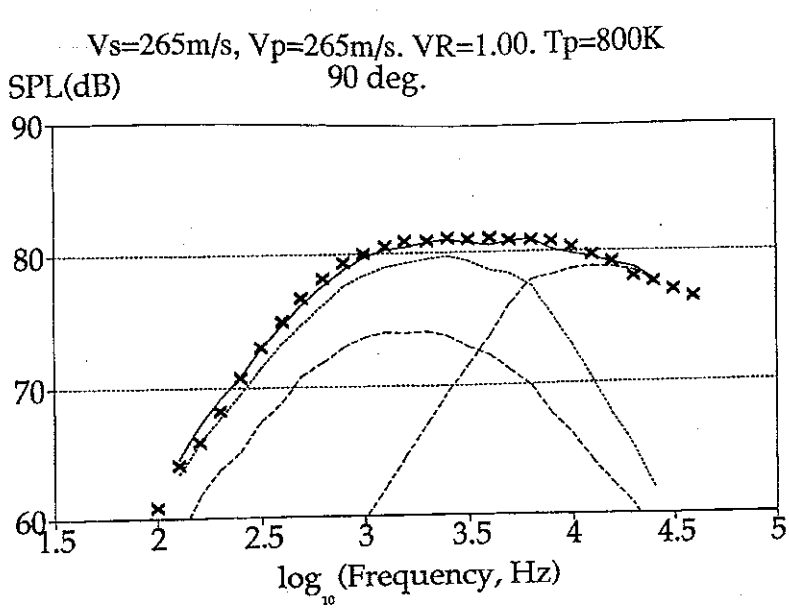
Vs=265m/s, Vp=265m/s. VR=1.00. Tp=800K
90 deg.
SPL(dB)
90
80
70
60
1.5
2
2.5
3
3.5
4
4.5
5
log10 (Frequency, Hz)

44 a)

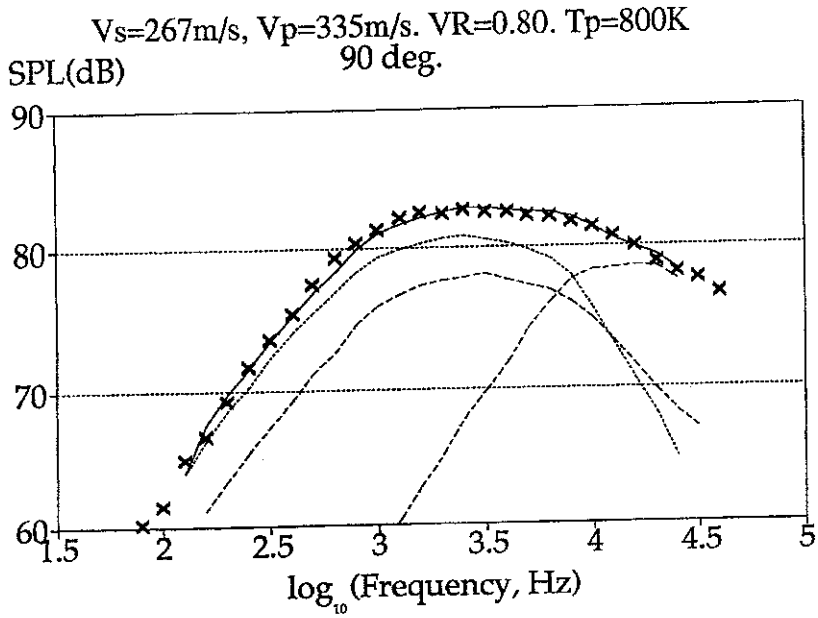
Vs=267m/s, Vp=335m/s. VR=0.80. Tp=800K
90 deg.
SPL(dB)
90
80
70
60
1.5
2
2.5
3
3.5
4
4.5
5
log10 (Frequency, Hz)

44 b)

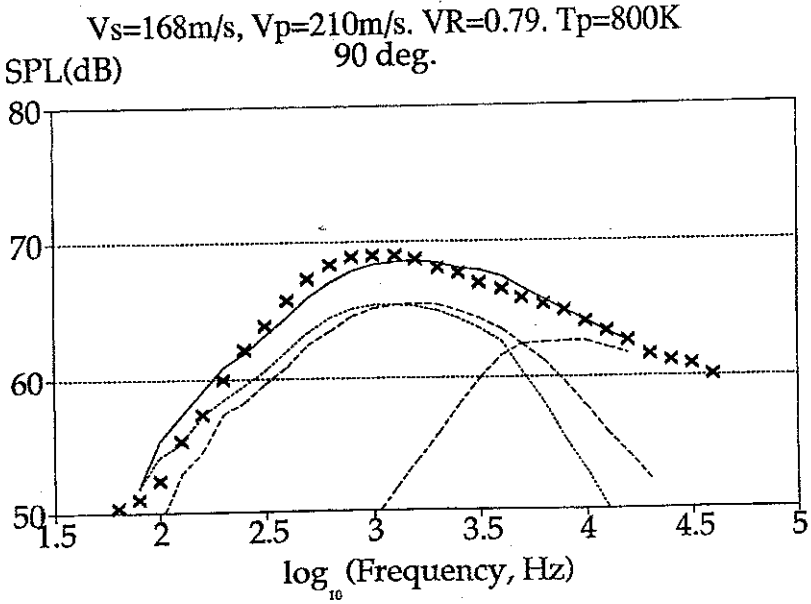
Vs=168m/s, Vp=210m/s. VR=0.79. Tp=800K
90 deg.
SPL(dB)
80
70
60
50
1.5
2
2.5
3
3.5
4
4.5
5
log10 (Frequency, Hz)

44 c)

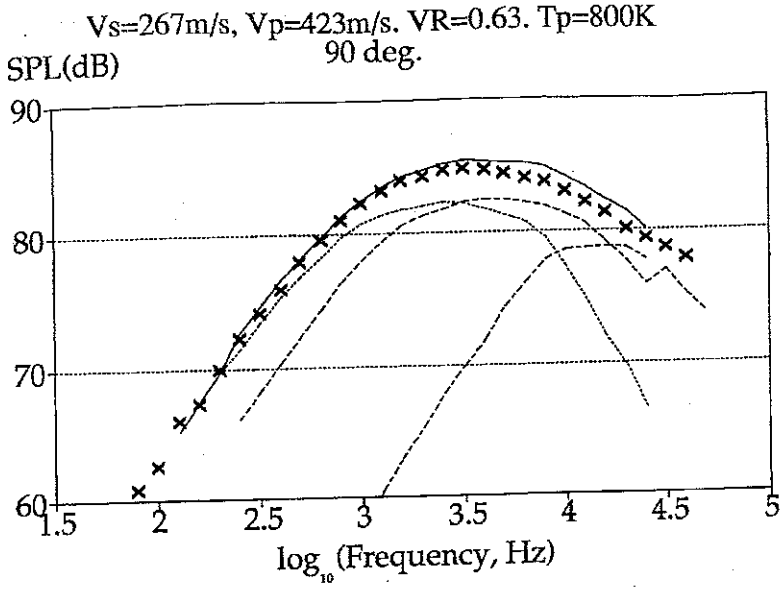
Vs=267m/s, Vp=423m/s. VR=0.63. Tp=800K
90 deg.
SPL(dB)
90
80
70
60
1.5
2
2.5
3
3.5
4
4.5
5
log10(Frequency, Hz)

44 d)

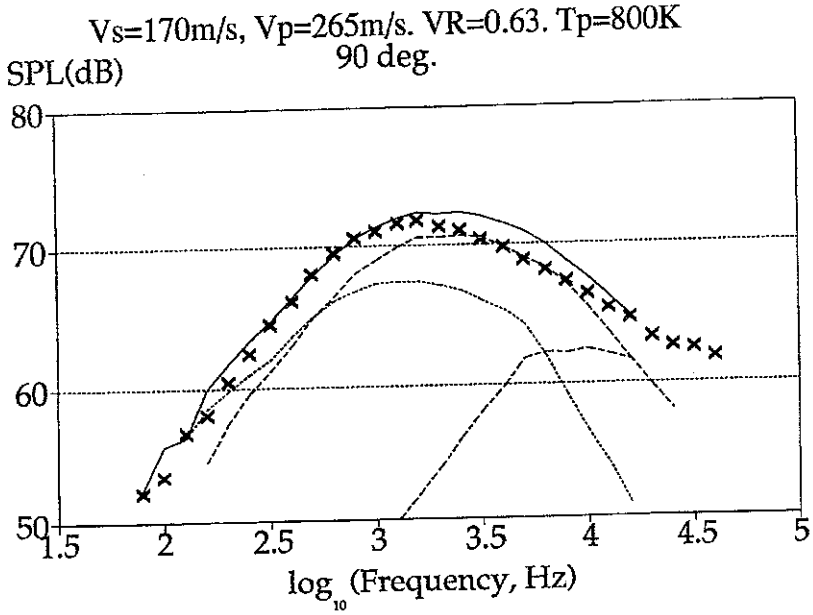
Vs=170m/s, Vp=265m/s. VR=0.63. Tp=800K
90 deg.
SPL(dB)
80
70
60
50
1.5
2
2.5
3
3.5
4
4.5
5
log10 (Frequency, Hz)

44 e)

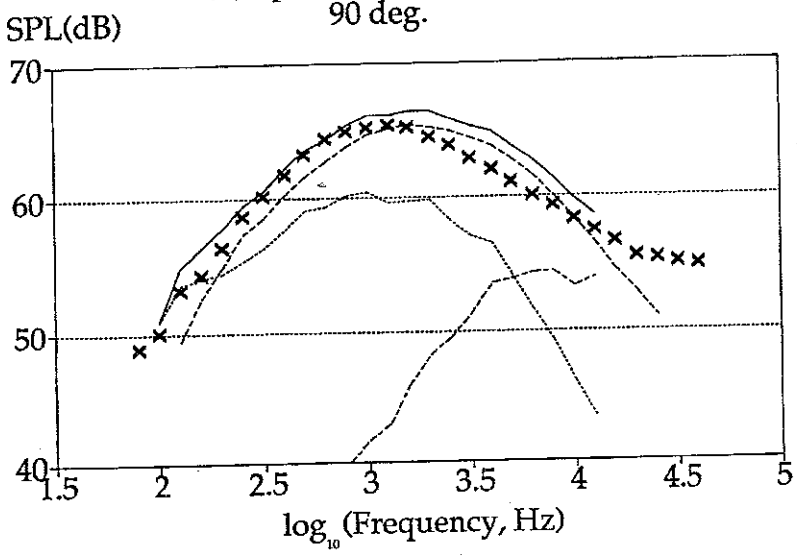
Vs=132m/s, Vp=210m/s. VR=0.63. Tp=800K
90 deg.
SPL(dB)
70
60
50
40
1.5
2
2.5
3
3.5
4
4.5
5
log10 (Frequency, Hz)

44 f)

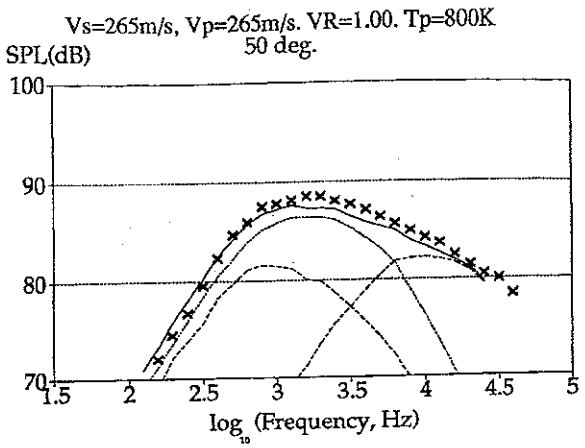

45 a)

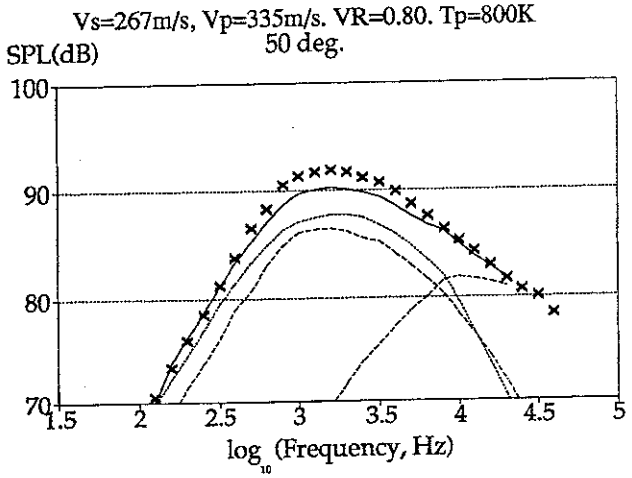

45 b)

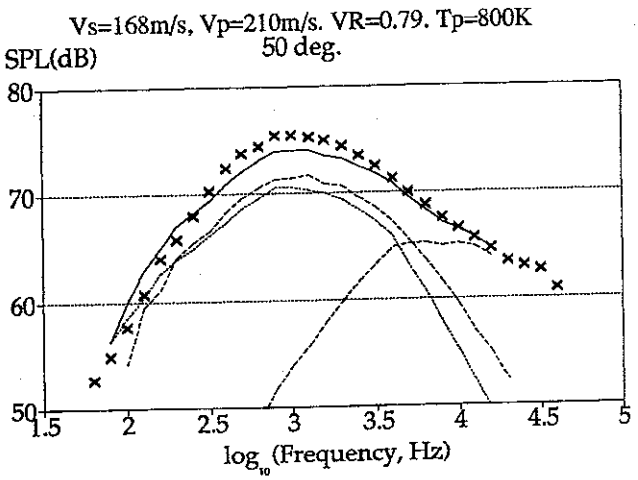

45 c)

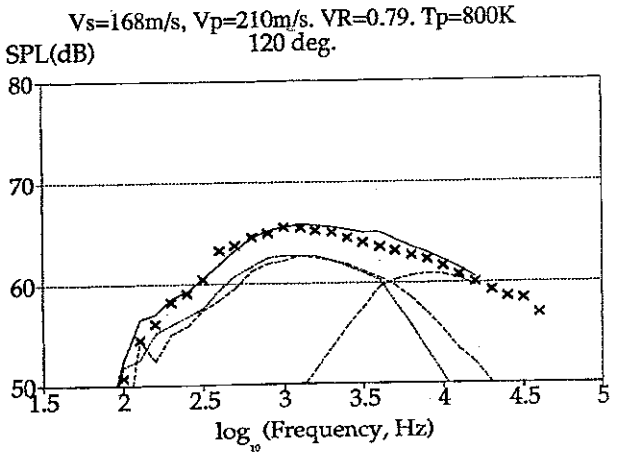

45 d)

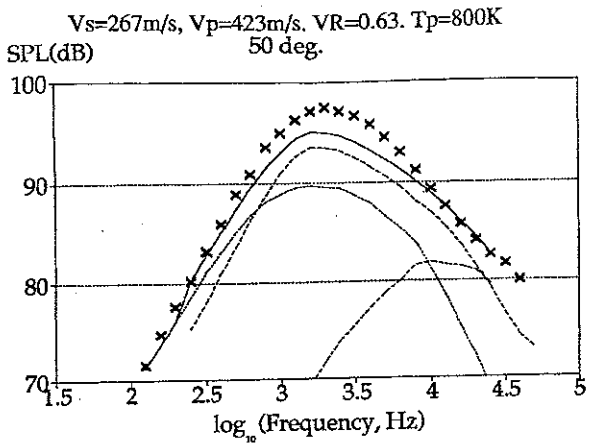

45 e)

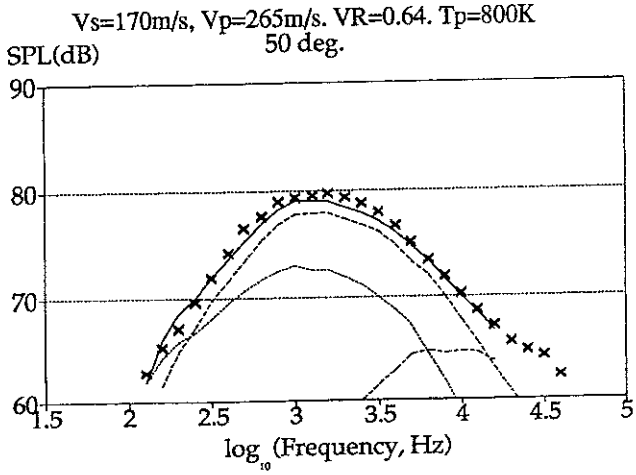

45 f)

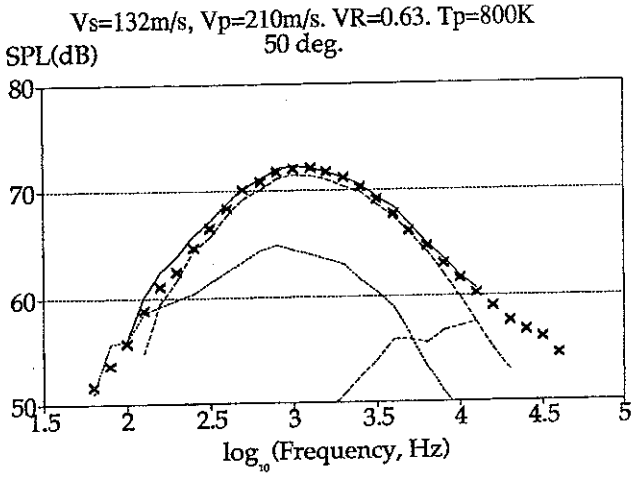

45 g)

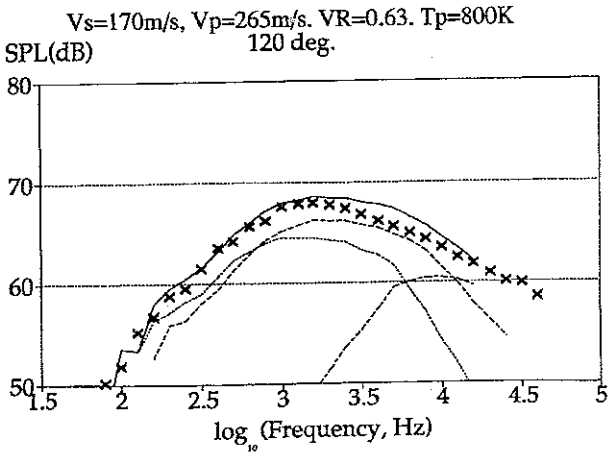

45 h)

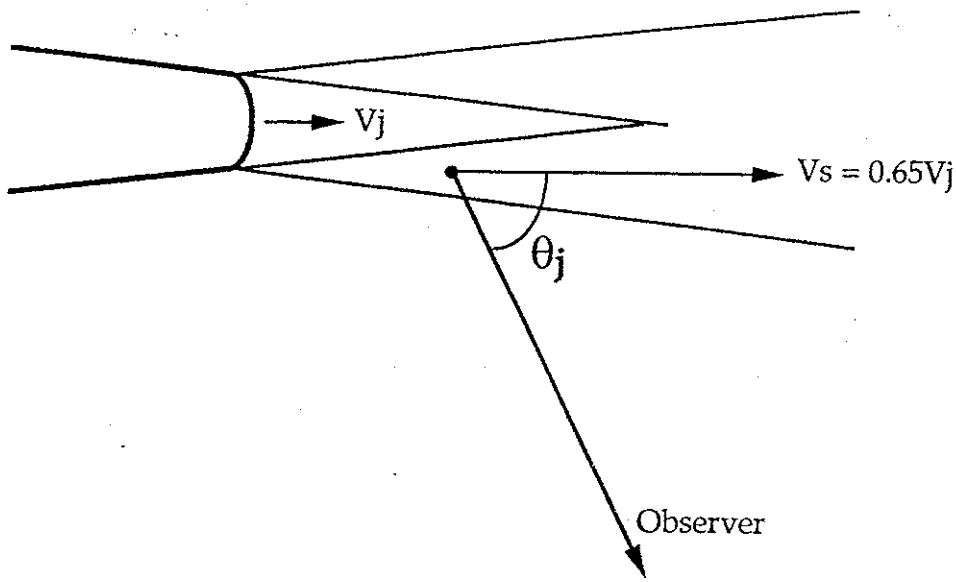

Figure 46 a) Source velocity and emission angle for a stationary jet.

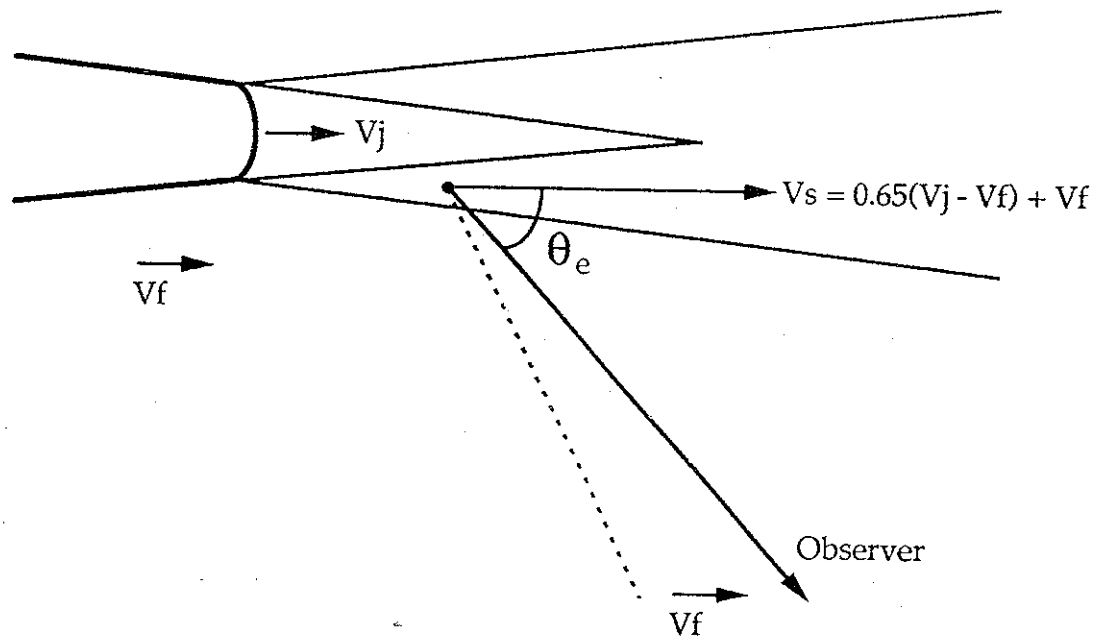

Figure 46 b) Source velocity and emission angle for a jet in a moving medium.

Figures 47.

o Static • Flight

a) Comparison of static and flight measured spectra for $V_p = 216 m/s, \lambda = 0.79$

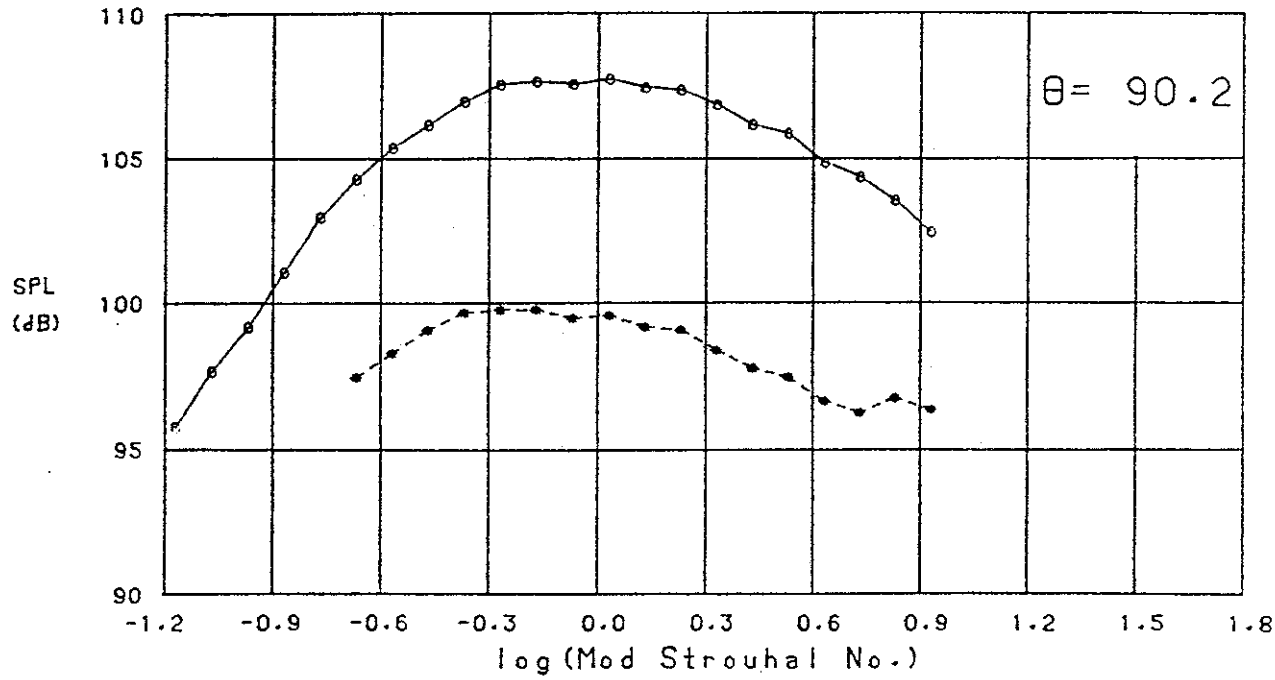

b) Comparison of static and flight measured spectra for $V_p = 301 m/s, \lambda = 0.56$

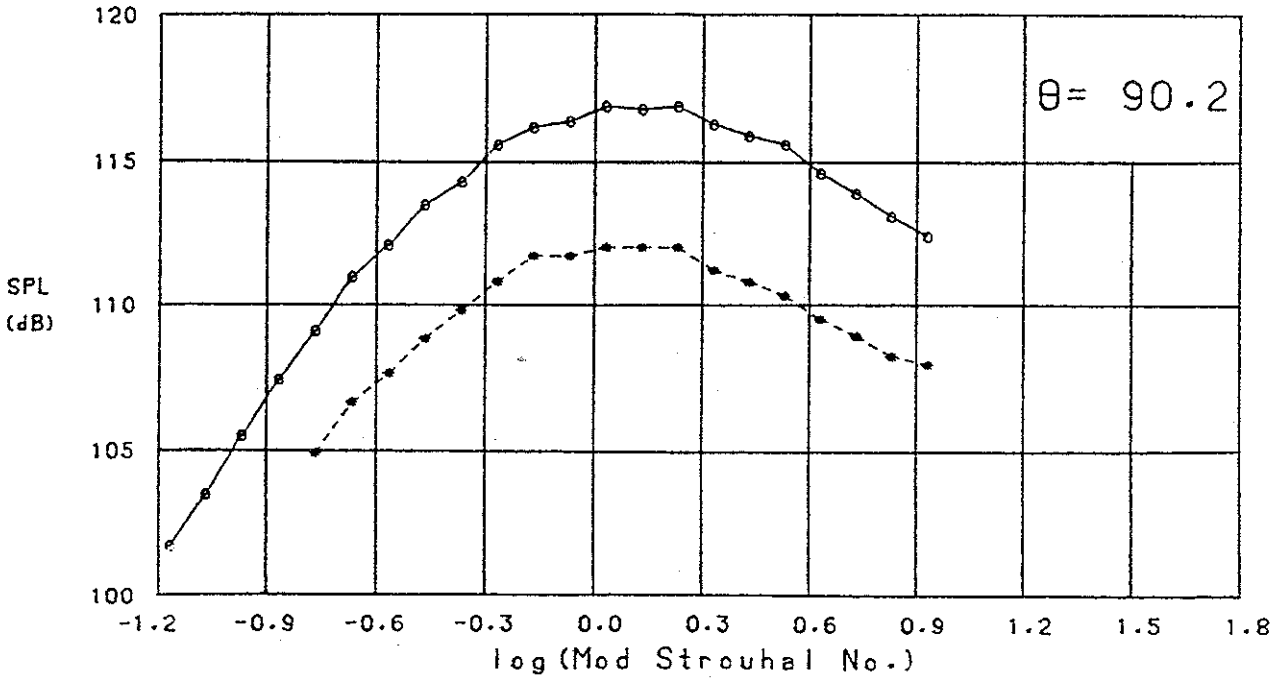

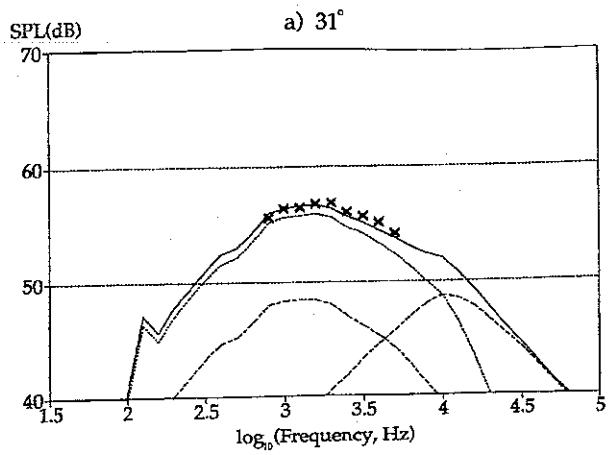

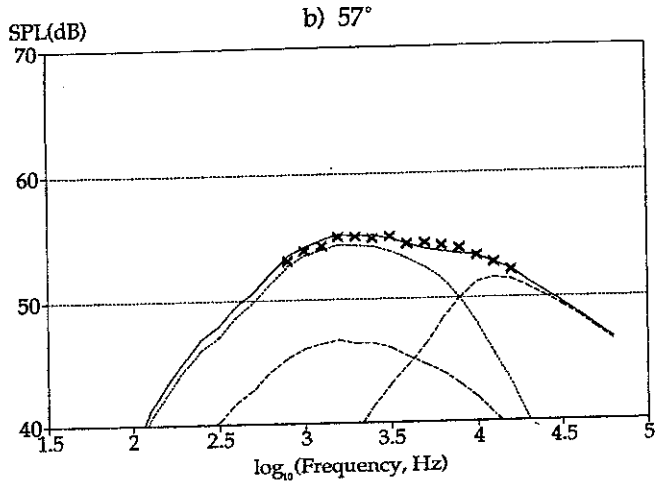

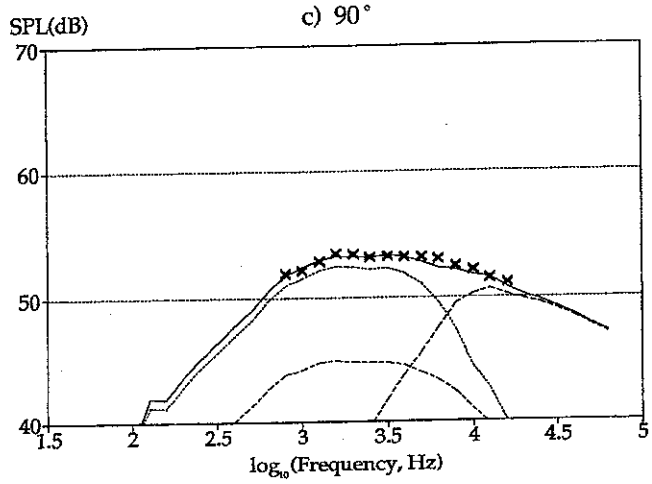

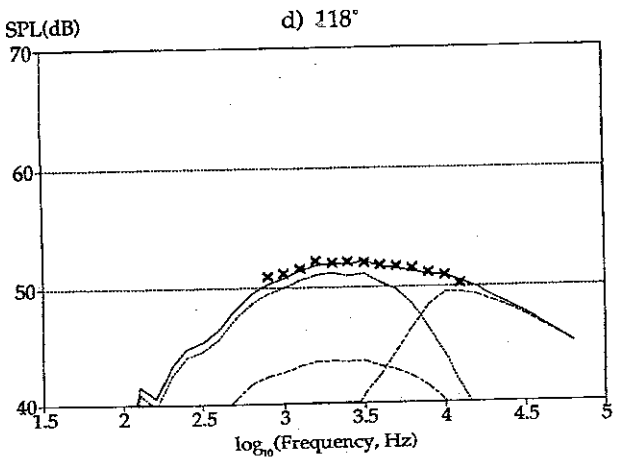

Figures 48.

Cold jet
Flight predictions,
$\beta = 2$, $\lambda = 1.0$,
$V_p = 171 m/s$

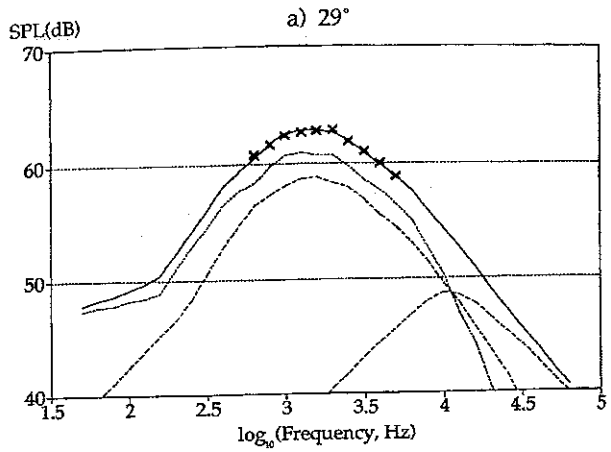

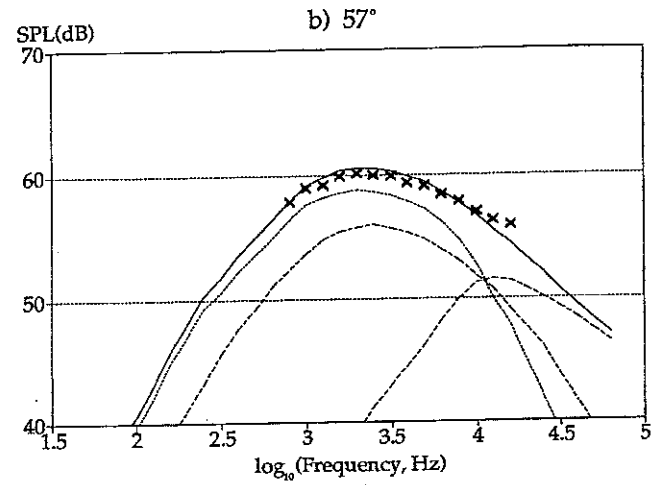

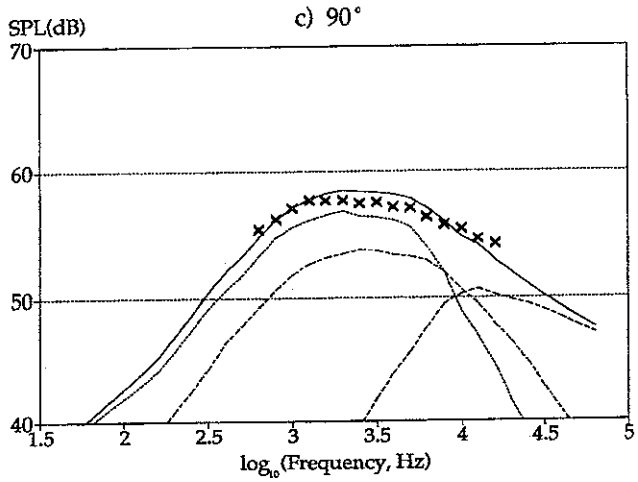

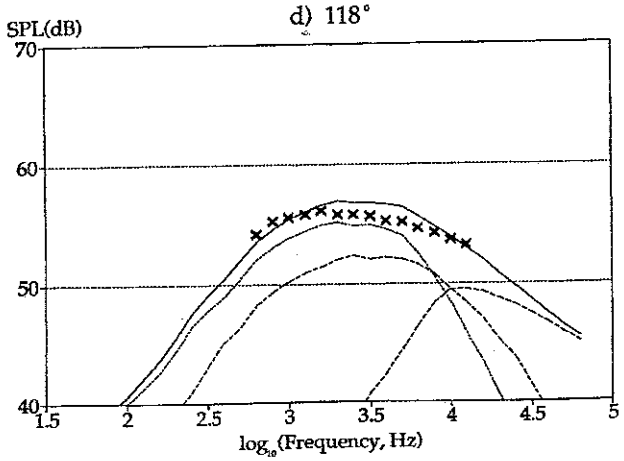

Figures 49.

Cold jet
Flight predictions,
$\beta = 2, \lambda = 0.8$
$V_p = 215 m/s$

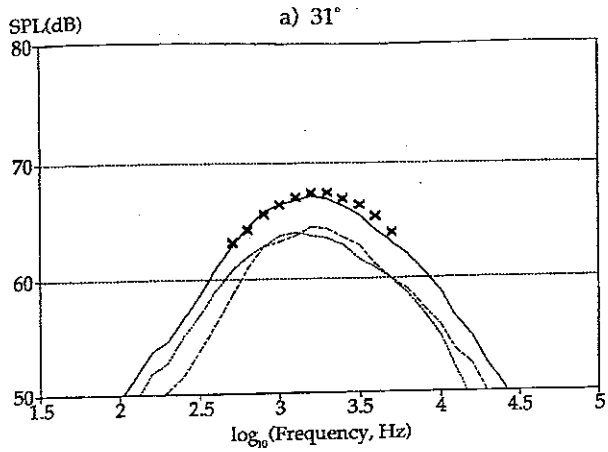

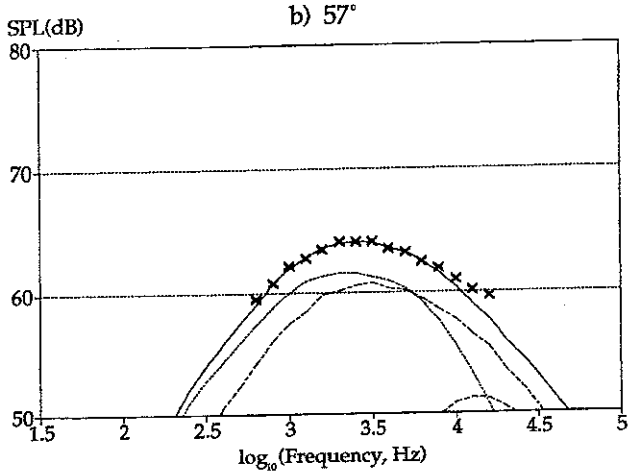

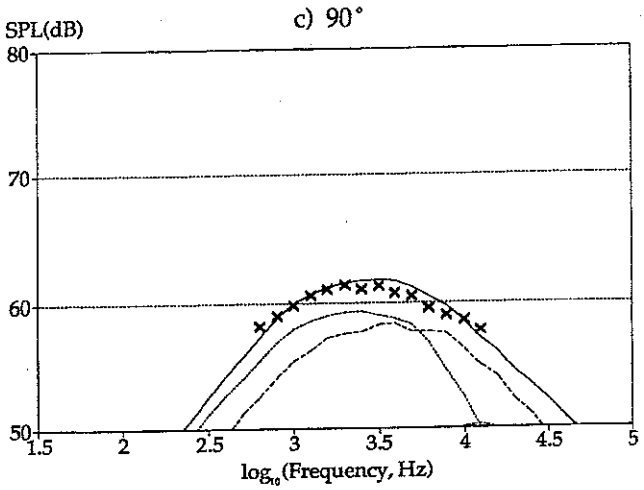

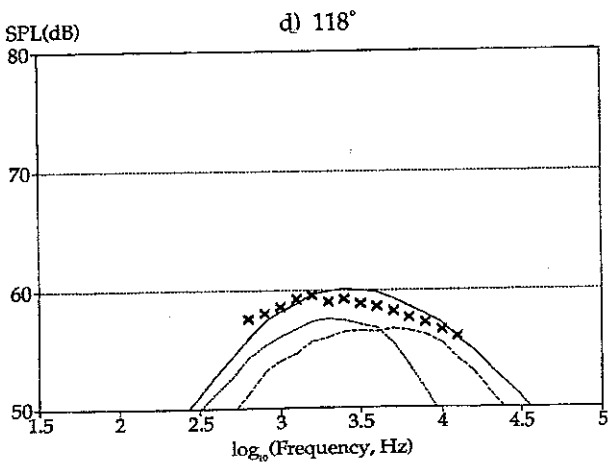

Figures 50.

Cold jet
Flight predictions,
$\beta = 2, \lambda = 0.7$
$V_p = 242 m/s$

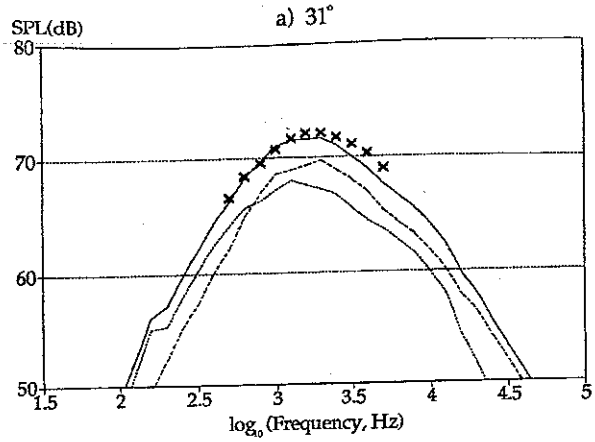

Figures 50.

Cold jet
Flight predictions,
$\beta = 2$, $\lambda = 0.63$
$V_p = 266 m/s$

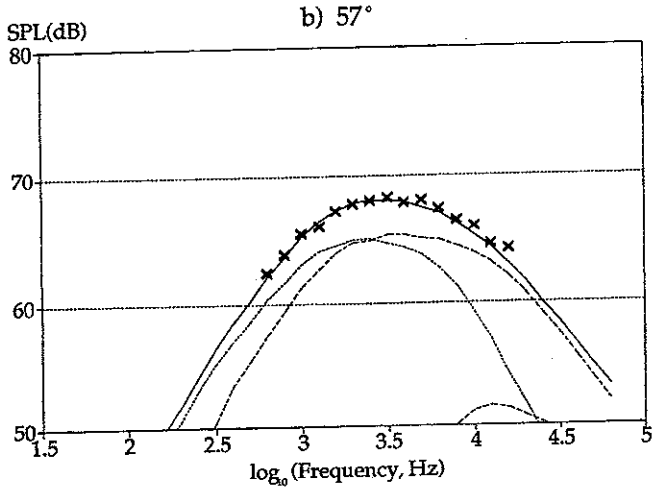

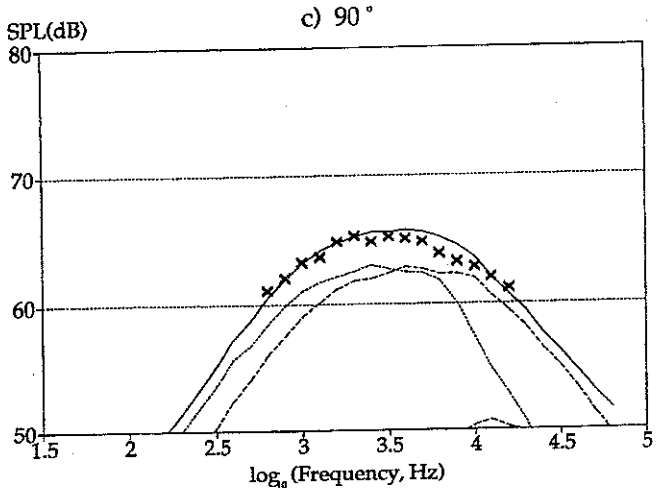

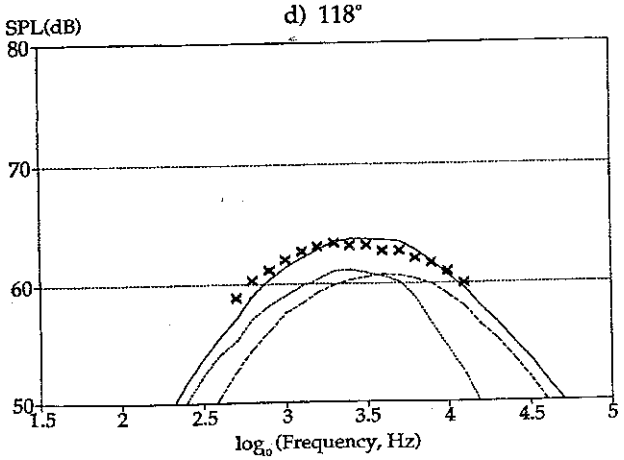

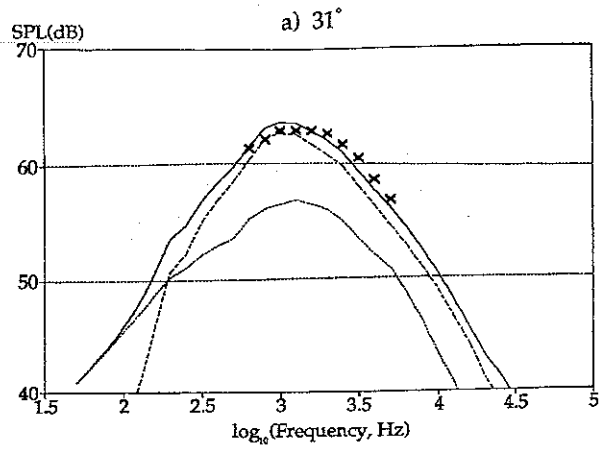

Figures 52.

Hot jet (600K)
Flight predictions,
$\beta = 2$, $\lambda = 0.63$
$V_p = 215 m/s$

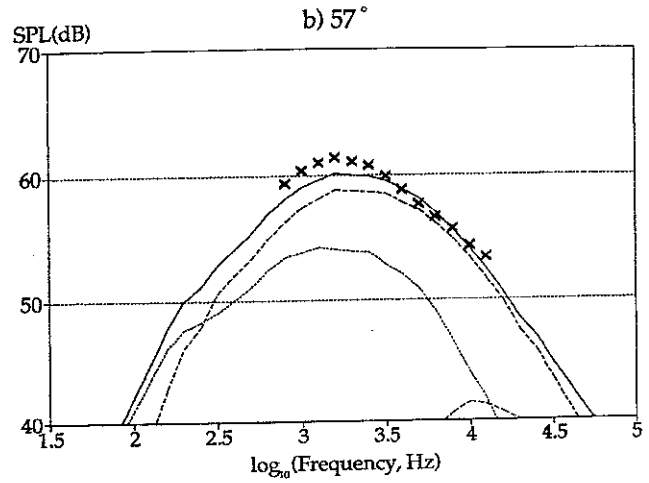

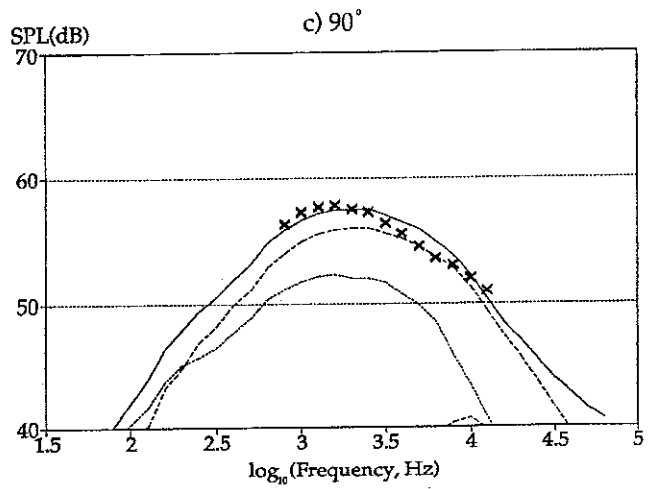

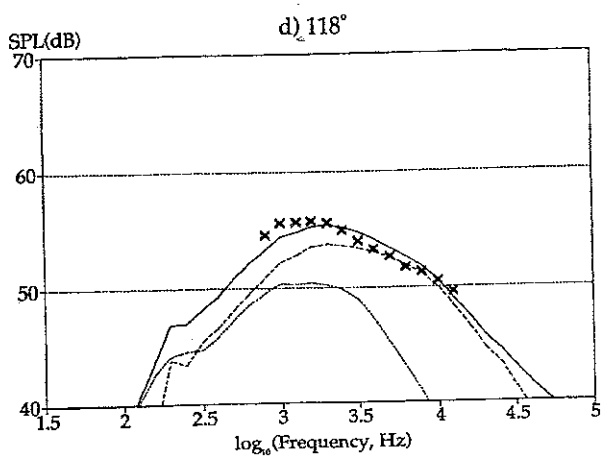

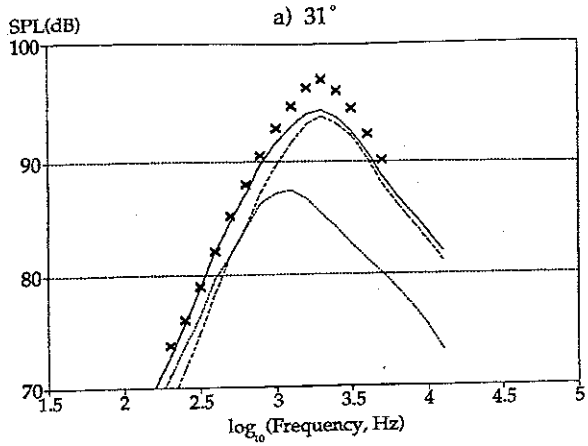

Figures 53.

Hot jet (800K)
Flight predictions,
$\beta = 2, \lambda = 0.63$
$V_p = 430 m/s$

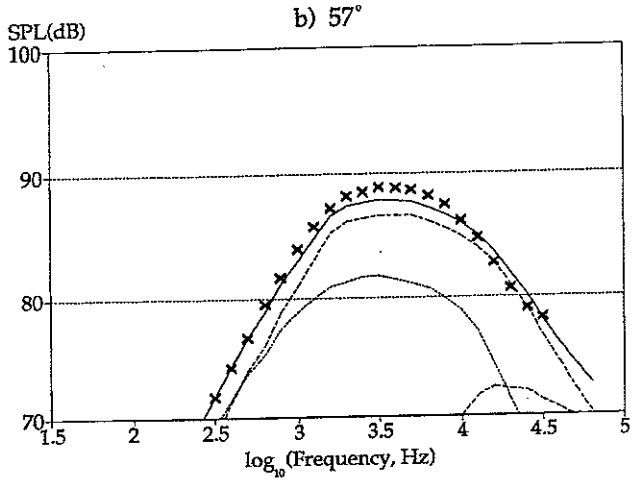

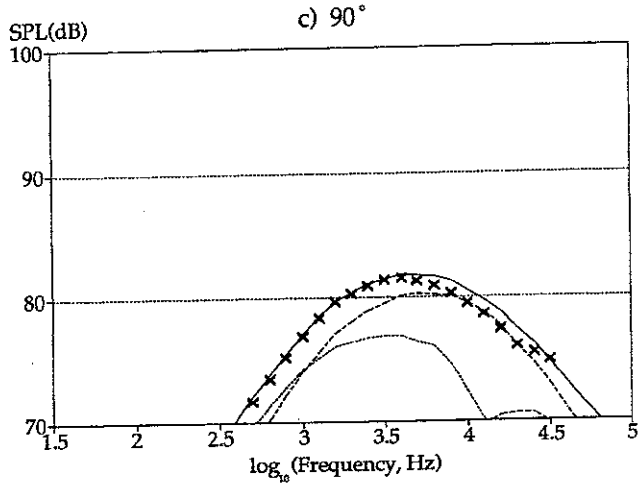

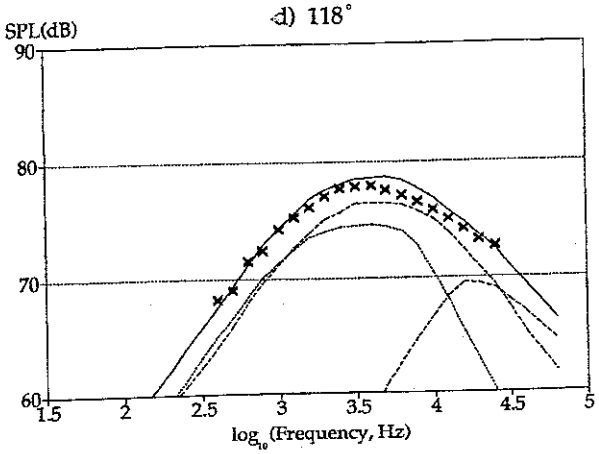

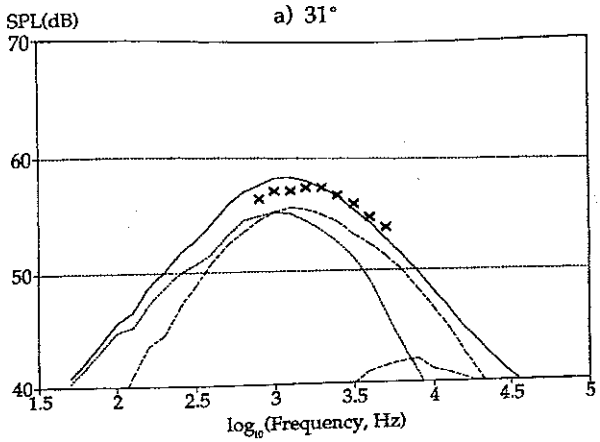

Figures 54.

Cold jet
Flight predictions,
$\beta = 4$, $\lambda = 0.63$
$V_p = 215 m/s$

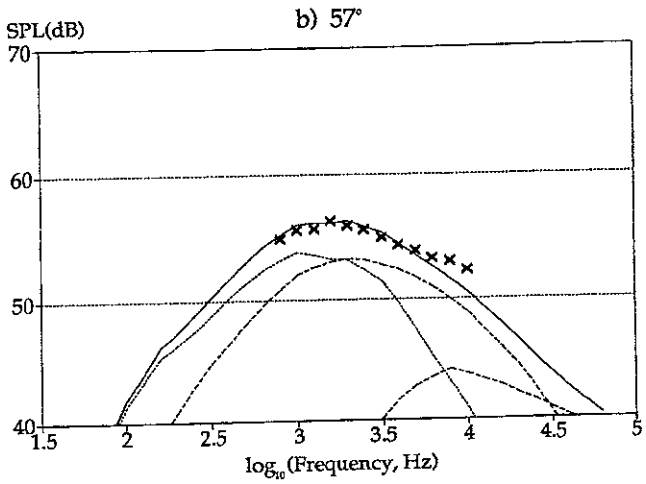

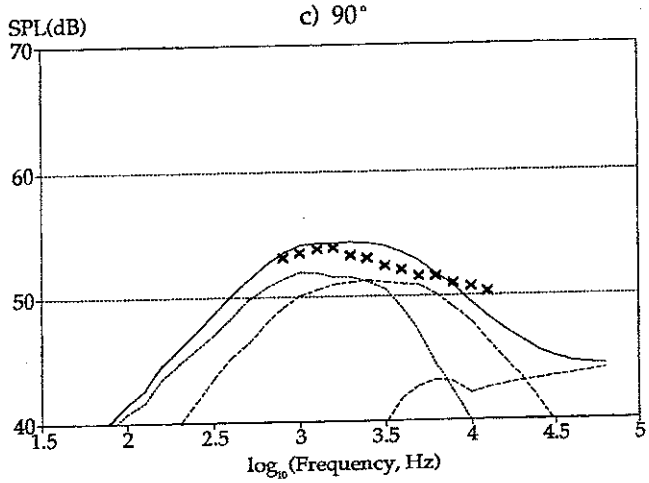

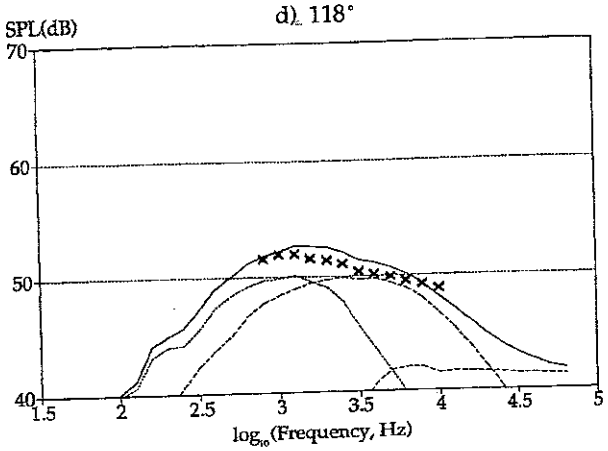

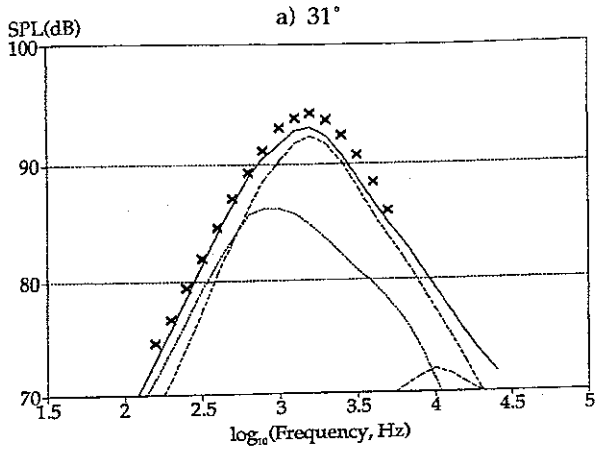

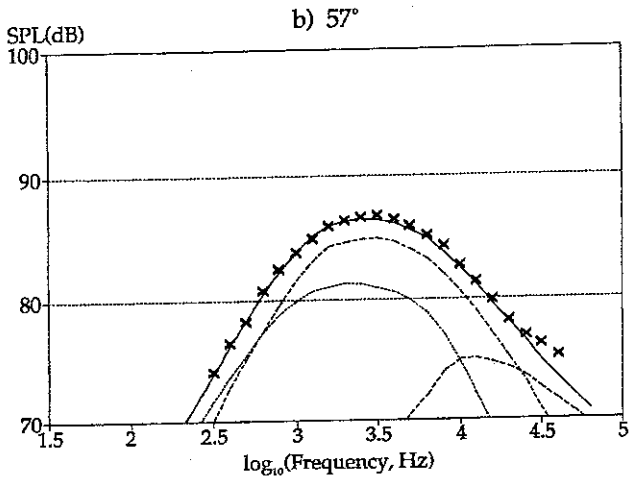

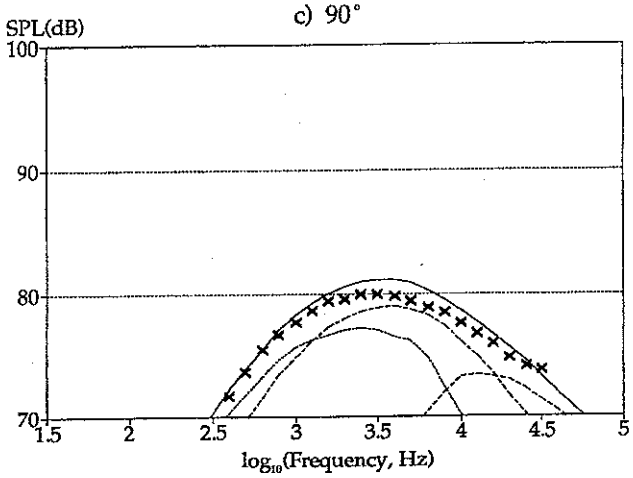

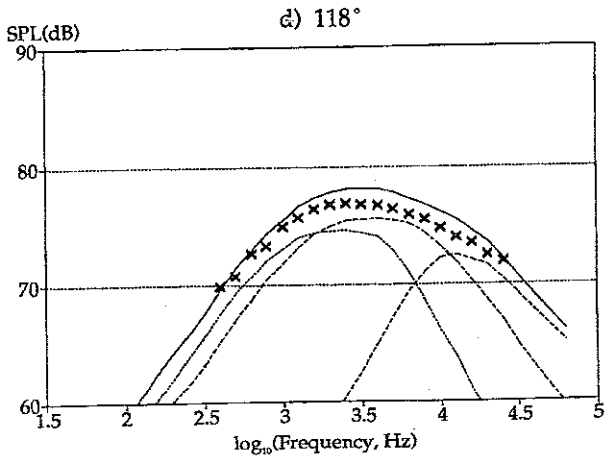

Figures 55.

Hot jet (800K)
Flight predictions,
$\beta = 4, \lambda = 0.63$
$V_p = 430 m/s$